Doctoral Dissertation
Doctoral Program in Electrical, Electronics and Communications Engineering
(36^{th} cycle)

Ultra-high bitrates Next Generation Optical Architectures and Passive Optical Networks

Giuseppe Caruso

* * * * *

Supervisor
Prof. Roberto Gaudino, Supervisor
Prof. Valter Ferrero, Co-supervisor
Dr. Giuseppe Rizzelli Martella, Co-supervisor

Doctoral Examination Committee:
Prof. Pierpaolo Boffi, Referee, Politecnico di Milano
Prof. Andrea Carena, Referee, Politecnico di Torino
Dr. Fernando Guiomar, Referee, Instituto de Telecomunicações
Prof. Josep Prat, Referee, Universitat Politecnica de Catalunya
Dr. Dario Pilori, Referee, Politecnico di Torino

Politecnico di Torino
May 07, 2024

I hereby declare that, the contents and organization of this dissertation constitute my own original work and does not compromise in any way the rights of third parties, including those relating to the security of personal data.

. . . . . .

Giuseppe Caruso
Turin, May 07, 2024

Summary

This thesis presents several novel contributions in the field of Passive Optical Networks (PON). The first part is devoted to the ITU-T 50G-PON standard, with its first recommendation released in September 2021. Being the first PON generation to foresee digital signal processing (DSP) in the form of Rx equalization to counteract bandwidth limitations and chromatic dispersion effect. Compared to previous PON generations, which required expensive reference equipment for compliance testing, 50G-PON introduces the transmitter dispersion eye closure (TDEC) as the metric for transmitter compliance testing. This new strategy allows to avoid an expensive reference transmitter and evaluate by means of mathematical tools the maximum amount of noise that can be added to the transmitted signal, therefore predicting the maximum channel penalty that can be allowed in order for a reference receiver to work properly. In this work, the rationale behind this metric is explained, including the modifications needed in 50G-PON to account for noise enhancement due to the receiver equalizer and shot noise introduced by avalanche photodiodes. Through a set of simulations and experiments, an optimization of parameters affecting the final measurement is performed. Two strategies of EQ adaptations and their effect on TDEC is analyzed, followed by a comparison between real-time and sampling oscilloscopes. Last and most important, a series of experimental results shows that TDEC is able to predict receiver sensitivity penalties due to typical impairments present in PON networks, such as limited extinction ratio and chromatic dispersion, being able to work also in negative chromatic dispersion region, where the interaction with positive chirp from electro-optical devices produces an improvement in signal quality going through the fiber.

The second part of the Thesis delves into a novel approach to counteract signal degradation due to system bandwidth limitations and chromatic dispersion. By exploiting a combination of conventional binary detection and electrical duobinary detection, a novel scheme, named Enhanced Electrical Duobinary, is analyzed through simulation and experiments in multiple working conditions. The results show that this scheme can obtain better sensitivity compared to binary detection in the case of severely reduced system bandwidth, while keeping limited sensitivity penalty in case of large system bandwidth.

In the last part, this work studies potential directions for Passive Optical Networks. Unnder the assumption that the next generation of PON will still use IM/DD and that two-level modulation will not be able to guarantee adequate performance when doubling the bitrate to 100 Gbps, a real-time PAM-4 PON testbed was implemented and studied. Different transmitter and receiver schemes (i.e. with and without optical amplification at both ends) and their sensitivities and power budgets were analyzed, showing promising results both for PON and Point-to-Point links.

Acknowledgements

I would like to express my sincere gratitude to the Optical and Quantum Communication Lab of Huawei, Munich for the opportunity to conduct my doctoral research within its dynamic and stimulating environment. Special thanks to Ivan Cano, my mentor and supervisor, whose advice, expertise, and support have been invaluable throughout this journey.

I thank the entire Optical and Quantum Communications team for their collaboration, encouragement, and insightful discussions that have enriched my research and shaped my understanding of the industry landscape. In particular, I extend my appreciation to Derek Nesset and Giuseppe Talli, who provided valuable insights and suggestions that have significantly enriched the quality of this work.

I extend my gratitude to my supervisor, Prof. Roberto Gaudino for the invaluable long-distance support and discussions.

A wholehearted thank goes also to my friends, both old and new, who have been a source of comfort, fun and joy in stressful times.

And, last but not least, I am grateful to my family for their unconditional encouragement and support during this journey.

Contents

List of Tables

List of Figures

Chapter 1

Introduction

In the past two decades, the global telecommunications industry has witnessed a rapid and transformative evolution, motivated by an insatiable demand for high-speed data transmission, increased bandwidth, and seamless connectivity, driven by bandwidth-intensive applications such as high-definition video streaming, cloud computing, virtual reality, and the Internet of Things (IoT).

The telecommunications networks serve as the crucial bridge connecting the vast expanse of the Internet to homes, businesses, and institutions around the world. In this context, one of the key enablers for massive broadband access deployment was the introduction of optical access network, particularly by means of Passive Optical Networks, or PON. These networks, as the name suggests, use passive optical components to facilitate data transmission over optical fibers without the need for active electronic components between the central office and the end-users. Thanks to its reduced cost and complexity compared to point-to-point networks, this architecture has enabled widespread deployments of Fiber-to-the-x (FTTx) services and in particular Fiber-to-the-home (FTTH), overcoming the limitations of traditional copper-based networks.

Furthermore, the introduction of 5G networks, with 6G already under study [58], promise low latency together with high capacity, that can only be provided when the cell sites are connected using optical access networks [19].

In addition, the adoption of PON is driven by the economic and social impact of the global digital transformation [59]. In fact, governments and enterprises around the world recognize the critical role of advanced telecommunications infrastructure in fostering economic development, innovation, and societal progress [79].

To give some numbers, according to Forbes Business Insight, it is estimated that the global PON market size will grow from the current $13.76 billion in 2023 to an estimated $35.59 billion by 2030 [62] and, when looking at adoption rate, in the first quarter of 2023 the fixed broadband subscribers were 1.377 billion [33], more than 77% of which are connected via Fiber-based links, as summarized in Table 1.1.

Broadband technology	Q1 2023 market share
Cable	15.78%
Copper	8.44%
Fiber	73.36%
Satellite	0.24%
Wireless	1.51%
Others	0.67%

Table 1.1: Market shares for broadband access technologies. Source: [33]

1.1 Passive Optical Networks

In order to understand why PONs have gained such an importance in the context of access networks, it must be understood what a Passive Optical Network is and what its main building blocks are.

Passive Optical Networks represent a class of fiber-optic communication systems designed to deliver high-speed data, voice and multimedia services to end users through a cost-effective and scalable architecture. Unlike traditional point-to-point fiber networks, PONs leverage passive optical components to distribute signals from a single point to multiple users, optimizing resource utilization and minimizing the need for active electronic equipment in the distribution network.

Three main blocks can be distinguished in a PON network, as depicted in Fig. 1.1. First, the Optical Line Terminal (OLT), typically located at the service provider's central office, while at the other end of PONs lies the Optical Network Unit (ONU), sometimes also referred to as Optical Network Terminal (ONT), situated at customer premises.

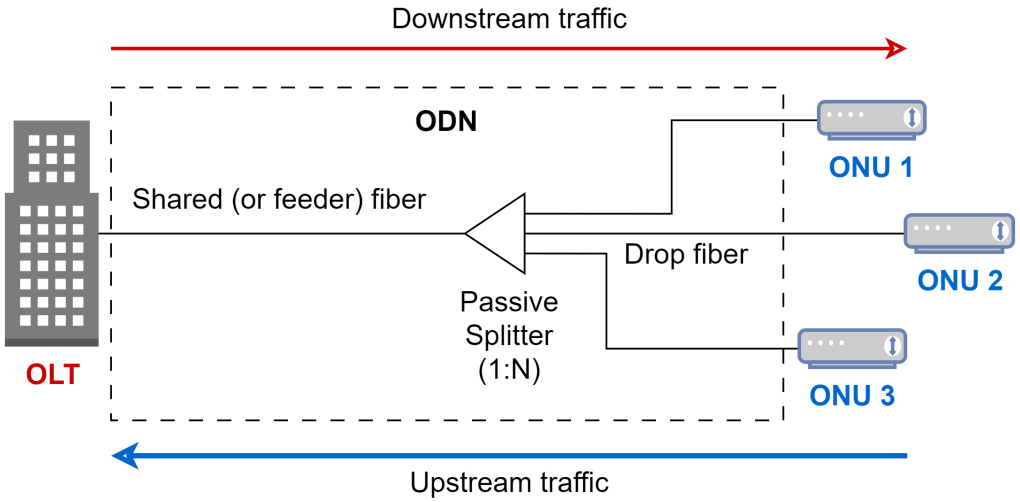

Figure 1.1: Structure of a PON

As the name suggests, PONs are inherently passive, which means that there is no active element between the OLT and the ONUs. This is achieved by using passive splitters, such as optical splitters and combiners, which enable branching of optical signals without the need for active components, such as repeaters or amplifiers. The use of passive splitters helps reduce Capital and Operational Expenditures (CapEx and Opex) associated with network deployment and maintenance. In fact, instead of having one fiber per user, as in the case of Point-to-Point networks, splitters allow the sharing of a fiber between multiple users and having only one transceiver per PON at the CO. Also, when N users are in the network, $N+1$ total transceivers are needed, compared to $2N$ in the case of a point-to-point network. At the Central Office (CO) side, in particular, the number of OLT drops from N to 1. Moreover, upgrading to higher bitrates is straightforward, since only the CO and the customer premises will require new devices. [22].

Passive splitters, together with optical fibers and connecting elements, form the third block of PONs, the ODN. Typically, the number of outputs of a splitter is a power of 2, and on this will depend the loss of the splitter itself. To give an example, a 1:2 splitter will give half of the input optical power to each output port, thus having a theoretical loss of 3 dB.

Since the fiber is shared between multiple users, some multiplexing and/or multiple access mechanisms are needed to transmit and receive to all users. In this configuration, in order to avoid collisions, Downstream (DS) and Upstream (US) use two different wavelengths. Moreover, due to the shared channel, when multiple ONUs try to transmit simultaneously, the signal cannot be detected properly by the OLT, and the most common approach to avoid collisions between ONUs is to employ Time Division Multiplexing (TDM). In TDM-based PONs, time slots are allocated for upstream and downstream communication, allowing multiple ONUs to share the same fiber link without interference. The OLT acts as the central hub of the PON and distributes and receives traffic to and from all users: the signal transmitted from the OLT is continuous and, in addition to providing data to the ONUs, it also conveys them timing and management information. Therefore, the OLT explicitly grants the ONUs the possibility to transmit in a given time slot, in which the ONU is allowed to send a burst of upstream data. The slots are assigned based on the ONU requirements, guaranteeing statistical multiplexing gain, and this is done via the so-called Dynamic Bandwidth Allocation algorithm, or DBA (for further reading, one can refer to [51] or [56].

The use of a shared medium, consequently, means that all ONUs share the capacity provided by the OLT: in the worst case where all users are active at the same time, each customer gets $1/N$ times the bitrate, minus the frame overhead used for control and signaling.

Standardization bodies such as the International Telecommunication Unit - Telecommunication Standardization Sector (ITU-T) and the Institute of Electrical and Electronics Engineers (IEEE) also published recomendations for Wavelength

Division Multiplexing (WDM) PON, which allocate several wavelengths for upstream and downstream traffic, enhancing the network's flexibility and scalability, and TWDM PON, that assigns each customer a given time slot and wavelength, thus exploiting both TDM and WDM. However, as of today TDM-PON is the most successful technology employed in PON.

1.2 Components and working principles of a PON

After describing the topology and building blocks of a PON, it is worth going more into detail and analyzing the working principles and the main physical components of this kind of network.

All PON standards up to now are based on Intensity Modulation and Direct Detection (IM/DD), which are the simplest and the most cost-effective systems in optical communications. These characteristics make them suitable for PON, where cost is of major concern due to the very large deployment scale.

IM consists in the variation of the intensity of the optical signal to encode information. The intensity of the light wave is modulated based on the data to be transmitted. Various modulation techniques can be used, such as on-off keying (OOK), where the signal is turned on or off to represent binary data, or pulse amplitude modulation (PAM) for multilevel signaling. All generations of PON until today employ the simplest modulation format, NRZ-OOK. IM can be achieved in two ways:

1. with *direct modulation*, the output power of a laser is modified by directly changing its driving current. Devices employing this kind of concept are called Directly Modulated Lasers (DML)

2. with *external modulation*, a laser produces a Constant Wave (CW) signal, which is then fed to an external modulator. PON typically employ Electroabsorption Modulators (EAM), devices based on the Franz–Keldysh effect, which allows to change the bandgap energy of the device by applying an external voltage [1].

At receiver side, direct detection consists in directly converting the optical signal to an electrical signal by means of a photodiode (PD), without attempting to recover any phase or polarization information. PDs convert variations in optical intensity directly into variations in electrical current, which are electrically amplified for subsequent processing. The most common choice, here, is to use a Transimpedance Amplifier (TIA), which provides high sensitivity together with a large bandwidth [1].

The sensitivity of an optical receiver is one of the most important parameters in PON, and it is defined as the minimum optical power level required to achieve a

certain level of performance. This performance level is often defined by the Bit Error Rate (BER), which represents the likelihood of errors in the received data. A lower sensitivity value indicates better performance, as it means the receiver can operate with lower optical power levels. Two main types of PDs can be distinguished, p-i-n and Avalanche Photodiodes (APDs). The latter are designed to have an internal gain mechanism which allows them to reach lower sensitivities compared to p-i-n, at the expense of a higher driving voltage.

A peculiarity of PON is that, in the US direction, the optical power is different from one ONU to another, and at the OLT Rx side the power of the input signal may differ more than 20 dB from packet to packet. As shown in Fig. 1.2, this means that the threshold used to detect the information bits must be adapted in a very short fraction of time, and this is typically performed during the preamble of each packet [61]. This poses also challenges for the clock recovery, since each packet arrives with a different phase, making the use of a conventional Phase-Locked Loop (PLL) unfeasible and requiring more elaborate techniques. Therefore, the OLT Rx is referred to as a Burst Mode Receiver (BM Rx).

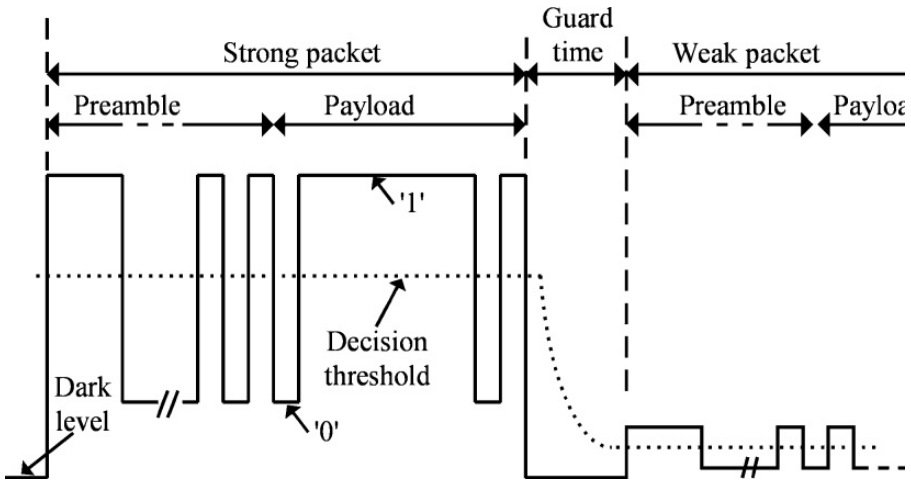

Figure 1.2: Input signal for a burst mode receiver [61]. © 2005 IEEE

Another fundamental concept in PON is the link budget, which is tightly connected to the receiver sensitivity. The link budget is a critical parameter that assesses the overall performance and viability of the optical communication link. It is, essentially, a comprehensive accounting of the optical power losses and gains throughout the PON, from the OLT in the central office to the ONUs or ONTs at the customer premises, and viceversa. The link budget is expressed in decibels (dB) and helps determine whether the optical power at the receiver end is higher than the receiver sensitivity. In that case, reliable data transmission is ensured. Since it accounts for all the losses along the network (splitters, connectors etc.), the link budget calculation also helps with designing a properly dimensioned PON,

in terms of distances and number of users that can be reached.

1.3 Development and standardization of PON

PONs have evolved over several decades, and their history can be traced through various stages of development. Please note that this Section does not aim to offer an exhaustive review of all PON standards; instead, its focus is on showing the principal technical decisions made in the design of the various generation of PONs.

The first proposals of using optical fibers for telecommunications date back to the 1960s; however, they became possible starting from the 1970s with the development of fibers having low attenuation, making them suitable for communications. Initially, optical fibers were mainly deployed using point-to-point links, connecting individual users directly to a central office. However, this architecture was not cost effective for widespread deployment, such as the one required for access networks. The need for a more cost-effective and efficient solution led to the development of PONs in the early 1990s [76].

The concept of PON emerged as a way to address the challenges of point-to-point networks. As already described, PONs were designed to share the optical infrastructure among multiple users by introducing passive components such as splitters and couplers. These passive components eliminated the need for active electronic devices at every network node, reducing both cost and complexity.

First standardization attempts: Early research efforts focused on developing protocols and standards to facilitate communication over PON architectures. Two main standards were developed in the 1990s, Asynchronous Transfer Mode PON (APON) and broadband PON (BPON). The first was defined by the Full Service Access Network (FSAN) and it used Asynchronous Transfer Mode (ATM) for data transmission. BPON, instead, was standardized by the ITU-T as G.983 [28], sharing similarities with APON but also including refinements, such as the possibility of using gigabit Ethernet traffic. BPON was the first PON system to reach more than 1 million users [21]. The two standards introduced both the concept of upstream and downstream channels, still in use in today's PON.

GPON: BPON was soon replaced by GPON (Gigabit PON, ITU-T G.984 [29]), whose first version was ratified by the ITU-T in 2003 [29]. This standard foresees a DS channel centered at 1490 nm and the US at 1310 nm. Different data rates are defined, but the most successfully employed combination was 2.5 Gbps in DS and 1.25 Gbps in US.

Several budget classes were defined, but two ended up being prevalent: class B+, with a link budget of 28 dB, providing a reach of 20 km and a 1:32 split ratio, and an extended class C+, supporting different configurations with up to 128 user

over 10 km or, alternatively, 16 users over 40 km. Since the deployment of a PON is an important investment from the operators point of view, the subsequent PON standards will have to be compatible with these budget classes, in order to coexist on the same network. Commercial deployments of GPON began in 2004, while it reached substantial market volume around 2008 and 2009 [38].

XG(S)-PON: Due to increased data rate demands, in particular from business and enterprise customers, ITU-T, after finalizing the G-PON recommendation, began studying the feasibility of a 10 Gbps capable PON. This work ended up first in the standardization of XG-PON, in 2010 [30] and in 2016 it was extended to include a symmetric version, named XGS-PON [31].

A fundamental requisite for PON standard is the backward-compatibility with already deployed networks and coexistence with installed equipment. Specifically, XG-PON uses a wavelength of 1577 nm for downstream traffic and a wavelength of 1270 nm for upstream traffic

Also in XG-PON multiple link budget classes were introduced, this time with extra margin in order to account for the insertion loss coming from the additional WDM elements ensuring coexistence with G-PON. The lowest-budget class, named Nominal 1 (N1), has a link budget of 29 dB, 1 dB more compared to class B+, while the highest, called Extended 2 (E2), foresees 35 dB.

One of the important features of XG(S)-PON was the introduction of Forward Error Correction (FEC). In fact, when increasing bitrate, maintaining the signal integrity becomes more and more difficult, and this reduces the sensitivity of the receiver. In order to overcome this issue, some redundancy is added to the transmitted signal, so that in case of errors, the receiver can still recover the information. In XG-PON, a Reed-Solomon (RS) FEC was defined, with 239 data bits and 16 redundancy bits, allowing to get a post-FEC BER of 1e-12 with a link-level BER of 1e-3.

Another choice, in order to get better sensitivity, is to employ APD-based receiver. These devices are more sensitive than PIN photodiode, thus requiring less transmitted power. However, APDs are typically more expensive than PINs, therefore a tradeoff is needed. The standard, for this reason, allows both solutions [38].

The first XG-PON field trial was performed in 2011 [46], while commercial deployment began in China, Japan, Korea and several other countries in 2015. Only in recent years, however, the demand for XGS-PON equipment became relevant compared to G-PON, as shown in Fig. 1.3.

50G-PON: In 2016, the ITU-T started an investigation of potential technologies to achieve beyond 10G PON connections. The final agreement was a PON based on 50 Gbps line rate, given that the operators require a four-times capacity increment between PON generations [96]. This resulted in the 50G-PON G.9804 series, whose

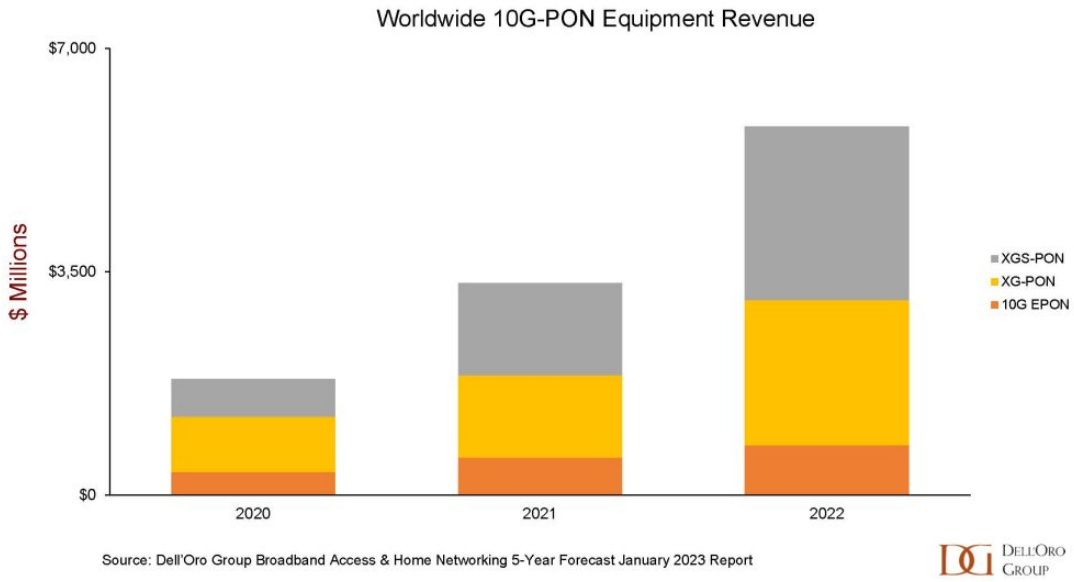

Figure 1.3: Worldwide 10 Gbps-Capable PON Equipment Revenue [36]. XG(S)-PON is the standard for 10 Gbps PON defined by the ITU-T [30, 31], while 10G EPON (Ethernet Passive Optical Network) is defined by the IEEE in [42].

first recommendation was released by ITU-T in September 2021 [26]. It defines a DS channel operating at 50 Gbps and two possibilities for the US, either 12.5 or 25 Gbps. Coexistence with GPON and XG(S)-PON was considered and therefore, to avoid colliding with existing networks, DS uses 1342 nm and US 1280 nm. An example of a network with legacy coexistence is depicted in Fig. 1.4.

One of the main challenges for this PON generation was to achieve Rx sensitivities to meet the link budgets of existing ODNs while keeping costs reasonably low: 50G-class APDs were still in the research stage and not commercially mature at the time. This led to the choice of ONU Rx based on APDs at 25 Gbps and, for the first time in PON, Rx-side equalization in order to overcome the bandwidth limitations, in addition to compensate for intersymbol interference introduced by chromatic dispersion. The Transmitter and Dispersion Eye Closure (TDEC) was introduced as a new metric to define the quality of the transmitters, keeping into account the effects of Rx-side equalization.

Together with improved receivers, the other solution to improve Rx sensitivity is to achieve a higher FEC gain. In 50G-PON, the RS codes introduced in XG-PON are replaced by Low-Density Parity Check codes (LDPC), specifically LDPC(17280, 14592), which allows to obtain a BER lower than 1e-12 with a link-level BER of 1e-2 [57]. To keep high launch power and low chirp at OLT side, EMLs integrated with Semiconductor Optical Amplifiers (SOA) are considered the main solution for

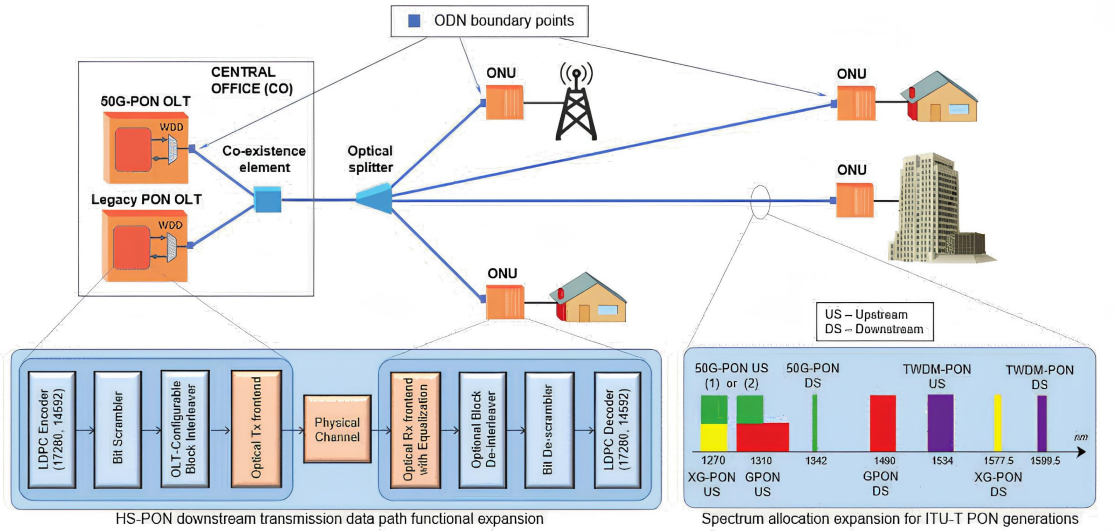

Figure 1.4: PON system with multiple generations deployed. Downstream transmission data path and PON spectrum allocation are also shown [6]. © 2022 IEEE

the OLT Tx.

In February 2023, the first amendment to the G.9804.3 standard [70], was released and, among its main addition, a 50 Gbps upstream link capability was added, made possible by technology progress in key components, such as burst-mode TIAs [34]. In order to keep costs low, the use of DMLs as ONU Tx will likely be required.

By looking at the timeline, a 50G-PON carrier trial [95] was already shown a few months after the publication of G.9804.3. Starting from 2022, operators in different countries have started performing field trial tests of 50G-PON on their deployed ODNs, such as Swisscom in Switzerland and OpenFiber in Italy. Market studies show that 50G-PON is expected to reach mass market from 2027 [36]

Table 1.2 reports the main features of the various ITU-T PON generation described earlier, in terms of achievable data rates (in downstream and upstream), wavelength allocation and presence (or absence) of FEC to improve sensitivity.

Table 1.2: Main technical features of the different ITU-T PON generations. The data rates are expressed in Gbps, while the wavelengths (λ) in nm.

ITU-T PON	DS Bitrate	US bitrate	λ (DS/US)	FEC
BPON	0.622	0.155	1490/1310	-
GPON	2.5	1.25	1480/1310	Optional
XG-PON	10	2.5	1577/1270	RS(255,239)
XGS-PON	10	10	1577/1270	RS(255,239)
50G-PON	50	12.5/25/50	1342/1260	LDPC(17280, 14592)

1.4 Outlook of this PhD Thesis

It is clear that PONs represent a cornerstone of the telecommunications infrastructure of the 21st century, offering a scalable and cost-effective solution to provide high-speed broadband access. As the demand for faster and more reliable Internet connectivity continues to increase, PON technology is emerging as a fundamental player in meeting these growing needs. Therefore, research in the field of PON is not merely an academic activity, but a pragmatic and forward-thinking endeavor. By understanding, optimizing, and expanding the capabilities of PON technology, research contributes to the evolution of advanced networks that are fundamental to addressing the challenges and opportunities of the digital age.

The research presented in this thesis was developed within the framework of an Industrial PhD agreement between Politecnico di Torino and Huawei Technologies, and the entirety of this work was developed within the Optical and Quantum Communication Laboratory of the Huawei Munich Research Center. This collaboration opportunity not only enriched the academic research but also directly contributed to addressing and solving pressing challenges within the PON industrial landscape. The convergence of academic expertise and industrial pragmatism underscores the significance and applicability of the findings presented in this Thesis.

With these motivations, this PhD thesis focuses on three key areas: standardization, novel techniques to counteract bandwidth limitations for higher bitrates, and future developments in PON. Chapter 2 delves into the latest ITU-T PON standard, 50G-PON, providing a detailed analysis and experimental verification of TDEC, the newly adopted transmitter compliance metric. Later, in Chapter 3 a novel DSP approach designed to enhance PON performance with limited-bandwidth components is introduced. Through a wide range of simulation and experimental tests, its advantages compared to conventional detection schemes are analyzed. Lastly, this research anticipates future challenges and opportunities, considering factors such as increased data rates and the development of novel components and technologies. In Chapter 4, the results of a set of real-time experiments for a 100 Gbps PON system employing PAM-4 are described, providing insight and directions for achieving PONs with data rates beyond 50 Gbps.

By addressing these aspects, the goal is to provide a practical and comprehensive understanding of PON technology, contributing to its efficiency, adaptability, and long-term relevance.

1.5 List of Publications

During the Ph.D. program, the following scientific contributions were published:

Peer-reviewed journals

1. Giuseppe Caruso, Ivan N. Cano, Derek Nesset, Giuseppe Talli, and Roberto Gaudino. "Real-Time 100 Gb/s PAM-4 for Access Links With up to 34 dB Power Budget". In: *Journal of Lightwave Technology* 41.11 (2023), pp. 3491–3497. DOI: 10.1109/JLT.2023.3244028

2. Jérémy Potet, Mathilde Gay, Laurent Bramerie, Monique Thual, Ivan N. Cano, Giuseppe Caruso, Ricardo Rosales, Derek Nesset, Fabienne Saliou, Gaël Simon, and Philippe Chanclou. "Real-Time DSP-Free 100 Gbit/s/λ PAM-4 Fiber Access Link Using EML and Direct Detection". In: *IEEE Photonics Technology Letters* 34.17 (2022), pp. 895–898. DOI: 10.1109/LPT.2022.3191460

3. Mariacristina Casasco, Giuseppe Caruso, Ivan N. Cano, Derek Nesset, Maurizio Valvo, Valter Ferrero, and Roberto Gaudino. "TDEC metric in 50G-PON: analytical and experimental investigation on several implementation aspects". In: *J. Opt. Commun. Netw.* 15.7 (July 2023), pp. 480–487. DOI: 10.1364/JOCN.489208. URL: https://opg.optica.org/jocn/abstract.cfm?URI=jocn-15-7-480

4. David Schaber, Patrick Schulte, Stefano Calabrò, Giuseppe Caruso, and Maxim Kuschnerov. "PON Downstream Scheme Supporting Simultaneously Different ONU Categories". In: *IEEE Photonics Technology Letters* 35.21 (2023), pp. 1171–1174. DOI: 10.1109/LPT.2023.3308372

International conferences

1. Giuseppe Caruso, Ivan N. Cano, Ricardo Rosales, Derek Nesset, Giuseppe Talli, and Roberto Gaudino. "Enhanced Electrical Duobinary Decoder with Low-BW Based Receivers for Short Reach Indoor Optical Links". In: *2021 European Conference on Optical Communication (ECOC)*. 2021, pp. 1–4. DOI: 10.1109/ECOC52684.2021.9606150

2. Ivan N. Cano, Giuseppe Caruso, Derek Nesset, and Giuseppe Talli. "Relation Between TDEC, Extinction Ratio and Chromatic Dispersion in 50G PON". in: *2022 13th International Symposium on Communication Systems, Networks and Digital Signal Processing (CSNDSP)*. 2022, pp. 555–557. DOI: 10.1109/CSNDSP54353.2022.9908040

3. Christian Bluemm, Heinrich von Kirchbauer, Giuseppe Caruso, Pablo Leyva, Ullrich Wuensche, Rongfang Huang, Jinlong Wei, Ivan N. Cano, Stefano Calabrò, and Giuseppe Talli. "FDMA Point-to-Multi-Point Fibre Access System

for Latency Sensitive Applications". In: *2022 European Conference on Optical Communication (ECOC)*. 2022, pp. 1–4

4. Giuseppe Caruso, Ivan N. Cano, Derek Nesset, Giuseppe Talli, and Roberto Gaudino. "Real-Time 100Gb/s Downstream PAM4 PON Link with 34 dB Power Budget". In: *2022 European Conference on Optical Communication (ECOC)*. 2022, pp. 1–4

5. Giuseppe Caruso, Ivan N. Cano, Giuseppe Talli, Derek Nesset, and Roberto Gaudino. "Study of TDEC for 50G-PON Upstream at 50 Gb/s in Negative Dispersion Regime using 25G-class Transceivers". In: *Optical Fiber Communication Conference (OFC) 2023*. Optica Publishing Group, 2023, Th1G.2. DOI: 10.1364/OFC.2023.Th1G.2

6. Mariacristina Casasco, Giuseppe Caruso, Ivan Cano, Annachiara Pagano, Roberto Mercinelli, Maurizio Valvo, Valter Ferrero, and Roberto Gaudino. "TDEC metric for 50G-PON using Optical Amplification". In: *2023 23rd International Conference on Transparent Optical Networks (ICTON)*. 2023, pp. 1–4. DOI: 10.1109/ICTON59386.2023.10207515

7. Ivan N. Cano, Giuseppe Caruso, Jinlong Wei, Giuseppe Talli, Christian Bluemm, Stefano Calabro, Heinrich von Kirchbauer, Ullrich Wuensche, Pablo Leyva, Huang Rongfang, Kuo Zhang, and Zhicheng Ye. "FDMA in Point-to-Multipoint Fibre Access Systems for Non-Residential Applications". In: *2023 23rd International Conference on Transparent Optical Networks (ICTON)*. 2023, pp. 1–4. DOI: 10.1109/ICTON59386.2023.10207353

Chapter 2

Transceiver compliance for IM/DD systems

In this Chapter, an overview of transmitter physical layer compliance testing for Passive Optical Networks is presented. The Chapter is divided into two parts: in the first, several testing methodologies will be discussed with their advantages and disadvantages, with a particular focus on describing the TDEC metric, recently introduced in the ITU-T 50G-PON standard [26].

The second part is dedicated to exploring and detailing the work carried out throughout the thesis on TDEC for 50G-PON, with analytical, simulations, and experimental results based on the following publications:

1. Mariacristina Casasco, Giuseppe Caruso, Ivan N. Cano, Derek Nesset, Maurizio Valvo, Valter Ferrero, and Roberto Gaudino. "TDEC metric in 50G-PON: analytical and experimental investigation on several implementation aspects". In: *J. Opt. Commun. Netw.* 15.7 (July 2023), pp. 480–487. DOI: 10.1364/JOCN.489208. URL: https://opg.optica.org/jocn/abstract.cfm?URI=jocn-15-7-480

2. Ivan N. Cano, Giuseppe Caruso, Derek Nesset, and Giuseppe Talli. "Relation Between TDEC, Extinction Ratio and Chromatic Dispersion in 50G PON". in: *2022 13th International Symposium on Communication Systems, Networks and Digital Signal Processing (CSNDSP)*. 2022, pp. 555–557. DOI: 10.1109/CSNDSP54353.2022.9908040

3. Giuseppe Caruso, Ivan N. Cano, Giuseppe Talli, Derek Nesset, and Roberto Gaudino. "Study of TDEC for 50G-PON Upstream at 50 Gb/s in Negative Dispersion Regime using 25G-class Transceivers". In: *Optical Fiber Communication Conference (OFC) 2023*. Optica Publishing Group, 2023, Th1G.2. DOI: 10.1364/OFC.2023.Th1G.2

4. Mariacristina Casasco, Giuseppe Caruso, Ivan Cano, Annachiara Pagano, Roberto Mercinelli, Maurizio Valvo, Valter Ferrero, and Roberto Gaudino. "TDEC metric for 50G-PON using Optical Amplification". In: *2023 23rd International Conference on Transparent Optical Networks (ICTON)*. 2023, pp. 1–4. DOI: 10.1109/ICTON59386.2023.10207515

2.1 Introduction

As already introduced in Chapter 1, access networks connect a large number of end users to the Internet, and this is made possible when the components needed are relatively inexpensive. For PON, this typically reflects that the ONU is much cheaper than the OLT, as the cost of the latter can be shared among many users. The residential customer market requires a large quantity of products at a low cost, which can only be achieved through a well-functioning industry supply chain. In this sense, industry standards guarantee that Passive Optical Network (PON) systems can coexist on existing infrastructure and allow interoperability between different vendors' equipment, thus increasing production volumes [92].

At the simplest level, interoperability in PON is guaranteed if, after choosing a target BER, a transmitter and a receiver can achieve the required link budget. In fact, in direct detection systems performance is typically limited by the sensitivity of the receiver, that is, the minimum received optical power required to operate at a given BER; a given receiver is said to be more sensitive than another if it requires less power to get the same BER. Sensitivity depends on the signal-to-noise ratio (SNR) and, by extension, on the noise effects that degrade the signal. As detailed in 5, a relationship between BER and signal quality can be expressed by the so-called Q factor [99], i.e.,:

$$Q = \frac{I_1 - I_0}{\sigma_1 + \sigma_0} \tag{2.1}$$

where I_1 and I_0 are the electrical currents corresponding to the 1 and 0 level, and σ_1 and σ_0 are the respective noise standard deviation values. It must be highlighted that the Q factor obtained in 2.1 is different from the Q function, that is, the tail distribution function of the standard normal distribution. To avoid confusion, throughout this Chapter the first is presented in italics, while the second term is in regular font. The BER can now be found as

$$\mathrm{BER} = \frac{1}{2}\,\mathrm{erfc}\left(\frac{Q}{\sqrt{2}}\right) \tag{2.2}$$

2.2 Bit Error Rate Testing

In principle, then, compliance could be tested by first measuring the output power of a transmitter, then connecting the receiver and varying the received optical power in order to check its sensitivity. The major components in a BER testing setup are the Pattern Generator, which provides the signal to be transmitted, and the Bit Error Rate Tester (BERT), which compares the received signal with the reference sequence.

Pattern Generation The pattern generator usually provides a pseudo-random binary sequence (PRBS) to simulate traffic in a real transmission system. PRBSs are periodic bit patterns characterized by their sequence length, number of consecutive 1s, and number of consecutive 0s. The most common PRBS for digital transmittion testing are PRBS-(N), whose length is $2^N - 1$ bits and N being an integer value. A typical implementation to generate a PRBS sequence is to use linear feedback shift registers (LFSR) [73]. Table 2.1 shows several PRBS polynomials and the resulting sequence periodicity.

Table 2.1: PRBS polynomials

Pattern	Polynomial	Length
PRBS-7	$1 + x^6 + x^7$	127
PRBS-9	$1 + x^5 + x^9$	511
PRBS-15	$1 + x^{14} + x^{15}$	32767
PRBS-23	$1 + x^{18} + x^{23}$	8388607
PRBS-31	$1 + x^{28} + x^{31}$	2147483647

The presence of long sequences of consecutive 0s and 1s allows one to test worst-case conditions in the system. In fact, typical clock recovery circuits work well when pattern alternates 0s and 1s, but not as good for long uninterrupted sequences of the same symbol, as they contain fewer clock frequency components. Furthermore, the frequency spectrum resolution of the transmitted sequence is determined by the inverse of the pattern length, following $\delta f = f_b/N_b$, where N_b is the length of the transmitted sequence. This means that, at the same bitrate, using longer PRBS pattern allows to test transfer function with better frequency granularity. At the same time, as the bitrate increases, it is possible to characterize the system without using extremely long sequences.

Error detection The other main component of a BER test set is the Error Detector (ED). Here, the signal transmitted through the system is compared to the PRBS sequence used as a reference. The two sequences go through an

XOR gate whose output is zero (0) when both inputs are identical or one (1) otherwise, the latter case indicating an error. For a proper BER estimation, it is fundamental that there is no timing mismatch when the two sequences are compared, i.e. the two must be synchronized in time. If the pattern generator and the error detector are in the same location, no external circuitry is needed, as they can share the same clock signal; alternatively, an external device that extracts the clock component from the received signal is necessary; this is typically referred to as Clock Data Recovery (CDR) module. A description of the clock recovery scheme and the synchronization mechanisms is beyond the scope of this work, but a good overview is provided in [41].

Being a time-dependent metric, the BER is typically measured until 100 errors are obtained in order to obtain statistical significance. This can lead to very long testing times, particularly at low target BER. In fact, the average time to see one error can be expressed as:

$$\Delta T = \frac{1}{BER \cdot R_b} \tag{2.3}$$

where R_b is the bitrate of the system. If, for example, we consider a transmitter at 1 Gbps (10^9 bit/s) and a target BER of 10^{-12}, the average time to obtain 100 errors will be 10^5 seconds, more than 25 hours. Increasing the bitrate helps because it is possible to shorten the test times (Eq. 2.3). At the same time, signal degradation at higher bitrates requires the introduction of some error correction, which reduces the link-level BER requirements while at the same time guaranteeing a low error probability after FEC.

However, BER testing is still not a desirable solution for compliance testing. A transmitter would have to be tested under all the potential working conditions with all available receivers on the market, which is as impossible as it sounds.

To make the process feasible, standards typically start by defining worst-case receivers. The primary reason for this is that the receiver's performance determines the system's overall capability to detect and correctly interpret the transmitted signals. Although a worst-case receiver is crucial, it is important to note that transmitters are also subject to design specifications and performance requirements. Transmitters must meet certain criteria to ensure that they generate signals within acceptable parameters and that their signal, after going through the worst-case channel, can still be properly detected [63].

In this context, a transmitter compliance metric is desirable when it can predict the sensitivity penalty caused by a degraded transmitted signal, so that, up to a certain degree, the transmitter can still meet the required link budget by increasing the transmitter power. In the context of PON, several metrics have been introduced and used over the years; in the following, three of them will be described: the Eye Mask test, the Transmitter Dispersion Penalty, and the Transmitter Dispersion Eye Closure.

2.3 Transmitter Eye Mask

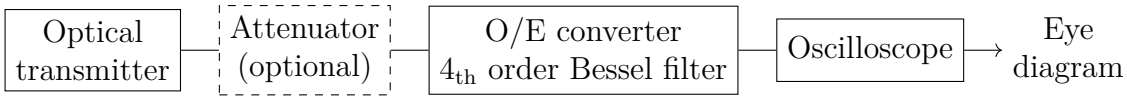

Figure 2.1: Setup for eye mask test as defined in ITU-T G.9807.1 [30]

The transmitter eye mask test is a fairly straightforward test. As shown in Fig. 2.1, after the optical signal is captured using an oscilloscope, the resulting eye diagram is generated.

On top of the eye diagram, several polygons are superimposed: usually, an inner polygon defines the minimum acceptable eye opening, while the outer ones define tolerable transients, i.e. over- and undershoot. Polygons are typically defined by assuming a given specification of rise time, fall time, pulse overshoot/undershoot, ringing, and jitter that may ensure proper operation with a compliant receiver.

The eye mask, despite hiding a nontrivial mathematical foundation (see, for example, [67]), is a fast test and very easy to interpret. However, several problems arise when working with eye mask tests: first, there is no single minimally acceptable transmitter due to the multitude of possible combinations that involve transmitter transition time, noise, and jitter. Each combination can result in a worst-case scenario, each with a distinct shape of the eye. Then, since the test is done back-to-back, it cannot give a prediction of the performance after fiber. Furthermore, the eye mask cannot completely ensure the interoperability of a transmitter, since a pass/fail test cannot be directly translated into a power penalty.

Despite the drawbacks, the eye mask test, because of its simplicity, is still a valuable preliminary tool to discard transmitters that generate too distorted waveforms, simplifying subsequent testing with the other metrics described in the following.

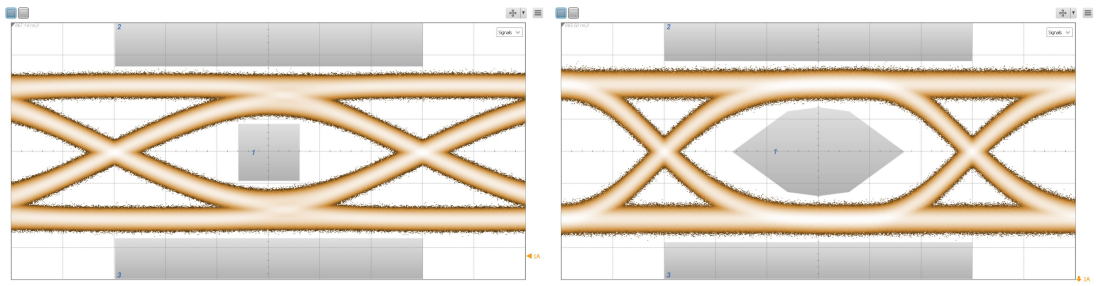

(a) (b)

Figure 2.2: Examples of ITU-T PON eye masks. (a) OLT for XG-PON. (b) ONU for GPON

As an example, Fig. 2.2a and Fig. 2.2b show the eye mask test for an XG-PON OLT transmitter at 10 Gbps and a GPON US Tx at 1.25 Gbps, respectively; in the figures, it is possible to see the captured signal and the superimposed inner, upper and lower polygons.

2.4 Transmitter and Dispersion Penalty

As already mentioned, a transmitter metric is desirable when it translates signal distortion into power penalties. In the IEEE 802.3ae (10G Ethernet, [43]) standard, a new metric was developed to assess the penalty due to transmitter quality and channel penalties, the Transmitter and Dispersion Penalty (TDP).

The main idea behind TDP is to evaluate the penalty of the device under test (DUT) compared to an ideal transmitter, and the setup for the evaluation of TDP is shown in Fig. 2.3.

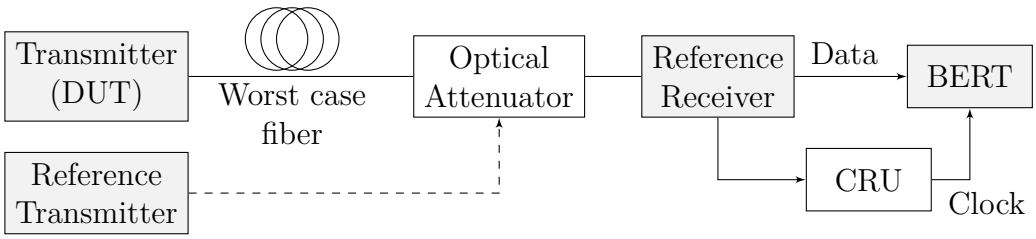

Figure 2.3: Reference TDP measurement setup

A reference transmitter is connected to a BER tester through an optical attenuator and a receiver, to measure its sensitivity at the target BER. A clock recovery unit (CRU) recovers the clock from the received signal and provides it to the BERT. Subsequently, the reference transmitter is replaced by the transmitter under test, and the attenuation is adjusted to achieve the BER of the reference transmitter. The difference in receiver sensitivity is the TDP for the DUT, and if it is smaller than the maximum allowed TDP, then the transmitter is compliant, since it can still meet the link budget by increasing the transmitted optical power. An example of a TDP sensitivity penalty is shown in Fig. 2.4.

Although being a very accurate metric up to very low error probabilities, the use of TDP as a transmitter compliance test has some drawbacks [50]. The requirements for the reference transmitter are very stringent, as is possible to see in IEEE 802.3ae (10G-Ethernet, [43]:

- Rise/fall times smaller than 0.15 Unit Intervals (UI) at 20% and 80%
- Output eye is symmetric and with good margin in the eye mask test
- Jitter is less than 0.2 UI peak-peak

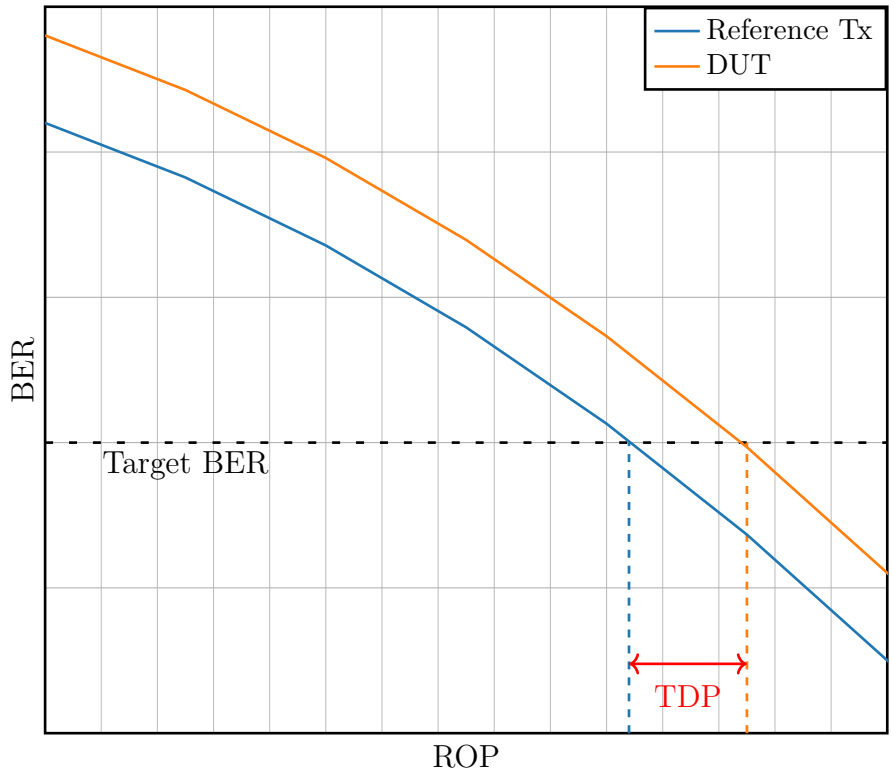

Figure 2.4: A typical TDP measurement curve. The blue curve is measured with the reference transmitter, while the orange is from the DUT

- Worst case vertical eye closure penalty (VECP) is less than 0.5 dB
- RIN should be less than -120 dB/Hz (100BASE-X) or -125 dB/Hz (1000BASE-X)

It becomes clear that as data rate increses, the hardware-based reference transmitter and receiver become more and more difficult to obtain and to calibrate. Furthermore, TDP is a sensitivity-based test, so it also requires a bit error rate tester (BERT), which makes the whole testbed very expensive. Together with the long time spans required to observe many bits for BER tests, these factors make it preferable to look for some alternative test method.

2.5 Transmitter and Dispersion Eye Closure

To overcome the limitations of the TDP test, a new transmitter compliance test was introduced in IEEE 802.3bm (Ethernet standard for a 100 Gb/s link using four multimode fibers [44]), the Transmitter and Dispersion Eye Closure (TDEC). It is

similar to TDP in the sense that it determines the launch power penalty for a transmitter under test compared to an ideal transmitter. Compared to TDP, however, TDEC has several advantages: first, the test is performed on an optical eye diagram captured by an oscilloscope, so it does not require an error detector; second, TDEC, as the name suggests, mathematically compares the closure of the measured eye to a theoretical two-level signal, thus taking out the need for a hardware reference transmitter. In addition, it is possible to measure the oscilloscope noise separately and de-embed it from the measurements. These features make TDEC an attractive solution for transmitter compliance testing. It must be once again highlighted that oscilloscope-based techniques are made possible by the introduction of forward error correction (FEC): with increasing data rates, obtaining low bit error probabilities can become difficult and expensive. By introducing FEC, it is possible to maintain a low post-FEC BER at the system level even with a high BER at the link level; if FEC is employed, it is possible to use measurement techniques that are based on the noise statistics of the signal and that do not rely on analysis at very low error probability (BERT-based), making them faster and cheaper overall [63].

TDEC working principle

It is possible to understand the working principle of TDEC by first looking at the TDEC test setup in Fig. 2.5.

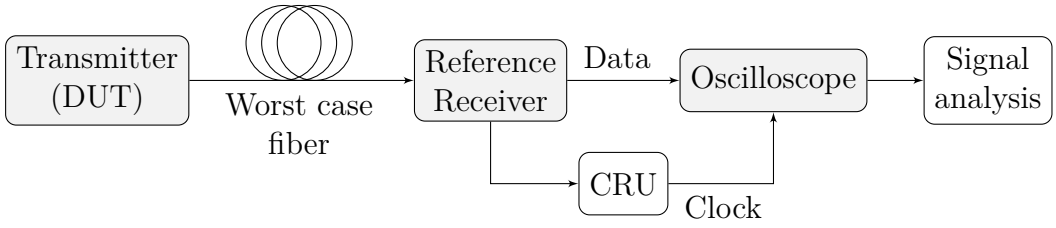

Figure 2.5: Reference TDEC measurement setup

A signal from the DUT is sent through a worst-case fiber and captured with a sampling oscilloscope. The histograms of the received eye diagram are calculated and, subsequently, the algorithm can be summarized in three steps [53]:

1. Estimate the amount of Gaussian noise we can add to the signal from the device under test (DUT) by using:

$$\frac{1}{2}\left(\frac{\int f_u(y)\,\mathrm{Q}\left(\frac{y-P_{avg}}{\sigma_G(y)}\right)\mathrm{d}y}{\int f_u(y)\,\mathrm{d}y}\right)+\frac{1}{2}\left(\frac{\int f_l(y)\,\mathrm{Q}\left(\frac{P_{avg}-y}{\sigma_G(y)}\right)\mathrm{d}y}{\int f_l(y)\,\mathrm{d}y}\right)=\mathrm{BER}_{target} \quad (2.4)$$

where f_u and f_l are the upper and lower distributions of the samples captured in the oscilloscope, P_{avg} is the average power, σ_G is the standard deviation of

the noise it is added to the signal, BER_{target} is the pre-FEC BER limit (1e-2 in [26]) and Q is the area under a normal distribution, as defined in Appendix 5. It follows that $\text{Q}\left(\frac{y-P_{avg}}{\sigma_G(y)}\right)$ gives the probability of error when noise is added to the samples with power y. The 1/2 terms in Eq. 2.4 are valid under the assumption that the probabilities of transmitting 0 and 1 are the same.

2. Estimate the noise that we can add to an ideal signal with the same optical modulation amplitude (OMA) according to [1]:

$$\text{BER}_{target} = \frac{1}{2}\,\text{erfc}\left(\frac{Q}{\sqrt{2}}\right) \tag{2.5}$$

3. Calculate TDEC as:

$$\text{TDEC} = 10\log_{10}\left(\frac{\sigma_{ideal}}{\sigma_G}\right) \tag{2.6}$$

Looking at Eq. 2.6, we can see that a lower TDEC value means that more noise can be added. Moreover, one can consider that the oscilloscope has intrinsic noise that is added to the signal at capture time. It is possible to account for it in the TDEC measurement by first measuring this noise component (i.e., capturing signal from the oscilloscope without any input connected) and then, considering it as an independent noise source, one can rewrite the noise as:

$$\sigma = \sqrt{N^2 + S^2} \tag{2.7}$$

In 2.7, N is the noise standard deviation found from 2.4 and S is the oscilloscope intrinsic noise standard deviation.

2.6 TDEC in ITU-T 50G-PON

The ITU-T adopted TDEC as a metric to assess transmitter compliance in 50G-PON [26]. In the G.9804.3 standard, a maximum value of 5 dB is set for TDEC to guarantee a minimum Tx quality level, when considering a given reference bandwidth-limited and equalized receiver. Beyond this value, the TDEC metric starts to diverge from the OMA penalty, becoming less reliable [86]. The relation between BER and TDEC can be derived as follows. If we consider the ideal signal, we will have $Q_{ideal} = \text{OMA}/2\sigma_{ideal}$. TDEC is the amount of noise that we can add to the captured signal to reach the target BER, that is, $\text{TDEC} = \sigma_{ideal}/\sigma_g$. Now, we capture a signal with a given amount of noise σ_s. If we assume that both σ_s and σg are independent Gaussian random variables, we can write $\sigma^2_{ideal} = \sigma^2_s + \sigma^2_g$. Recalling the definition of OMA, we can rewrite it as

$$\frac{1}{Q^2_{ideal}} = \frac{1}{Q^2_s} + \frac{1}{Q^2_g} \tag{2.8}$$

The BER of the captured signal will be [99]:

$$\mathrm{BER} = \frac{1}{2}\,\mathrm{erfc}\left(\frac{Q_{ideal}}{\sqrt{2}}\sqrt{\frac{\mathrm{TDEC}^2}{\mathrm{TDEC}^2-1}}\right) \tag{2.9}$$

Having defined the basics of TDEC, two main changes were made to the original definition to adapt it to a 50G-PON system [96], described in the following paragraphs.

Effect of the receiver equalizer

As already stated in Chapter 1, to overcome receiver bandwidth limitations and compensate for the chromatic dispersion penalty as such a speed, 50G-PON is the first generation of passive optical networks that includes equalization on the receiver side. The main consequence, regarding the TDEC measurement, is that when a signal goes through an equalizer the eye opening is increased, but at the same time the signal has enhanced high-frequency noise components. This effect must be taken into account in the noise evaluation process. This effect was already considered for Transmitter Dispersion Eye Closure Quaternary (TDECQ) [45], where the noise enhancement factor C_{eq} was introduced. C_{eq} is a coefficient that compensates for the noise enhancement factor of the reference equalizer when the equalizer has been optimized for the minimum TDEC. One can derive C_{eq} as follows:

$$C_{eq} = \sqrt{\int_f N(f)\cdot|H_{eq}(f)|^2\,\mathrm{d}f} \tag{2.10}$$

where $N(f)$ is the noise power spectral density and $H(f)$ is the frequency response of the reference equalizer, which is, for the 50G-PON downstream case, a 13-taps T-spaced feedforward equalizer (FFE). $N(f)$ is equivalent to white noise filtered by a fourth-order Bessel-Thompson filter with a 3-dB bandwidth of 18.75 GHz (the TDEC reference filter). After including the equalizer contribution, the noise calculation from Eq. 2.4 now becomes:

$$\frac{1}{2}\left(\frac{\int f_u(y)\,\mathrm{Q}\left(\frac{y-P_{avg}}{C_{eq}\cdot\sigma_G(y)}\right)\mathrm{d}y}{\int f_u(y)\,\mathrm{d}y}\right)+\frac{1}{2}\left(\frac{\int f_l(y)\,\mathrm{Q}\left(\frac{P_{avg}-y}{C_{eq}\cdot\sigma_G(y)}\right)\mathrm{d}y}{\int f_l(y)\,\mathrm{d}y}\right)=\mathrm{BER}_{target} \tag{2.11}$$

Extending TDEC for APD-based receivers

It was already mentioned in Chapter 1 that in order to improve receiver sensitivity, PON receivers typically employ APD photodiodes. Although PIN photodiode performance is primarily affected by a thermal noise component, mainly coming from the transimpedance amplifier (TIA), in APDs the avalanche gain effect creates power-dependent noise components [1]. Specifically, for a two-level signal, the

noise on the 1 level will be higher than the noise on the 0 level. Thus, an APD will have two noise components affecting the generated current, thermal and shot noise. The two can be considered as independent random processes with Gaussian statistics, so we can write

$$\sigma^2 = \sigma^2_{s_{0,1}} + \sigma^2_{th} \tag{2.12}$$

The 0,1 pedix in $\sigma^2_{s_{0,1}}$ indicates that the noise component depends of the input power level, according to:

$$\sigma^2_{s_{0,1}} = 2q\, M^2 F_A R\, \Delta f\, P_{0,1} \tag{2.13}$$

where q is the elementary charge, M is the APD gain, F_A is the excess noise factor of the APD, R is the photodiode responsivity, Δxf is the bandwidth and $P_{0,1}$ is the input optical power.

From Eq. 2.13, it is clear that the avalanche gain of the APD, produces a higher noise level on the one-bits in comparison to the zero-bits. This is taken into account by defining the *noise asymmetry variable* as

$$m = \sigma_1/\sigma_0 \tag{2.14}$$

Recalling the definition of Extinction Ratio and defining the ratio between thermal and shot noise on the one bits

$$\rho_1 = \sigma_{th}/\sigma_{sh_1} \tag{2.15}$$

we can rewrite 2.14 as

$$m = \sqrt{\frac{1+\rho_1}{1/ER+\rho_1}} \tag{2.16}$$

For a PIN photodiode, the dominant term in Eq. 2.15 is the thermal noise σ_{th}, which results in $\rho_1 \gg 1$ and leads to $m = 1$. In an Rx limited by shot noise, like, for example, APDs working at very low error probabilities (e.g. BER $\approx 10^{-10}$), the shot noise term dominates and we get $\rho_1 \ll 1$, which leads to the noise asymmetry value becoming dependent on the ER as $m = \sqrt{ER}$. This relation is represented by the dashed line in Fig. 2.6 and can be considered as the upper bound.

For the purpose of measuring TDEC, the noise from the DUT must be compared with that of an ideal device, referred to as σ_{ideal}, including also the APD noise. For this purpose, we can rewrite Eq. 2.5 as:

$$2 \cdot \mathrm{BER}_{target} = \mathrm{Q}\left(\frac{\mathrm{OMA}}{2\sigma_{ideal}}\right) + \mathrm{Q}\left(\frac{\mathrm{OMA}}{2m\sigma_{ideal}}\right) \tag{2.17}$$

Eq. 2.17 is a reformulation of 2.5 for APDs, under the assumption that the same number of zeros and ones are transmitter. Given BER_{target}, there is no direct way to extract σ_{ideal} from Eq. 2.17, however a simple numerical search can be implemented for this purpose.

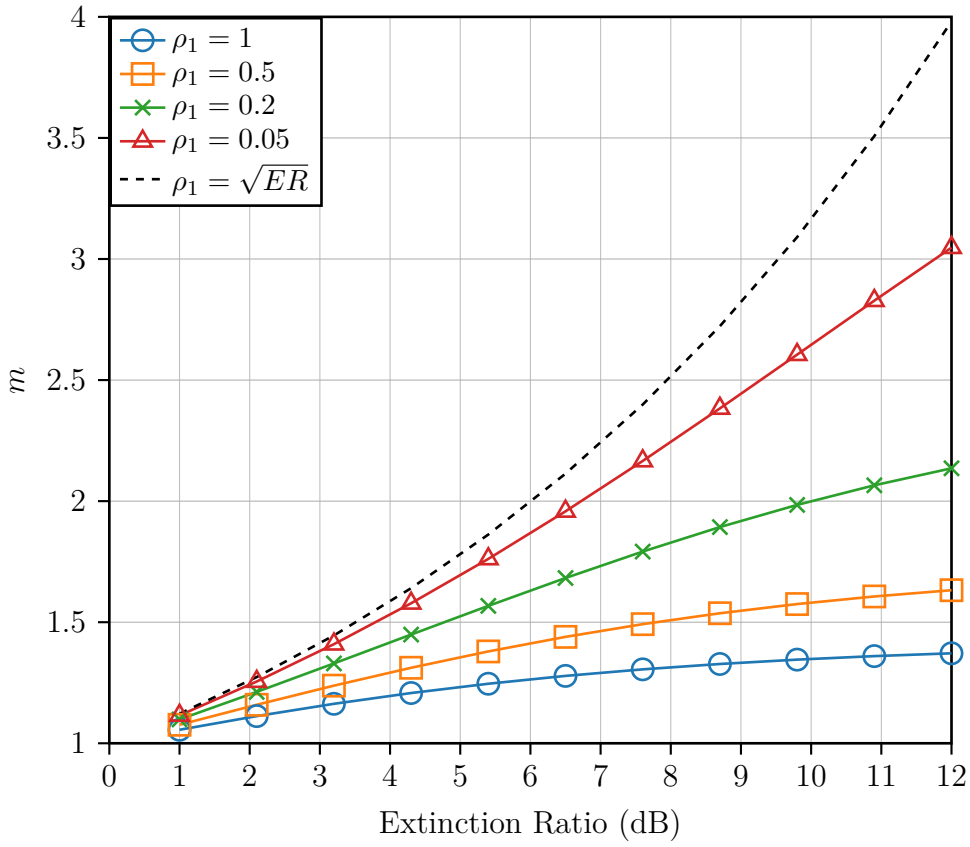

Figure 2.6: Asymmetric noise value (m) against ER

In 50G-PON, the selected target pre-FEC BER is 10^{-2} and in this situation the signal power is so low that σ_{th}^2 becomes non-negligible and even comparable to the shot noise. Fig. 2.6 plots the value of m against typical ER values of PON transmitters when varying ρ_1. We can observe that in the range $0.2 < \rho_1 < 1$ the value of m is bound between 1 and 2.5, depending on the ER. Furthermore, when approaching the limit of ER $\to \infty$, m tends to converge. Therefore, for values of ER up to 8 dB, the asymmetric noise is in the range $1 < m < 2$. In the current 50G-PON recommendation, a value of 1.5 has been selected.

After introducing m to account for the contribution of the shot noise, it must be adopted for the samples that appear inside a histogram. A linear relation between m and the signal power can be adopted, considering $m = 1$ for the 0-level and $m = 1.5$ for the 1-level. Then, the following equation is obtained:

$$M(y) = \begin{cases} \frac{m(y-y_0)+(y_1-y)}{y_1-y_0} & \text{for } y \geq y_0 \\ 1 & \text{for } y < y_0 \end{cases} \tag{2.18}$$

The value of M depends on the power of the sample and it modifies the noise

standard deviation according to [26]:

$$\sigma_G(y) = \sqrt{\left(M(y) \frac{y - y_0}{y_1 - y_0} (\sigma_0^2 + S^2) - S^2 \right)} \tag{2.19}$$

The other terms appearing in 2.19 are the following: y_0 and y_1 are the power levels of 0-bits and 1-bits, respectively, σ_0 is the noise to be added to the captured signal (without considering the extra noise of the APD) and S is the standard deviation of the intrinsic noise coming from the oscilloscope.

2.6.1 Parameter optimization in the TDEC implementation

The preceding Sections have comprehensively reviewed the state-of-the-art of transmitter compliance testing in Passive Optical Networks, providing a thorough understanding of existing research and methodologies. Moving forward, the focus shifts to the novel contributions produced during this Ph.D. work.

When looking at the TDEC in the ITU-T 50G-PON standard, it is evident that several parameters are left free, up to the implementer. Some of them were evaluated and optimized to obtain a consistent value. The procedure depends on the parameters that will be explained in detail in the following: calculation of the average power (P_{avg}), number of bins (N_{bins}) for each of the four histograms, and increase step of the noise power. The procedure to assess P_{avg} is defined in [26]. Power levels are measured by searching for sequences of 72 consecutive 0 or 1, present in the SSPR test signal, and then P_{avg} is obtained as the average of the two values: $P_{avg} = (P_1 + P_0)/2$.

After computing P_{avg}, the number of histogram bins N_{bins} must be evaluated. When doing the actual TDEC measurement, the first difference from the theoretical formulas comes from the fact that we cannot use continuous PDFs since we are dealing with discrete (sampled) data. Therefore, the number of bins for the histogram will influence the distribution of the samples, as in Eq. 2.11, and it is important to evaluate how much this parameter will affect the final measurement. For this purpose, we first find the minimum and maximum signal level for each of the four sampling locations and then create histograms using a variable number of bins (N_{bins}) and evaluate the TDEC. Fig. 2.7 shows the resulting TDEC against N_{bins}. If $N_{bins} < 30$, the TDEC is overestimated, as we introduce a quantization error (power levels are rounded to the central value of the histogram bin). On the other hand, when using $N_{bins} > 30$, the improvement in TDEC is marginal, at the expense of increased computation time. For the rest of this section, the choice is to employ $N_{bins} = 50$.

TDEC is an iterative process in which the noise is gradually increased until the target BER is reached, therefore the noise increment step ($\Delta\sigma_G$) plays an important

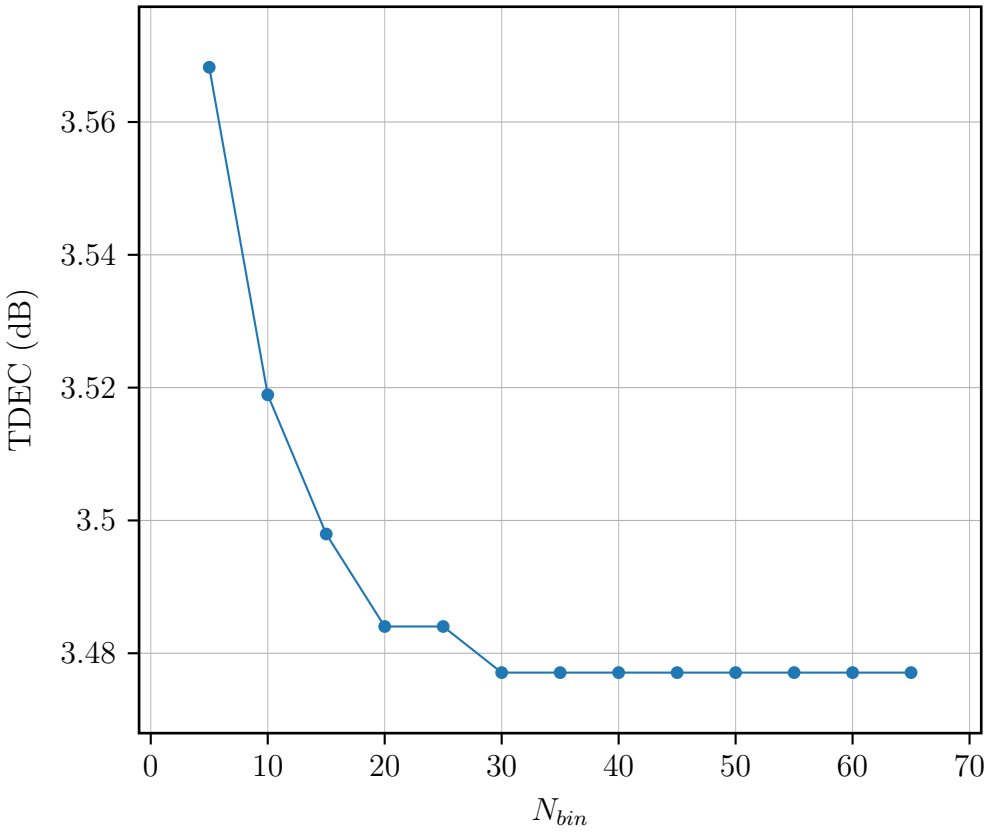

Figure 2.7: TDEC dependency on the number of histogram bins

role in the computation. Using a step size that is too coarse means that the iterative process will stop too quickly, leading to an underestimated TDEC value; on the other hand, a very fine granularity will slow the execution time of the algorithm.

Based on these considerations, some tests were performed by varying $\Delta\sigma_G$, expressed as a fraction of the average signal power, and calculating the TDEC with it. The results of this are reported in Fig. 2.8. As expected from the considerations expressed above, TDEC is underestimated when using an excessively large $\Delta\sigma_G$, since the noise value will quickly produce a signal with BER_{target}. From the Figure, it is possible to see that $\Delta\sigma_G < P_{avg}/500$ is needed to provide a convergent TDEC value. As a good trade-off between speed and accuracy, a value of $\Delta\sigma_G = P_{avg}/5000$ is used for the rest of this Section.

TDEC evaluation using real-time and sampling oscilloscopes

After optimizing the parameters in the TDEC measurement procedure, another topic of interest is related to the measurement of actual devices, specifically the way that waveforms are captured. Two families of oscilloscopes can be used to acquire

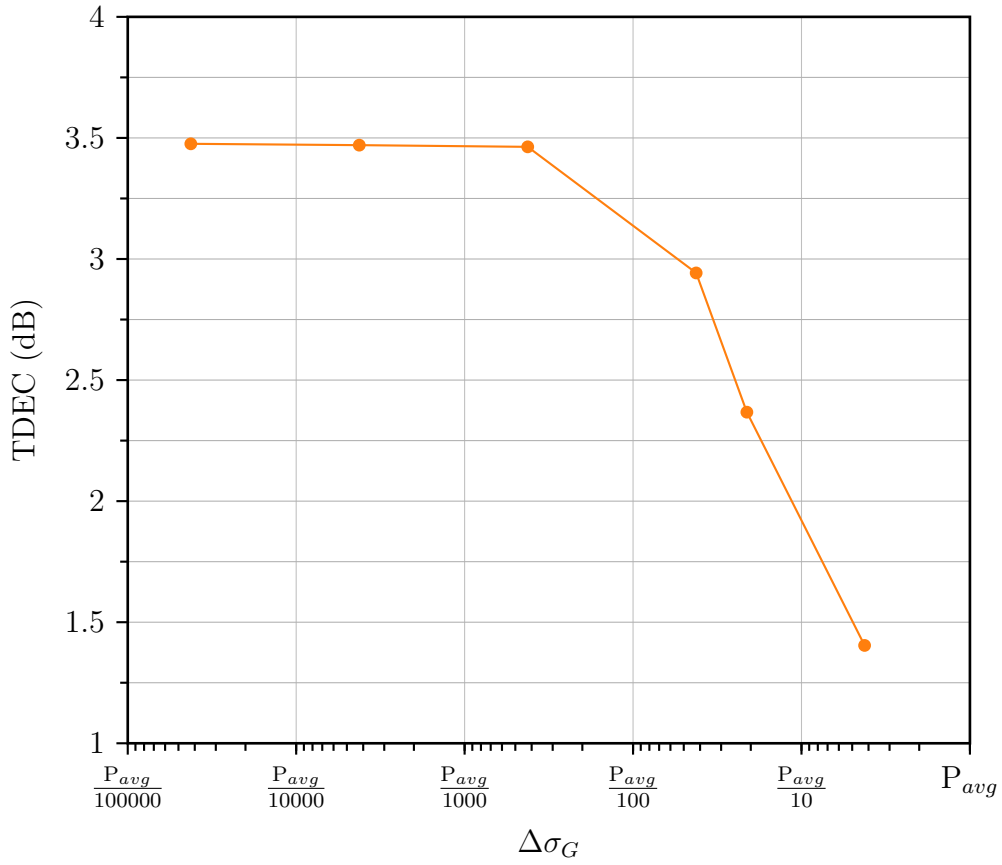

Figure 2.8: TDEC dependency on the noise step size

ultra-high-frequency waveforms: real-time oscilloscopes (RTOs) and equivalent-time oscilloscopes, also known as sampling oscilloscopes. The main difference between the two categories is in the way they digitize their input. For real-time oscilloscopes, they are able to capture in real time the incoming signal, with a limited number of samples. They typically use an internal sample clock and a trigger signal and sample uniformly over time using a high-speed analog-to-digital converter (ADC). For example, when sampling a 50 Gbps signal, a 200 GSamples/s RTO continuously acquires 4 samples/bit uniformly spaced Δ_{RTO}=5 ps, storing them in an internal random access memory (RAM) for the following post-processing and display.

On the other hand, sampling oscilloscopes use a different technique to capture signals. The acquisition here is done over multiple iterations and requires an explicit (or recovered) clock signal; a repetitive pattern is required, since on each trigger event, the sampling instant is slightly delayed compared to the previous iteration. This technique allows one to overcome the sampling rate limitations of a real-time oscilloscope, managing to digitize signal up to the analog bandwidth of the sampling

oscilloscope. An illustration of the two operating principles is shown in Fig. 2.9.

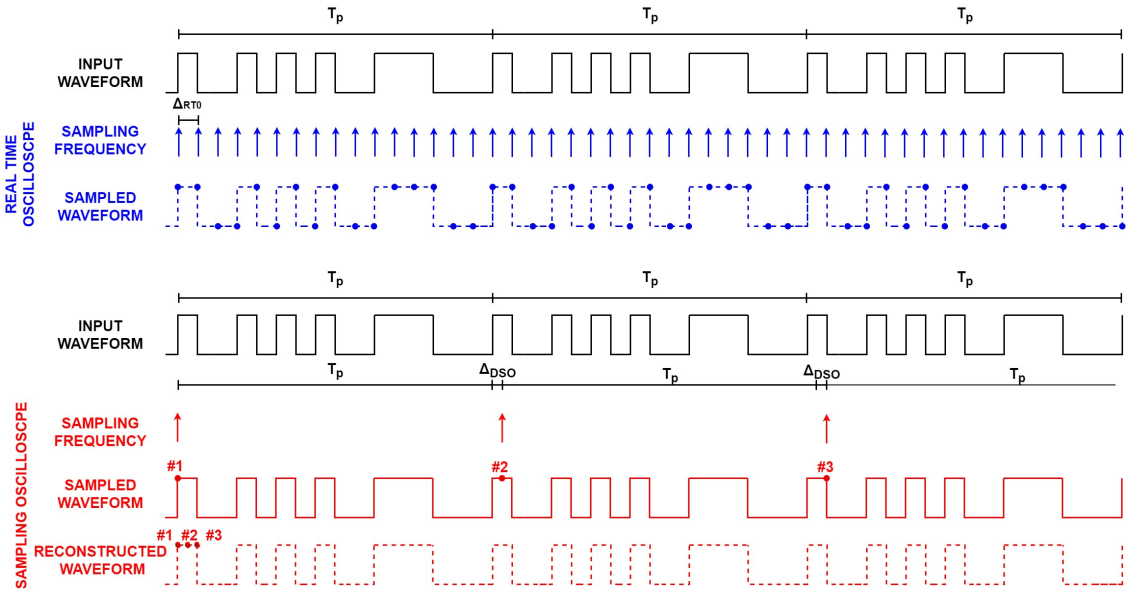

Figure 2.9: Sampling mode of real-time oscilloscopes (blue) and equivalent-time (red) oscilloscope on the same input waveform (black).

In the context of transmitter compliance, it would be of interest to compare the TDEC behavior on waveforms captured from the two types of oscilloscope and assess if both can be used for this purpose. For this task, a comparison of TDEC on waveforms captured with the two types of oscilloscope was performed, following the setup depicted in Fig. 2.5. The results are shown in Fig. 2.10, where the TDEC is shown compared to the number of points after upsampling (N_{up}). The value obtained from the sampling oscilloscope is represented by a blue line. It can be seen that the TDEC estimates obtained by upsampling the RTO output converge almost perfectly to the DSO value provided that at least N_{up}=16 samples/bit are used.

For the RTO, the 50 Gbps optical signal is converted to the electrical domain using a PIN PD with a 3-dB bandwidth of 36 GHz and is acquired at a sampling rate of 200 GSa/s. It is clear that when using a limited number of samples, the two time windows of the histogram cannot be properly determined; for example, when 4 samples per bit are used, it is possible to evaluate the histograms at 0, 0.375, 0.75 and 1 UI. The waveforms are therefore digitally upsampled using a polyphase anti-aliasing filter. Starting from the 4 samples/bit captured, different upsampling rates were evaluated and the subsequent TDEC result was compared against the one obtained from the sampling oscilloscope. This is reasonable since when using N_{up}=16, the samples end up being spaced 1.25 ps, which, for a bitrate of 50 Gbps, corresponds to 0.0625 UI, close enough to the 0.04 UI histogram width specified in

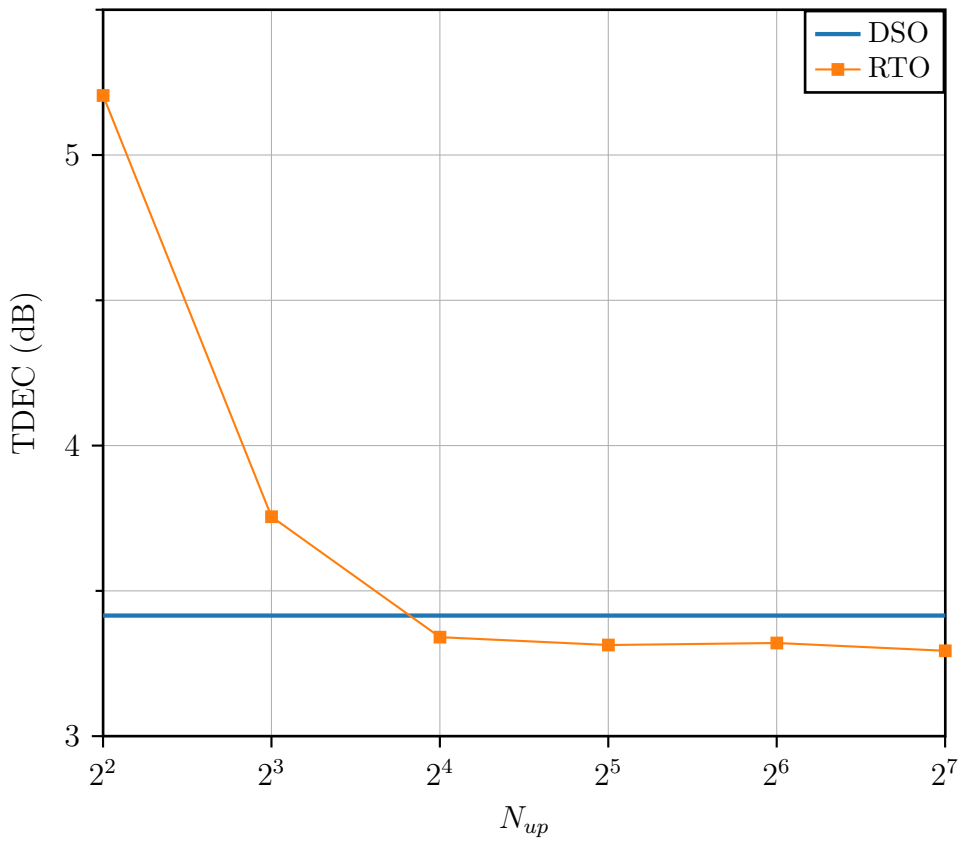

Figure 2.10: TDEC vs. N_{up} (samples per symbol after upsampling in for the RTO). The DSO reference TDEC value is reported as a green line as a comparison.

the ITU-T standard [26]. Furthermore, the left and right histograms are located at 0.4375 and 0.5625 UI, respectively, again very close to the sampling windows of the standard (0.425 and 0.575 UI). A higher value of N_{up} changes the resulting TDEC estimate only marginally, so it can be concluded that at least 16 samples per bit should be used.

As a final observation, for sufficiently high N_{up}, the TDEC estimate from the RTO is around 0.1 dB lower than the DSO. This mismatch can have the following causes: first, the difference in the specifications of the two oscilloscopes, in terms of analog bandwidth and effective number of bits; then, for the RTO case, a commercial PD is employed, which has a non-ideal frequency response, whereas for the DSO the Rx module is well calibrated; last, when performing the digital upsampling, noise is not taken into account, which may also explain the discrepancy.

Equalizer tap adaptation strategy

As already seen in previous Sections, the G.9804.3 50G-PON recommendation [26] uses a 13-tap T-spaced FFE in the reference receiver, whose tap coefficients are optimized to give the MMSE for eye opening. Since the implementation of the algorithm is left to manufacturers, another topic of interest would be evaluating how much the equalizer tap adaptation strategy affects the final TDEC measurement. In the literature, two algorithms are commonly used to compute FFE coefficients [24, 68]:

1. zero-forcing, where the taps are optimized to obtain zero inter-symbol interference (ISI) on the equalized eye diagram without considering the presence of noise on the input signal; in the following this will be named the noiseless (NL) equalization strategy.

2. MMSE that maximizes the signal-to-noise ratio at the equalizer outputs jointly considering ISI and noise on the input signal; in the following this will be referred to as noise-enhancement reduction (NER) equalization strategy.

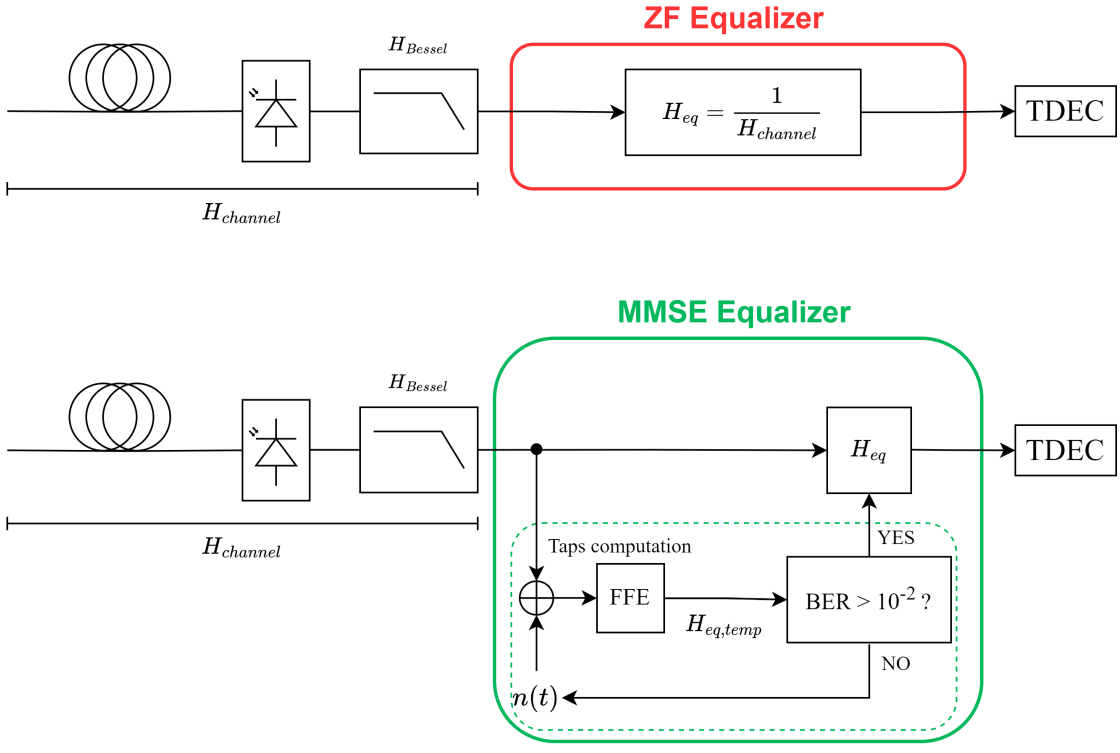

Figure 2.11: Block diagram of TDEC equalizer adaptation techniques: (a) Noise-Less (NL) equalizer and (b) Noise-Enhancement-Reduction (NER) equalizer.

When using NL, the FFE taps optimization algorithm minimizes the ISI at the equalizer output in a noiseless condition. Fig. 2.11(a) illustrates the working principle of this equalizer. For the experiments in this Section, an adaptive stochastic gradient descent [68] with a step size of 10^{-3} is used to adapt the equalizer taps, after normalizing the input samples to be in the range [-1,+1]. To find the best sampling instant, the tap optimization strategy is repeated N times, where N is the number of samples per bit, and the sample that gives the minimum TDEC value is selected. In Fig. 2.12, the TDEC for each sampling instant is shown when $N = 32$ is used. A typical bathtub curve can be observed, and, as expected, the optimal sampling instant is close to the middle. Similar observations are reported in [75].

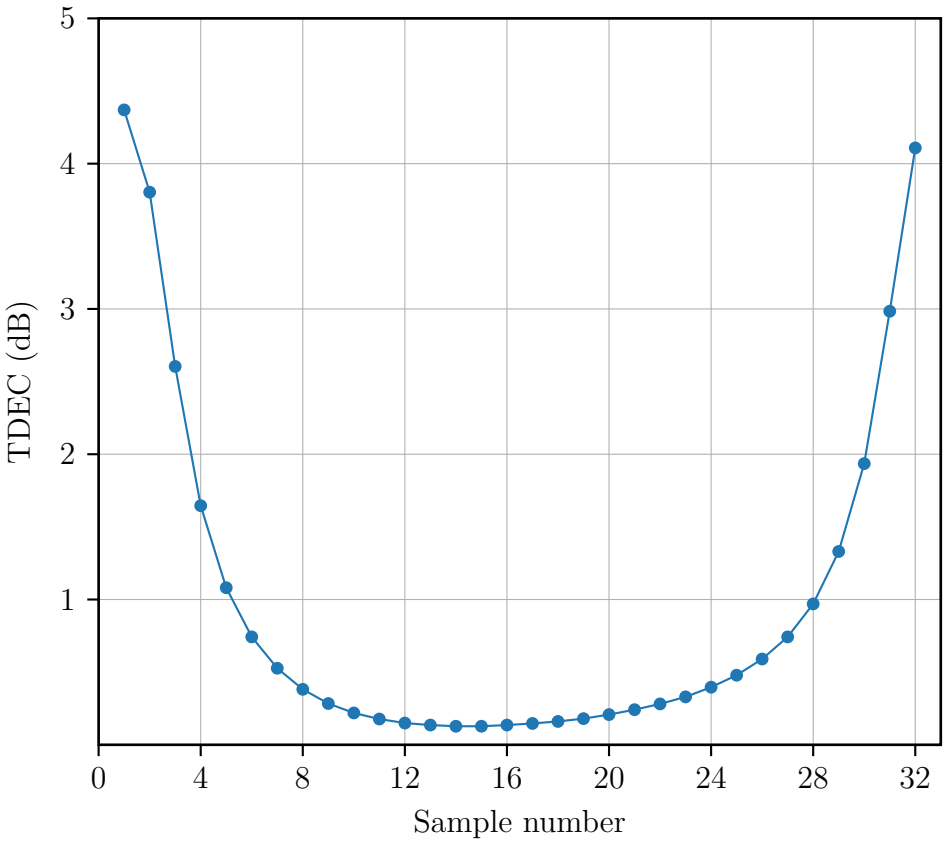

Figure 2.12: TDEC vs. sampling instant position for the NL tap optimization strategy

For the NER strategy time-domain Gaussian noise samples are added to the signal, and the taps are optimized according to the MMSE criterion. The process is iterated, increasing the variance of the input noise until the target BER of 10^{-2} is reached; also in this case, the procedure is done on each of the sampling instants. The one where the highest noise variance can be added is selected and TDEC is calculated. The block diagram is shown in Fig. 2.11(b).

The two equalization strategies, NL and NER, are tested by transmitting an SSPR sequence [60] at 50 Gbps. For capturing the samples, a 200 GSa/s RTO was employed, and the captured 4 samples/bit waveform is then oversampled to 32 via digital interpolation. The samples are then filtered with a 4^{th} order low-pass Bessel filter with 3-dB BW of 18.75 GHz ([26]) and equalized following the NL and NER approaches. The resulting TDEC and C_{eq} values are reported in Table 2.2 for the two cases. Both equalizers give quite similar TDEC values, with NER giving a value 0.17 dB lower than NL. However, a significant variation is visible in C_{eq}, as expected from theory. The NL equalizer tries to minimize ISI at the FFE output, regardless of noise. For a typical BW-limited channel, it tends to enhance the high frequency components not only of the signal but also of the noise, which is reflected in a higher C_{eq}. On the other hand, the NER jointly minimizes ISI and noise, limiting noise enhancement and, consequently, obtaining a lower C_{eq}.

Table 2.2: TDEC and C_{eq} using NL and NER equalizers

	TDEC (dB)	C_{eq} (dB)
NL	3.47	3.29
NER	3.30	2.49

In Fig. 2.13 the experimental non-equalized eye diagram and the equalized eye diagrams using the two methods are shown. A larger opening can be seen after the NL equalizer compared to the NER, at the expense of increased noise at high frequencies; this is noticeable from the higher standard deviation at the bit transitions (Fig. 2.13(b)).

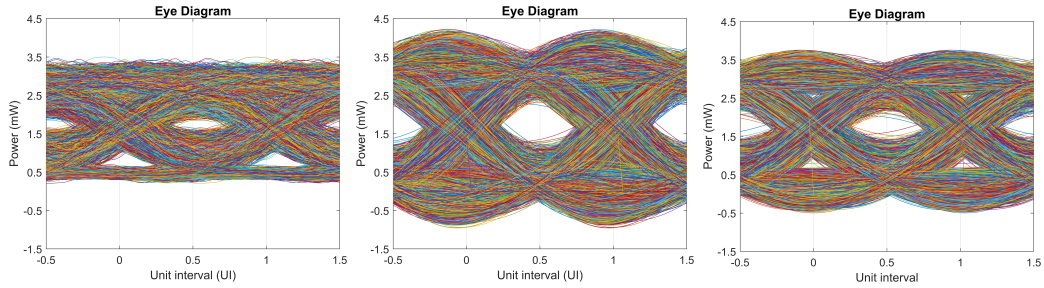

(a) (b) (c)

Figure 2.13: Eye-diagrams from experimental data. (a) Back-to back received waveform (b) Waveform after NL equalizer (c) Waveform after NER equalizer

To further evaluate the NL and NER strategies, a set of simulations is carried out. The bandwidth limitations of an optical transmitter are modeled by using a 2^{nd}-order Butterworth filter with variable 3-dB bandwidth. An SSPR sequence [60] oversampled at 4 samples/bit is used to emulate the RTO and TDEC and C_{eq} are calculated as previously described.

Fig. 2.14 shows TDEC and C_{eq} for the two equalization strategies (NL in red, NER in green) when changing the Tx 3-dB BW. The plots indicate that when there is enough BW ($\approx$ 30 GHz), both NL and NER produce the same TDEC and C_{eq}.

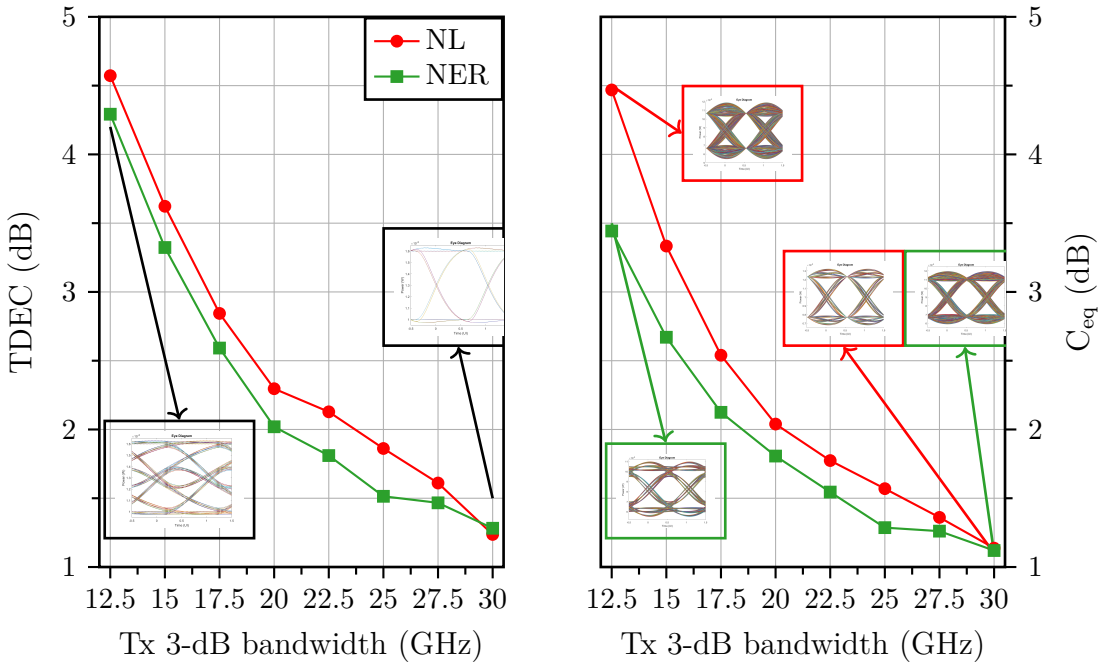

(a) (b)

Figure 2.14: TDEC (a) and C_{eq} (b) against 3-dB electrical BW for NL and NER equalizer. Insets of (a) report the eye-diagrams before equalization at the highest and lowest BW under test. Insets of (b) show the eye diagrams after NL and NER equalization

As the BW reduces, the NER equalizer produces a slightly lower TDEC, as it also takes noise into account. This is more evident when one looks at the C_{eq} curve in Fig. 2.14(b), where the NL strategy significantly enhances the noise. The different effects of the two equalizers can be clearly seen when looking at the insets of Fig. 2.14(b) linked to the lowest BW. The final message here is that both NL and NER produce similar TDEC results, but care should be taken to properly consider C_{eq}.

2.6.2 Experimental validation of TDEC for 50G-PON

In this Section, it was verified if TDEC is able to predict OMA sensitivity penalties typical of a PON scenario. A high-level block scheme of the experimental setup is shown in Fig. 2.15. Since TDEC is a metric for characterizing transmitters, a selection of them will be tested, and they will be specified case by case.

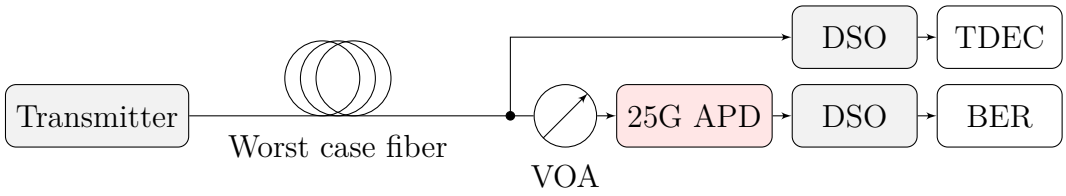

Figure 2.15: Setup for TDEC against Rx sensitivity measurements

As for the receiver, it is the same for all cases: first, the sensitivity of the system at a target BER of 10^{-2} is evaluated by varying the received optical power (ROP) through a variable optical attenuator (VOA). The optical to electrical conversion is done by a 25G-class APD followed by a transmipedance amplifier (TIA). The electrical signal is then captured by a digital sampling oscilloscope (DSO), and the BER is calculated offline by direct error counting. Then TDEC is evaluated by directly capturing the optical signal with the DSO, which includes a built-in reference receiver, and evaluating TDEC on it.

Extinction Ratio

In a first round of experiments, we focus on the dependence on the ER. It is well known that a finite extinction ratio causes a penalty on receiver sensitivity [1]. The BER, in fact, is influenced not only by the average received optical power (ROP), but also by the separation of the 1 and 0 levels (see Appendix 5). In order to account for this, the performance of receivers in PON are expressed in terms of optical modulation amplitude (OMA), which is defined as $P_1 - P_0$. This metric may look equivalent to the ER, but in case of a system with linear attenuation, the extinction ratio will stay constant, while the OMA is decreased by a factor equal to the attenuation. By knowing the transmitted ER and the average ROP (P_{avg}), the OMA can be calculated as:

$$\text{OMA} = 2P_{avg}\frac{\text{ER}-1}{\text{ER}+1} \tag{2.20}$$

This equation highlights that when two signals are received with the same average power, the one with the lower ER will have a lower OMA, leading to an increased BER.

To evaluate whether TDEC can predict this penalty, the setup of Fig. 2.16 was implemented, in which a 25G-class EML emitting at 1299 nm was employed as transmitter.

The Tx ER is then changed from 5 to 9 dB in 1 dB steps, values that are reasonable for an EML-based Tx in the OLT. Since the target here is only to assess penalties from ER variation, TDEC and Rx are only measured in a back-to-back configuration in these experiments. The impact of the asymmetric noise parameter

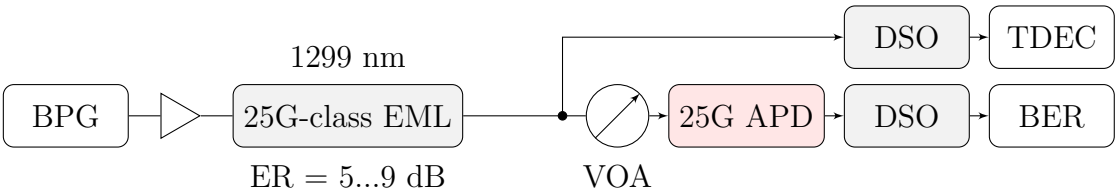

Figure 2.16: Setup for TDEC against ER variation

m was examined to verify the considerations for the APD receivers explained in the previous section.

The results of this test are depicted in Fig. 2.17, where the TDEC against the sensitivity of Rx (in OMA) is plotted. As expected, increasing the ER improves the quality of the eye diagram, leading to a better (smaller) TDEC value.

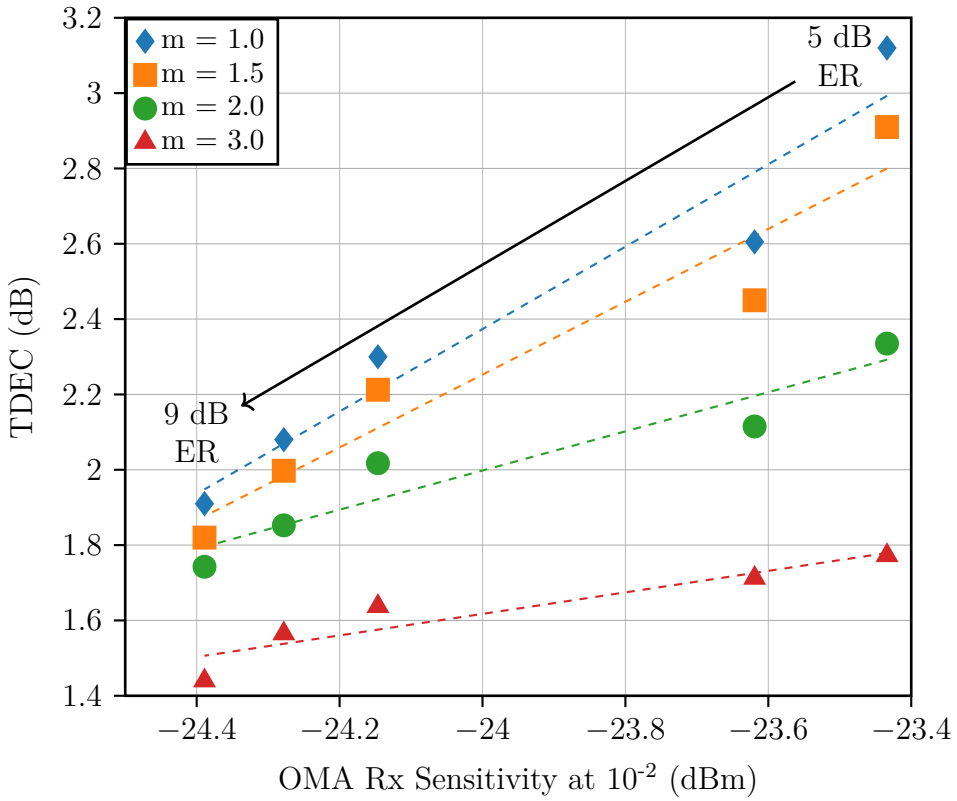

Figure 2.17: TDEC against OMA Rx sensitivity when varying m and Tx Extinction Ratio

If the linear regression between the two variables (Table 2.3) is calculated, it is possible to see that, using a m value of 1.5 as defined in the 50G-PON standard, a coefficient of determination (R^2) of 0.924 and a slope of 0.97 are obtained, indicating an almost 1:1 correlation between the two variables.

Table 2.3: Linear regression equation and correlation coefficients for results in Fig. 2.17

m	Regression equation	R^2
1.0	$y = 1.095\,x + 28.65$	0.935
1.5	$y = 0.97\,x + 25.48$	0.924
2.0	$y = 0.52\,x + 14.48$	0.9045
3.0	$y = 0.29\,x + 8.48$	0.8637

Chromatic Dispersion

Another well-known source of power penalty is fiber chromatic dispersion. To verify the validity of the TDEC in assessing the chromatic dispersion penalty, another set of experimental tests was performed. Using the configuration of Fig. 2.18, this time the Tx ER is fixed at 7 dB and the relationship between TDEC and Rx sensitivity is measured when the accumulated CD of the link changes. A Standard Single Mode Fiber is used, going from BtB to 25 km by adding 5 km spans.

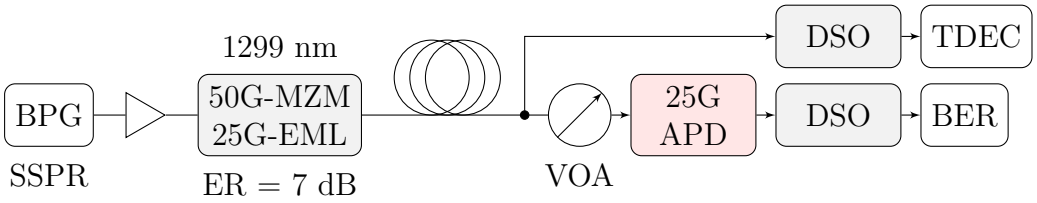

Figure 2.18: Setup for TDEC against chromatic dispersion measurement

The path penalty obtained with TDEC and Rx sensitivity after 25 km with respect to BtB is almost identical (≈1.4 dB), as it is possible to see in Fig. 2.19. Furthermore, when combining the two metrics, a linear regression yields a slope of 0.97 and $R^2 = 0.923$, indicating a very good correlation between the two variables. For comparison, a full-bandwidth Mach-Zehnder Modulator (MZM) was also tested. The light source in this case was an External Cavity Laser (ECL) emitting at 1360 nm. Fig. 2.19 includes the MZM results of TDEC against OMA at BER=10^{-2} from BtB to 25 km.

Since TDEC is a metric that indicates the quality of Tx, we expect it to indicate a difference between using EML and MZM. In BtB, the measured TEC is 2.2 dB and 2.4 dB for MZM and EML, respectively, with the corresponding OMA Rx sensitivity of -24.1 dBm and -23.9 dBm. Interestingly, TDEC perfectly follows the Rx sensitivity penalty, demonstrating that it is a useful metric for Tx qualification. From Fig. 2.19 it is also possible to see that TDEC and Rx sensitivity when used with EML improve after fiber transmission. This behavior is explained by the EML wavelength (1299 nm) being in the negative CD regime, which opens

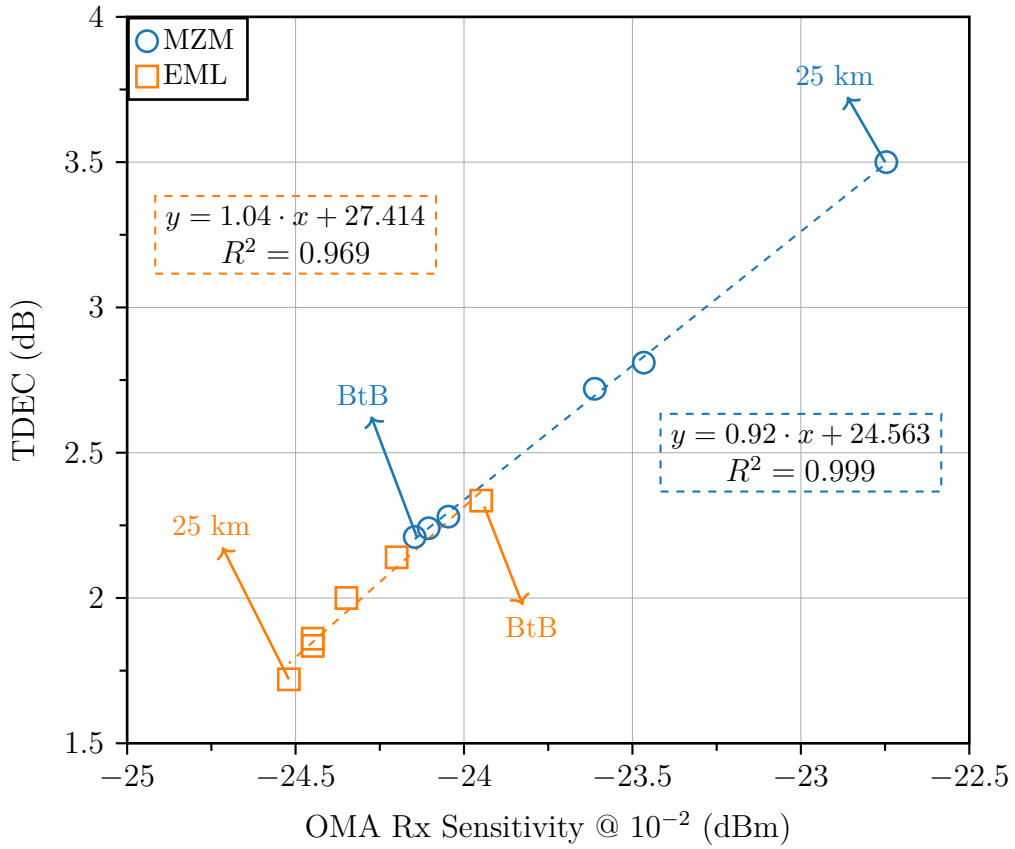

Figure 2.19: TDEC against OMA Rx sensitivity when varying fiber length (steps of 5 km). Inset boxes show regression line and R2 coefficient for MZM (blue) and EML (orange)

the eye diagram after fiber transmission. Furthermore, after 20 km the measured TDEC and OMA Rx sensitivity are 1.8 dB and -24.5 dBm respectively, which are 0.5 dB and 0.4 dB better than in BtB, indicating that the variation in TDEC and Rx sensitivity go hand in hand. Additionally, when performing a linear regression, the slope is 0.92 for the MZM and 1.04 for the EML, again indicating a good correlation between the variables. Therefore, TDEC clearly follows the Rx sensitivity and is a good indicator of the penalty that the system can experience after fiber transmission.

Validating TDEC for 50G-PON upstream

After the initial recommendation of September 2021, where 50 Gbps downstream and 12.5/25 Gbps upstream links were defined, the interest of ITU-T focused on the upstream at 50 Gb/s. Here, some of the wavelengths under study (1260-1280 nm and 1290-1310 nm) can fall into the negative chromatic dispersion

(CD) regime. Furthermore, although potential 50G US Tx devices are becoming commercially available, 25G components can be used to keep costs low. For these kinds of system, negative dispersion, mixed with the positive chirp factor of EMLs and DMLs, could lead to an improved eye diagram after fiber transmission and, consequently, to better Rx sensitivity; it had to be verified whether TDEC was able to predict this behavior. The setup for these tests is depicted in Fig. 2.20. Specifically, two devices were tested, which should be representative of those that will be used in a real ONU: a 25G class directly modulated laser (DML) and an electroabsorption modulated laser (EML).

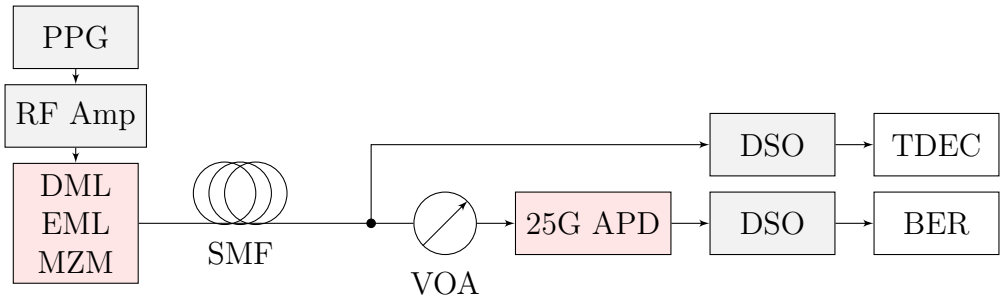

Figure 2.20: Setup for TDEC measurements for 50G upstream

A pulse pattern generator (PPG) produces either a PRBS-15 for the measurement of the BER or an SSPR for TDEC. The electrical signal is adjusted to modulate the DML, then the ElectroAbsorption Modulator (EAM) section of the EML, or MZM to produce an optical NRZ signal, which is subsequently sent through different lengths of Single-Mode Fiber (SMF). The emission wavelengths for the DML and EML are 1293 nm and 1300 nm, respectively, while the light source for the MZM is an ECL emitting at 1310 nm. Both DML and EML are packaged in optical subassemblies, and the measured Extinction Ratio (ER) is 4 dB for the DML and 6 dB for the EML. The low ER of DML is mainly due to non-optimal electrical connections. Table 2.4 summarizes the values of the key parameters for both Tx studied. The output power (P_{out}) from the DML is reported considering the expected insertion loss of the optical multiplexer (3.5 dB) included in the Transmitter Optical Sub-Assembly (TOSA). On the Rx side, the optical signal is captured by a Digital Sampling Oscilloscope (DSO) with an embedded 4th order Bessel-Thompson filter with 18.75 GHz BW. TDEC is then measured after applying a 13-tap T-spaced FFE.

When computing the BER, a Variable Optical Attenuator (VOA) limits the input power into an InP 25G APD, whose electrical output is then captured by the DSO and processed with a 13-tap T-spaced FFE followed by a 1-tap DFE. The equalizer coefficients were optimized following a Zero-Forcing (ZF) algorithm. It should be noted that the FFE used in these experiments used 13 taps with six precursors, following the DS recommendation, since at the time of the experiments

Table 2.4: Transmitter parameters for TDEC against chromatic dispersion measurements

Parameter	Device		Unit
	EML	DML	
DFB I_{bias}	60	85	mA
EAM V_{bias}		1.9	V
Wavelength	1293	1299	nm
Extinction Ratio	4	6	dB
Output Power	+6.2	+4	dBm
3-dB Bandwidth	22	17	GHz

the ITU-T had not reached consensus on the US specification. Subsequently, due to the equalizer convergence timing constraint in the upstream direction, the 50G-PON standardization group agreed for an FFE with 7 taps and 2 precursors; the authors in [86], however, showed that there is a negligible TDEC penalty when reducing the tap number from 13 to 7. Same as in the last step, the average BER is calculated by direct error counting after capturing 40 PRBS-15 sequences.

Fig. 2.22a reports the results with solid lines for Back-to-Back (BtB) and dotted after SMF. The OMA at a pre-FEC target BER of 10^{-2} for the DML is -21.1 dBm. The reduced Tx and Rx BW, together with some electrical reflections that still appear in the signal, limited the Rx sensitivity. Furthermore, the eye diagram in BtB after equalization is skewed, as seen in Fig. 2.21a.

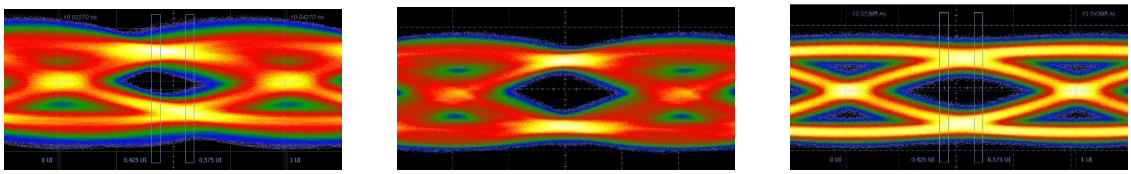

(a) (b) (c)

Figure 2.21: Measured eye-diagrams for (a) 25G-class DML, (b) 25G-class EML and (c) 50G-class MZM

In comparison, EML has a more symmetric eye in BtB as seen in Fig. 2.21b and, reflecting the improvement in eye quality, the measured OMA at 10^{-2} is reduced to -24.4 dBm. A full BW MZM, with an ER of 6 dB, is reported as a reference. For this device, the Rx sensitivity achieved is -25.2 dBm, and the corresponding eye diagram in BtB shown in Fig. 2.21c is clearly more open than the other Tx devices.

TDEC is then measured after capturing at least 20 consecutive waveforms with an SSPR sequence to obtain repeatable and stable values. In BtB, the obtained transmitter eye-closure (TEC) values are 5.2 dB, 2.3 dB and 1.6 dB for DML, EML,

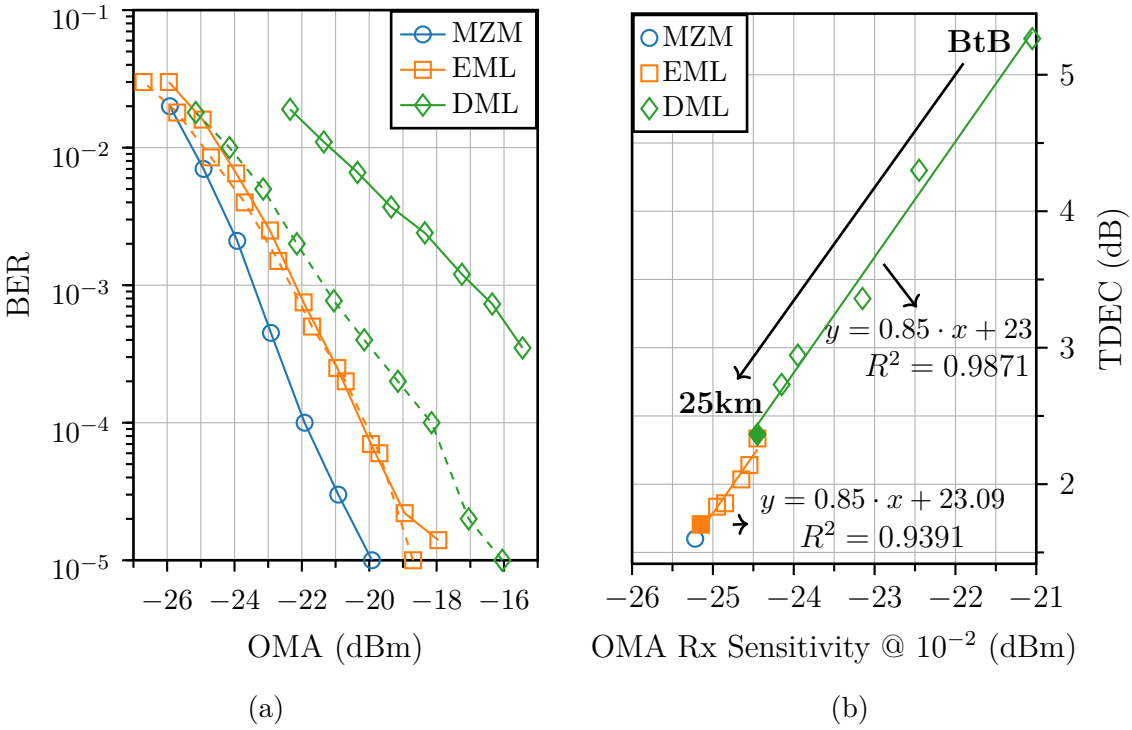

Figure 2.22: TDEC and sensitivity for Tx in the negative dispersion regime

and MZM, respectively. The high TEC for DML confirms its poor eye quality (Fig. 2.21a) and is reflected in low Rx sensitivity. More significantly, it is possible to see that the variation in TEC between Tx is accurately correlated with the sensitivity of Rx. The TEC for DML is almost 3 dB higher than for EML, and the difference in Rx sensitivity between them is nearly the same (3.3 dB). Between DML and MZM, TEC and Rx sensitivity change by 3.6 dB and 3.9 dB, respectively, and comparing EML and MZM, both variables differ by around 0.7 dB. Fig. 2.22b plots the TDEC against the ROP for DML and EML Tx. Each point corresponds to an additional 5 km SMF spool up to a total length of 25 km (Table 2.5 shows the total measured CD). In BtB, the signal quality produced by each Tx measured with the TEC is reflected in its Rx sensitivity, as previously described. The emission wavelength of the DML (1293 nm) is well below the zero-dispersion wavelength of the SMF. The interaction of the positive chirp of this device with the negative CD leads to pulse compression and results in a more open eye diagram as the signal travels through the SMF [20].

Therefore, both TDEC and Rx sensitivity improve after fiber transmission, as can be seen in Fig. 2.22b. When performing a linear regression of points at various lengths of the SMF, the coefficient of determination (R^2) is around 0.99, indicating that there is a very good correlation between both variables. Another thing to be noticed from the linear regression curve is that the slope is around 0.85, so one

Table 2.5: Measured chromatic dispersion

Distance [km]	Chromatic dispersion [ps/nm]	
	1290 nm	1310 nm
10	-24.2	-14
20	-44.7	-28
30	-57.6	-36

could derive that TDEC is not able to precisely predict the sensitivity penalties. However, this discrepancy is very likely due to improper optimization of the APD gain. Moreover, it can be noticed that both the DML and the EML results fall on the same line.

The EML also operates in the negative CD regime, the total accumulated CD (after 25 km is -36 ps/nm) and the chirp of this device are lower than those of the DML: therefore, there is only a slight improvement in the TDEC and Rx sensitivity after fiber transmission. If the linear regression of TDEC against Rx sensitivity is calculated after several lengths of the SMF, a R^2 value of 0.94 is obtained, indicating once again the correlation between the two parameters. It should be noted that the DML exhibits, in BtB, a TDEC of 5.2 dB, which is above the maximum allowed by the 50G-PON standard. This indicates that with this device the receiver will not work properly. Performance could be improved by adding a more complex equalizer on the Rx side, but this would still mean that the device is not compliant. Alternatively, to improve TDEC, the Tx quality should be improved. To test this latter option, an analog FIR filter with 6-taps spaced at 7.5 ps was added as a pre-emphasis in the Tx and its coefficients were optimized offline by compensating the BW. The curves of BER against OMA with and without the pre-emphasis FIR filter are shown in Fig. 2.23.

At BER=10^{-2}, the Rx sensitivity improves by 1.5 dB to -22.8 dBm, while the measured TDEC decreases accordingly to 3.8 dB (from 5.3 dB). The improved TDEC value is also confirmed by looking at the eye diagram before and after the introduction of the FIR filter (Fig. 2.21a). Again, TDEC can predict the DML performance. Furthermore, from the Rx sensitivity achieved with pre-equalized DML (P_{out}=+6.2 dBm), a power budget of 29 dB can be realized. After fiber transmission, the Rx sensitivity is further improved, and the link budget is ensured.

2.7 Final remarks

In summary, this Chapter serves as a comprehensive exploration of several transmitter compliance testing methodologies. After introducing the Transmitter Eye

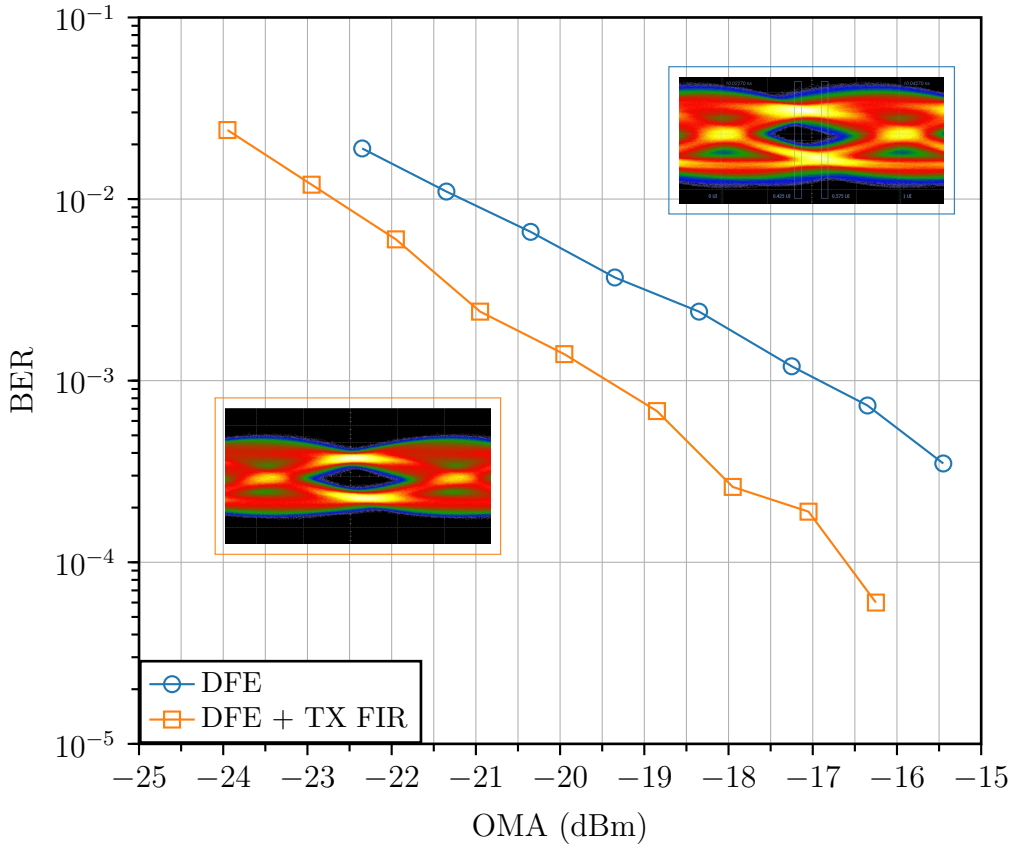

Figure 2.23: Sensitivity improvement of a bandwidth-limited DML when including an analog FIR filter for pre-emphasis

Mask and Transmitter Dispersion Penalty, the discussion shifts to the TDEC metric, initially developed for IEEE Ethernet and later adopted in 50G-PON.

The Chapter outlines the advantages of adopting the TDEC metric, offering a distinct improvement in terms of simplicity and cost reduction over previously employed testing methods. The rationale behind this change is carefully explained, underscoring the unique strengths and contributions of the TDEC approach. The rationale behind this metric shift is explained, highlighting the modifications needed to adapt it to 50G-PON.

A significant portion of the Chapter is dedicated to detailing the optimization of parameters within the TDEC algorithm, showcasing its robustness and reliability in evaluating transmitter performance in PON environments.

Through a series of exhaustive experimental tests, the Chapter convincingly demonstrates the TDEC metric capability to anticipate and predict various factors contributing to link budget penalties within PON networks. This predictive prowess positions the TDEC metric as a cornerstone for transmitter compliance testing,

offering invaluable insights to optimize PON network performance.

In essence, the novel contributions presented in this work underscore the TDEC importance and utility in PON deployments, solidifying its role as a fundamental tool for manufacturing cost reduction and network optimization.

Chapter 3

Addressing bandwidth limitations through enhanced detection

In this Chapter, we delve into the critical aspects of Passive Optical Networks (PONs), focusing on the challenges posed by bandwidth limitations and CD. Bandwidth constraints and chromatic dispersion are inherent in optical fiber communication systems, significantly impacting signal quality and network performance within PON architectures, particularly for 50G-PON.

One solution to mitigate the effects of bandwidth limitations and chromatic dispersion is the adoption of duobinary modulation. This technique offers a promising approach to enhance spectral efficiency while minimizing the impact of signal distortions. By encoding data in a more bandwidth-efficient manner, duobinary modulation enables PONs to achieve higher data rates and improved signal quality, even in the presence of bandwidth constraints and chromatic dispersion. However, the use of duobinary comes at the price of a reduced eye opening and receiver sensitivity.

For this reason, this Chapter introduces a novel technique that combines binary and duobinary detection to further enhance PON performance. Through detailed analysis and experimentation, the efficacy of this new technique in improving signal integrity is discussed and its validity in optimizing PON efficiency in real-world scenarios is evaluated.

The results shown in this Chapter are based on the following work:

1. Giuseppe Caruso, Ivan N. Cano, Ricardo Rosales, Derek Nesset, Giuseppe Talli, and Roberto Gaudino. "Enhanced Electrical Duobinary Decoder with Low-BW Based Receivers for Short Reach Indoor Optical Links". In: *2021 European Conference on Optical Communication (ECOC)*. 2021, pp. 1–4. DOI: 10.1109/ECOC52684.2021.9606150

3.1 Introduction

It was already discussed in the previous Chapters that efficiency and cost effectiveness are fundamental factors for the success of Passive Optical Networks (PONs). However, achieving high data rates is challenging and not very cost-effective, as state of the art components are needed. The use of lower bandwidth components is a common strategy to minimize expenses, particularly on Optical Network Units (ONUs). However, this approach can introduce signal degradation, leading to performance penalties. An effective solution to mitigate these issues is the integration of DSP equalization techniques at the ONU side. This way, the received signals can be effectively corrected, restoring their integrity and reducing the impact of bandwidth limitations. Furthermore, DSP-based equalization not only aids against bandwidth limitations but also helps in counteracting chromatic dispersion. This is confirmed by the results shown in [78], where the authors report the feasibility of an experimental 50G-PON link with penalties of around 1 dB after 20 km SMF, using an FFE+MLSE equalizer.

However, equalization also has several drawbacks worth considering. The increased complexity associated with implementing equalization implies additional hardware and computational resources. This often results in higher costs and increased power consumption, particularly in high-speed communication systems.

In this sense, alternative approaches have been proposed for to overcome chromatic dispersion and bandwidth limitation impairments and, as a result, to enhance signal quality.

3.1.1 Duobinary signaling

One of the techniques worth considering is duobinary modulation. Duobinary modulation offers a method of data encoding that can effectively mitigate the impact of bandwidth limitations while maintaining spectral efficiency. Shown for the first time by Lender in 1963 [52], the duobinary encoding introduces on purpose a given amount of ISI into the signal, thus reducing its bandwidth requirements. The input binary data stream is encoded into a three-level signal using a delay-and-add filter, that sums the current symbol to the previous one. A possible implementation of the encoder is shown in Fig. 3.1a. It can be shown that the new signal has no +1 to -1 transitions or viceversa; this means, that the fastest-rising edges of the signal are removed, reducing the bandwidth of the signal [85]. This narrower bandwidth results in a slower signal transition between levels, which inherently reduces susceptibility to dispersion-induced distortion and allows to significantly increase the transmission distance [47].

On the receiver side, as shown in Fig.3.1b, two thresholds (V_{high} and V_{low}) are used to detect the three levels of the received signal, followed by a XOR-gate which determines the binary data from the duobinary symbols.

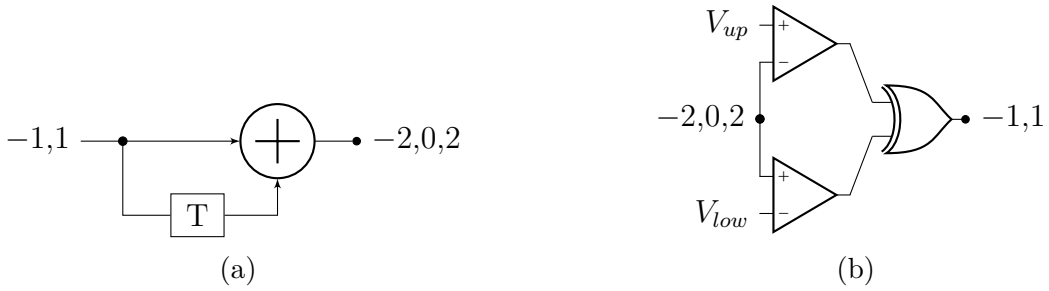

Figure 3.1: Encoder (a) and Decoder (b) for Electrical Duobinary signaling

Some examples of EDB for PON can be found in [88] and [40], where the authors show a TDM-PON based on EDB with distances of up to 40 km at 26 Gbps and 40 Gbps, respectively, or [83], where a comprehensive analysis of modulation formats (PAM-2, PAM-4 and EDB) and DSP techniques for PON is provided. There are two main disadvantages with this scheme: first, it requires a precoder at transmitter side to avoid error propagation [85], that could cause problems with interoperability; second, it has an inherent sensitivity penalty compared to OOK-NRZ, due to its reduced eye aperture. Furthermore, the 3-levels must be clearly identified. For this reason, in [83] the authors propose a receiver scheme that switches from binary (BD) detection to 3-level detection depending on the total BW of the system.

Another approach is the so-called optical duobinary scheme, the three-level signal is generated by overdriving a Mach-Zehnder modulator, and the latest results have shown the validity of this scheme to combat dispersion effects up to 100 Gbps [39]. However, the high driving voltage required to fully overdrive the MZM and the higher cost of these devices compared to EMLs still have made them not ideal for application in PON scenarios.

What makes EDB interesting for PON is that when an NRZ-OOK signal is transmitted, the presence of chromatic dispersion and/or a limited bandwidth receiver act as a low-pass filter, generating a signal where three levels are distinguishable, as we can see in Fig. 3.2a. The impact of adding an FFE at receiver is depicted in Fig. 3.2b, where it can be seen how the two levels are more distinguishable, compared to the case without FFE.

Trying to overcome these issues, during the course of this PhD a novel approach was developed, exploiting both binary and EDB detection. For this reason, it was named Enhanced Electrical Duobinary, or EEDB.

3.2 Enhanced Electrical Duobinary

The EEDB scheme takes into account the correlation that exists between neighboring bits in a BW-limited channel, through the scheme shown in Fig. 3.3a. For each received symbol, two decisions take place: first, a typical binary detection

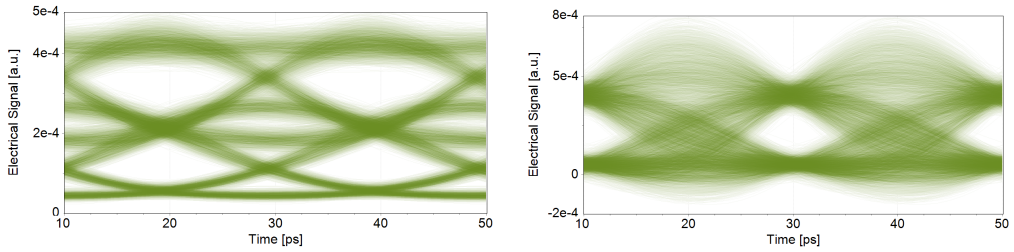

(a) (b)

Figure 3.2: Eye diagram at 50 Gbps before (a) and after FFE (b)

takes place with a conventional mid-level threshold (V_{th}) at the center of the bit. In the following, it will be referred to as BD. Half a bit later, two more thresholds (upper and lower) are used to detect the three levels, as for conventional EDB.

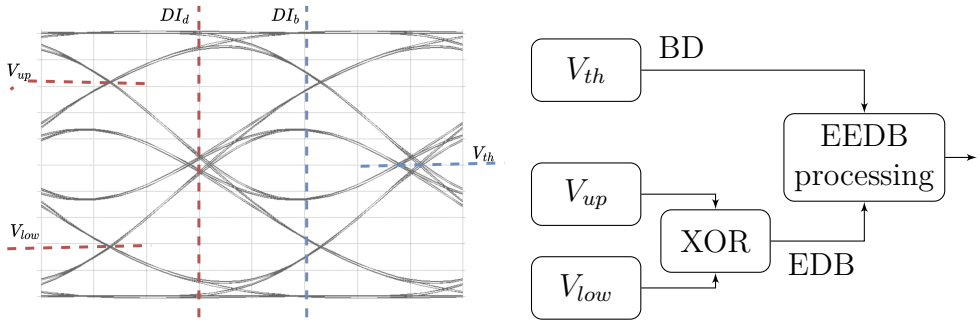

(a) (b)

Figure 3.3: Decision thresholds and instants on the eye diagram (a) and logical scheme of EEDB detection (b).

Fig. 3.3b illustrates the logical scheme of the EEDB, while 3.3a depicts the decision instants (DI) and the thresholds for BD (DI_b, V_{th}) and EDB (DI_d, V_{up}, V_{low}). Afterwards, the decoder in the EEDB is based on the relation between the detected NRZ and EDB symbols, namely:

$$\hat{z}[n] = y[n] \oplus y[n-1] \tag{3.1}$$

where $y[n]$ is the current NRZ decided bit and $\hat{z}[n]$ is the EDB symbol computed from NRZ $y[n]$. We then compare the detected EDB symbol $z[n]$ with a calculated $\hat{z}[n]$ from the current and previous BD bits (3.1).

In a BW limited system, the duobinary eye is more open than the binary eye (Fig. 3.2a). Therefore, it can be assumed that errors will be more likely to appear in $y[n]$, so the information in $z[n]$ is more reliable than the one in $\hat{z}[n]$. Furthermore, since $y[n]$ is used in two consecutive computations of $\hat{z}[n]$, an error in the detected

$y[n]$ will generate two errors in $z[n]$. Therefore, when the result of the comparison gives two consecutive errors (i.e. $z[n] \neq \hat{z}[n]$ and $z[n-1] \neq \hat{z}[n-1]$), we consider it more likely that it was caused by a wrongly detected $y[n]$, and we reverse it (at the decision instant n, it is $y[n-1]$). In case there is an isolated error, it can be assumed that $z[n]$ was not correctly detected and keep $y[n]$.

Since the processing is performed only with bits, the scheme could in principle be implemented using only logic gates, like in the example illustrated in Fig. 3.4

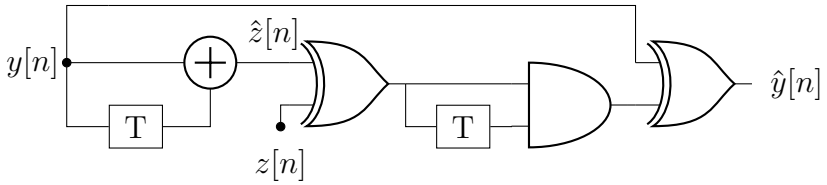

Figure 3.4: Implementation of EEDB using logical gates

One important feature of the EEDB is the lack of a precoder in Tx and, as long as the DI are properly selected, it can also work when the system is only partially limited in BW. As will be shown in the following Sections, additional DSP can be included, like adding an FFE for the BD and EDB branches to open their respective eye diagrams. It will also be shown that with the aid of simple equalization, EEDB can work using a single decision instant placed between DI_b and DI_d.

The EEDB method is capable of rectifying isolated errors and consecutive identical errors within $y[n]$, given the presence of adequate inter-symbol interference (ISI). To ensure the functionality of the receiver even when its bandwidth is not severely limited, the algorithm can be expanded to consider the case where errors are more likely to occur within the EDB detection scope. For this, a new check is added, considering the two-bit delay relation between EDB and BD:

$$z[n] - z[n-1] = y[n] - y[n-2] \tag{3.2}$$

The comparison takes place every four EDB symbols and, when 4 consecutive errors appeared, the symbols $y[n-3]$ and $y[n-2]$ are inverted at time instant n. The EEDB scheme first performs the 1-bit error correction and then the 2-error in a sequential way.

3.2.1 Simulations

Following a comprehensive discussion of the theoretical foundations supporting the proposed scheme, the next step in its validation involved several tests through simulations. These simulations served as a crucial initial step in assessing the scheme's performance under various conditions and scenarios, providing valuable insights into its potential effectiveness and limitations.

A simulation setup for the evaluation of the EEDB scheme was developed and verified using the VPI TransmissionMaker™simulation software. In order to emulate a typical PON network, the setup of Fig.3.5 was implemented. On the transmitter side, the bitstream consists of a 50 Gbps pseudorandom binary sequence (PRBS) of $2^{15} - 1$ bits. An electrical signal is therefore generated and filtered through a 4th order Bessel Filter with 3-dB bandwidth of 37.5 GHz. The optical signal is provided by a DFB laser source emitting at 1342 nm with linewidth of 1 MHz and it is modulated through an external modulator with a chirp value of 0.2 and 6 dB ER.

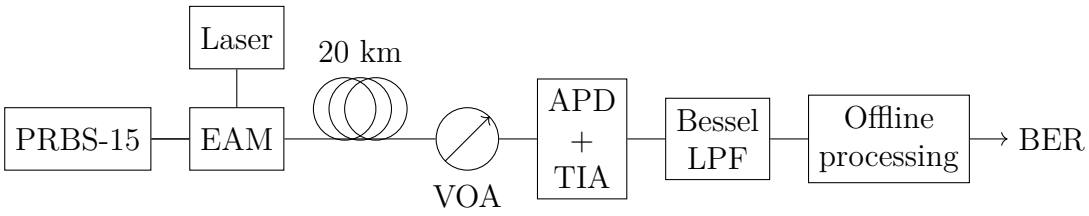

Figure 3.5: Simulation setup for EEDB assessment

After going through 20 km of SMF (77 ps/nm, as in [26]) and a VOA that emulates ODN losses, the optical signal is detected by an APD with a responsivity of 1 A/W, gain of 8, and k_A of 0.4. The photodiode is followed by a transimpedance amplifier (TIA) with an input-referred noise density of 10 pA/$\sqrt{\text{Hz}}$ and resistance of 1 kΩ. A fourth-order Bessel filter with variable 3-dB cutoff frequency is used to emulate limitations in receiver bandwidth. The filtered electrical signal is post-processed using self-developed Python code, implementing the scheme described in the previous Section, and lastly the BER is computed with binary, duobinary, and EEDB detection. A summary of all the simulation parameters is shown in Table 3.1.

Receiver Bandwidth

As a first test, the sensitivity was measured in the case of a receiver with limited bandwidth, which is the initial use case of EEDB. When using a Rx BW of 15 GHz, at a pre-FEC BER of 1e-2 (as defined in 50G-PON [26]), the Rx sensitivity in back-to-back (BtB) is found to be -23.5 dBm, -25.7 dBm, and -27.4 dBm for BD, EDB, and EEDB, respectively. Interestingly, the EDB sensitivity in this case is higher than BD since, given the BW limitation, the EDB eye is more open. This is very helpful for EEDB, which, in fact, is able to outperform BD by almost 4 dB.

Subsequently, the 3-dB bandwidth of the Rx electrical filter was swept from 80% to 20% of the bitrate, to emulate different receivers, and then the corresponding receiver sensitivities for the three detection schemes were measured. Fig. 3.6 shows the penalty in sensitivity (measured at a target BER of 1e-2) compared to the best

Table 3.1: Simulation parameters for EEDB

Parameter	Value	Unit
Transmitter side		
Sequence length	2*32767	Bits
Samples per bit	8	Samples
DFB wavelength	1342	nm
EAM extinction ratio	6	dB
EAM chirp	0.2	
Output Power	0	dBm
Receiver side		
APD responsivity	1	A/W
APD avalanche multiplication	8	
TIA input-referred noise density	10^{-12}	$A/\sqrt{Hz}$
TIA transimpedance	1000	Ω
APD dark current	300	nA
Filter type	4th order Bessel	

performance achieved using conventional binary detection. It can be seen that with higher Rx Bw, conventional BD performs better than EDB; the opposite is true when the receiver bandwidth is reduced.

As noted in [82], there is a point where the Rx sensitivity curves of BD and EDB cross (around $0.3{\cdot}R_b$, in our case), and one could switch between the two detection schemes depending on Rx BW. The objective of EEDB is to improve the Rx sensitivity of the EDB detection with low-BW receivers, thus avoiding the need to switch between detection schemes. This is achieved successfully, as can be seen in the left section of Fig. 3.6, where for $BW < 0.4 \cdot Rb$ EEDB is able to reduce the penalty up to a maximum of 2.6 dB in the worst case, obtained when $B = 10$ GHz.

Chromatic dispersion

In a second set of simulations, two different receiver configurations were investigated in a system operating at 50 Gbps: one with a full bandwidth receiver and another with a reduced bandwidth receiver operating at 0.3 times the bitrate (15 GHz). The purpose was to understand how chromatic dispersion affects the performance of EEDB, compared to classical BD and EDB detection.

The setup is the same as the one shown in Fig. 3.5, with the only differences being the change of Rx electrical bandwidth for the two cases and the introduction of variable chromatic dispersion, which was systematically varied from 0 to 100 ps/nm in steps of 40 ps/nm. The results are shown in Fig. 3.7a and 3.7b, where the y-axis represents the penalty compared to the BD sensitivity at 0 ps/nm CD

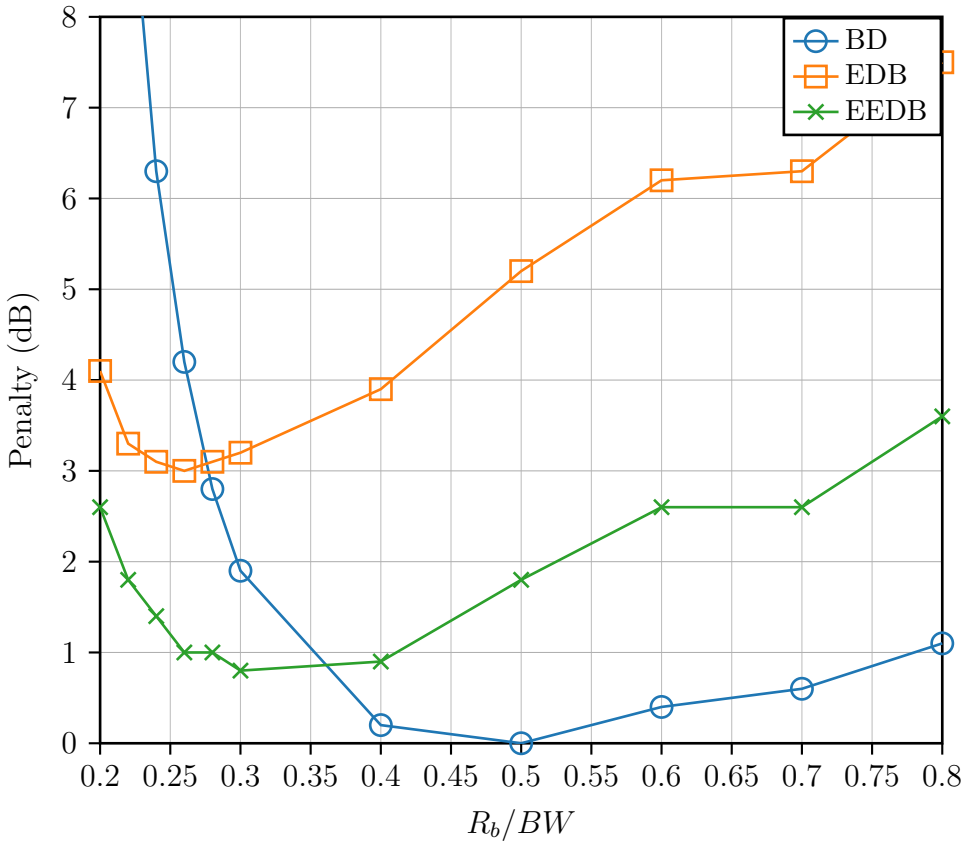

Figure 3.6: Sensitivity performance of EEDB when simulating changes in Rx bandwidth

(BtB case), assuming a full-BW receiver and one with $B = 15$ GHz, respectively.

In the first scenario, the EDB detection receiver exhibits significantly poorer performance compared to BD in BtB. Despite this consistent underperformance, its penalty remains relatively stable across different levels of CD. This confirms the well-known result of EDB having good performance against CD, due to its reduced bandwidth compared to NRZ-OOK. Conversely, BD initially maintains the best sensitivity levels but becomes unusable when going beyond 80 ps/nm, with a penalty greater than 4 dB. When looking at the EEDB scheme, its performance are in between BD and EDB. The initial penalty is around 2 dB, which increases only slightly with 100 ps/nm CD, reaching 2.7 dB.

In the second configuration, the EDB penalty reduces to around 1 dB, due to the reduced Rx bandwidth. While BD performs already worse than EDB with 40 ps/nm, this time EEDB outperforms both detection schemes, confirming the validity of this detection scheme with reduced bandwidth receivers.

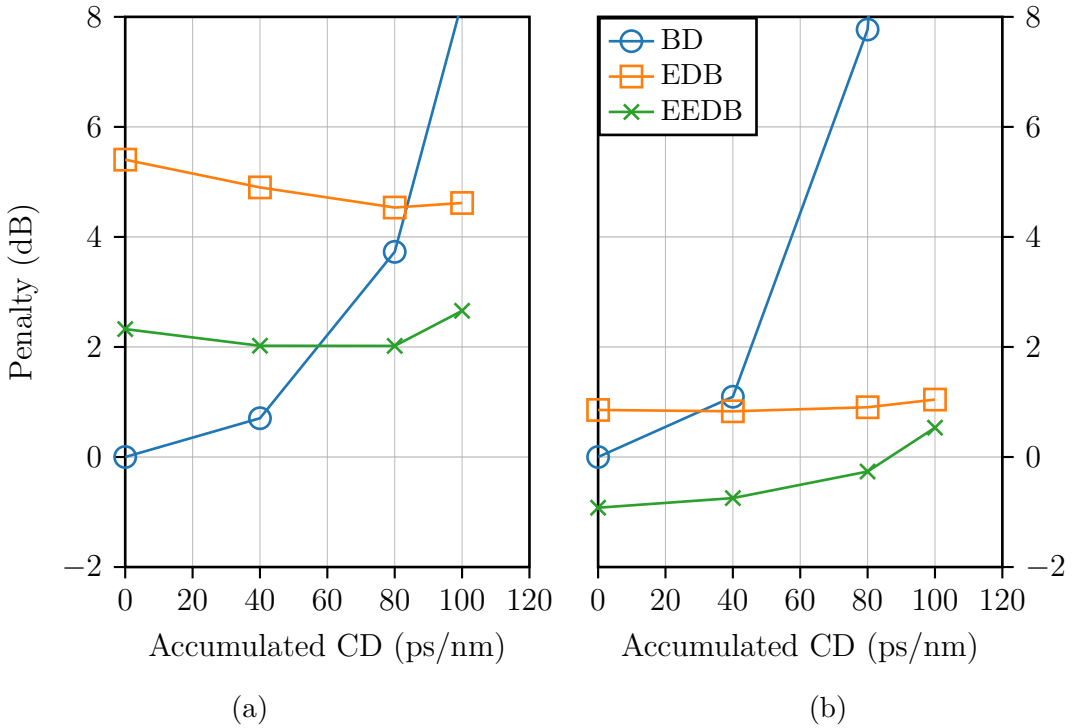

Figure 3.7: Effect of chromatic dispersion on EEDB for (a) full BW Rx and (b) Rx with BW = 0.3 R_b

EEDB in presence of reflections

After verifying the scheme for the cases just described, a last set of simulations is performed to evaluate the effect of potential reflections present in the system.

Reflections can be caused by various factors, including discontinuities in the optical medium (such as changes in fiber diameter or splices), bends and curves in the fiber causing partial reflections and contaminants on the connector surfaces. These are double reflections which travel in the same directions of the signal and can degrade signal quality, cause interference, and contribute to system instability. It is therefore important to either reduce reflections by properly deploying the optical network or, in the case where this is not possible, try to minimize the impact of this effect. The setup emulating the reflections is shown in Fig. 3.8.

The only variation, compared to the previous tests, is the addition of a second optical path by means of one splitter after the transmitter and a coupler before the receiver, to emulate partial reflection of the transmitted signal along the path. The sensitivity is measured at 1e-2 and the power of the reflected signal is varied. A fiber spool is added so that the two signal mixing in the photodiode are decorrelated. For these simulations, a signal-to-noise ratio is defined as SNR = $\frac{P_{signal}+P_{refl}}{P_{refl}}$ which represents the total signal ($P_{signal}+P_{refl}$) compared to the reflected signal ($Prefl$).

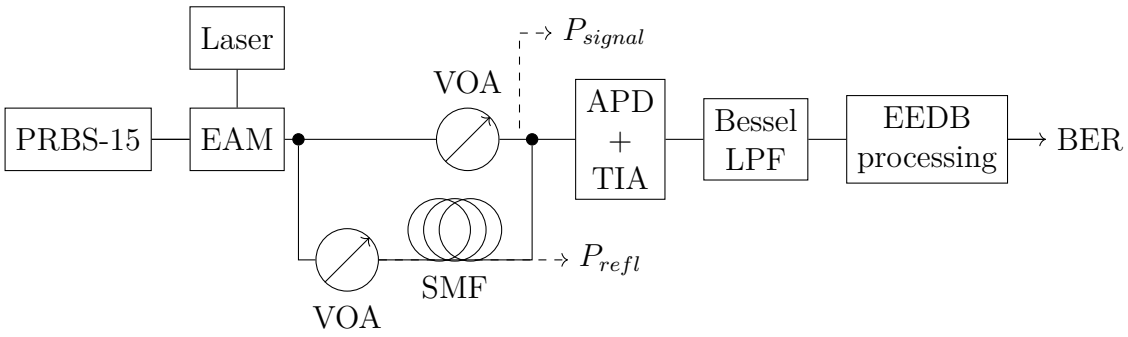

Figure 3.8: Simulation setup to evaluate reflection effects within the system.

The plot in Fig. 3.9a displays the absolute penalty compared to BD detection when the reflection is minimized (SNR = 20 dB), while Fig. 3.9b shows the relative penalty for each detection scheme.

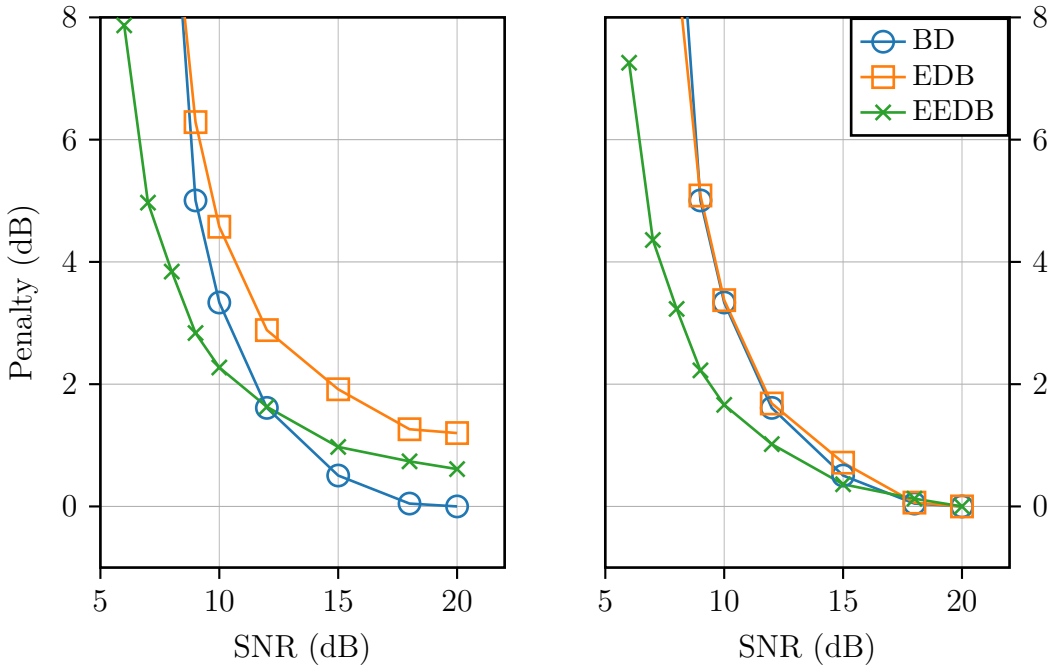

Figure 3.9: Sensitivity penalty when varying reflected signal power for BD, EDB and EEDB. (a) Absolute penalty compared to BD at $SNR = 20$ dB (b) Relative penalty compared to each scheme at $SNR = 20$ dB

It is interesting to see that, despite BD performing the best among the three

detection schemes up to a SNR of 12 dB, the EEDB scheme manages to keep a relative penalty below 2 dB up to around an SNR value of 9 dB, meaning a 10 times increase in reflected power compared to the initial SNR of 20 dB. The other two schemes have similar performance, reaching 2 dB relative penalty at around 12 dB, meaning half of the reflected power compared to the EEDB case. It must be emphasized, however, that several other factors have an impact on the system performance in case of reflections, as thoroughly described in [91]. With that said, this last set of simulations is just an initial step in this direction and its simplicity does not invalidate the obtained result.

3.2.2 Experimental results

The comprehensive set of simulations conducted indicates that the proposed scheme demonstrates significant potential in addressing challenges related to receiver bandwidth limitations, CD and reflections encountered within the optical channel. However, to fully validate and determine the practical applicability of these results, experimental verification is imperative. After completing simulations to model various scenarios, the research transitioned into the experimental phase, to verify the accuracy of the model and to analyze details that simulations might have missed.

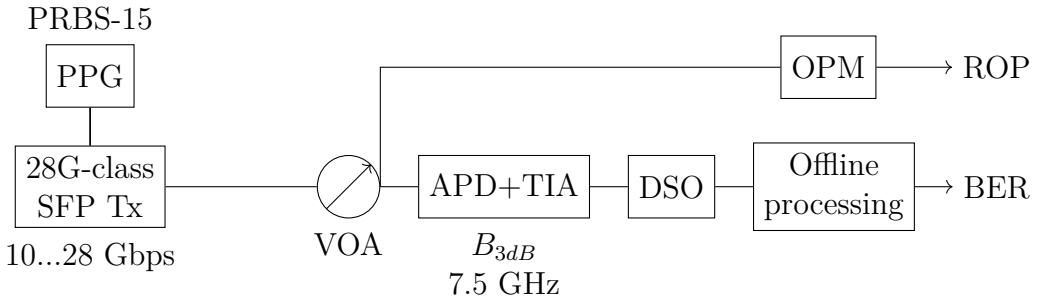

Figure 3.10: Experimental setup for EEDB

At the beginning of our experiments, due to a lack of component availability in the laboratory, the initial tests were performed using a commercial 25G-class transmitter and a 10G-class receiver, working up to 25 Gbps. As it will be shown, these initial limitations did not invalidate the proposed scheme, but rather provided valuable insights into its robustness and adaptability. The goal is to experimentally investigate the validity of the EEDB scheme when varying the receiver bandwidth, similar to what was done with the simulation described in 3.2.1. The setup, shown in Fig. 3.10, comprises a PPG generating a PRBS-15 electrical NRZ-OOK signal, which is fed to a 25-class commercial transceiver module. A 10G-class APD is

employed as the receiver, with a 3-dB bandwidth of around 7.5 GHz and an integrated TIA. Since for this experiment the goal is to evaluate the effects from the reduced system bandwidth only, any potential CD effect is avoided by connecting the transmitter and the receiver with a short spool of SMF, followed by a VOA to change the amount of power entering the photodiode. The received electrical signal is then captured using a sampling oscilloscope and the offline processing is the same described in the previous section.

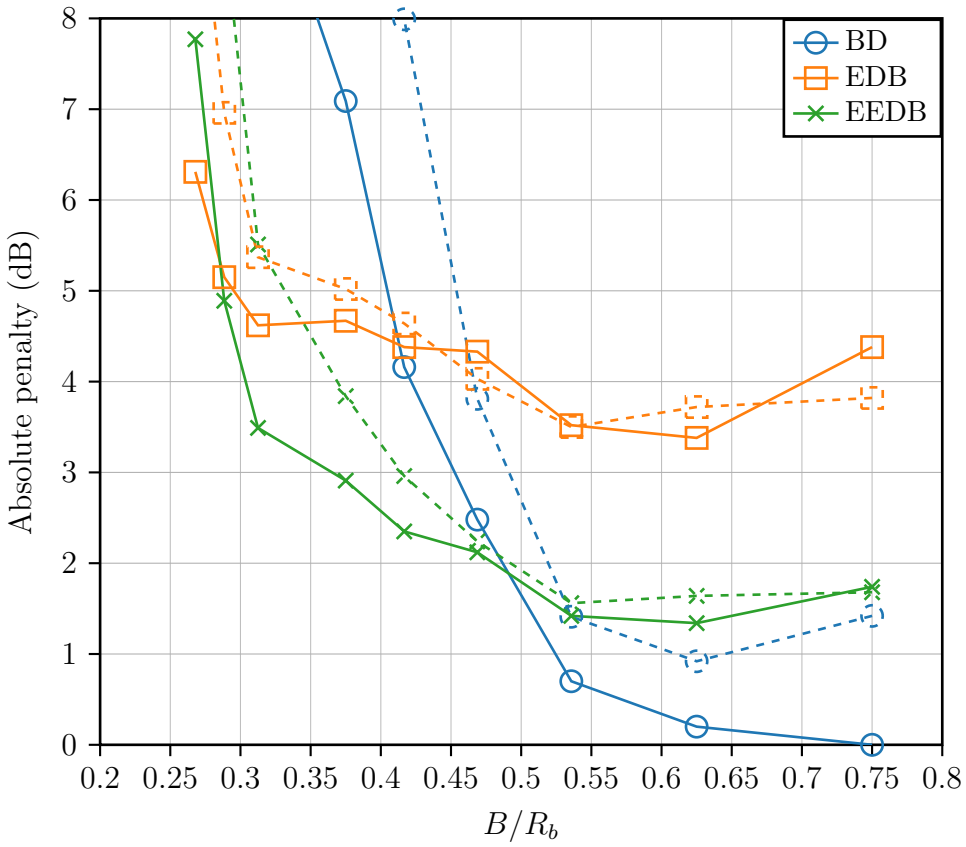

Figure 3.11: Measured sensitivity penalty when varying bitrate with a fixed Rx bandwidth. Dotted line shows results after 20 km

The bitrate is dynamically adjusted between 10 and 28 Gbps during the course of the experiment, resulting in a system bandwidth going from 75% to around 27% of the bitrate. This variation allows to assess the system's resilience to different levels of bandwidth limitation when using BD, EDB or EEDB, respectively. For each of the bitrates, the attenuation of the system is swept in order to find the sensitivity of the system at a target BER of 1e-2 [26]. The experimental outcomes are graphically depicted in Fig. 3.11, where the x-axis indicates the ratio between Rx bandwidth and bitrate and the y-axis shows the penalty compared to the binary

detection at 10 Gbps using a receiver with 7.5 GHz bandwidth.

Following the thorough evaluation of bandwidth limitations, the subsequent imperative was to assess the influence of CD on the performance of the proposed scheme. In this phase of experimentation, a setup was implemented to assess the effects of chromatic dispersion across varying lengths of single-mode fiber (SMF). The experimental setup is the one shown in Fig. 3.11, but this time the bitrate was fixed to 10 Gbps, so that bandwidth limitations did not affect the results, and the SMF length was gradually increased, ranging from 5 to 30 km in steps of 5 km. Fig. 3.12 depicts the results from this set of tests, showing the absolute penalty against fiber distance and also the optical path penalty (OPP), measured as the difference in sensitivity with respect to the BtB case.

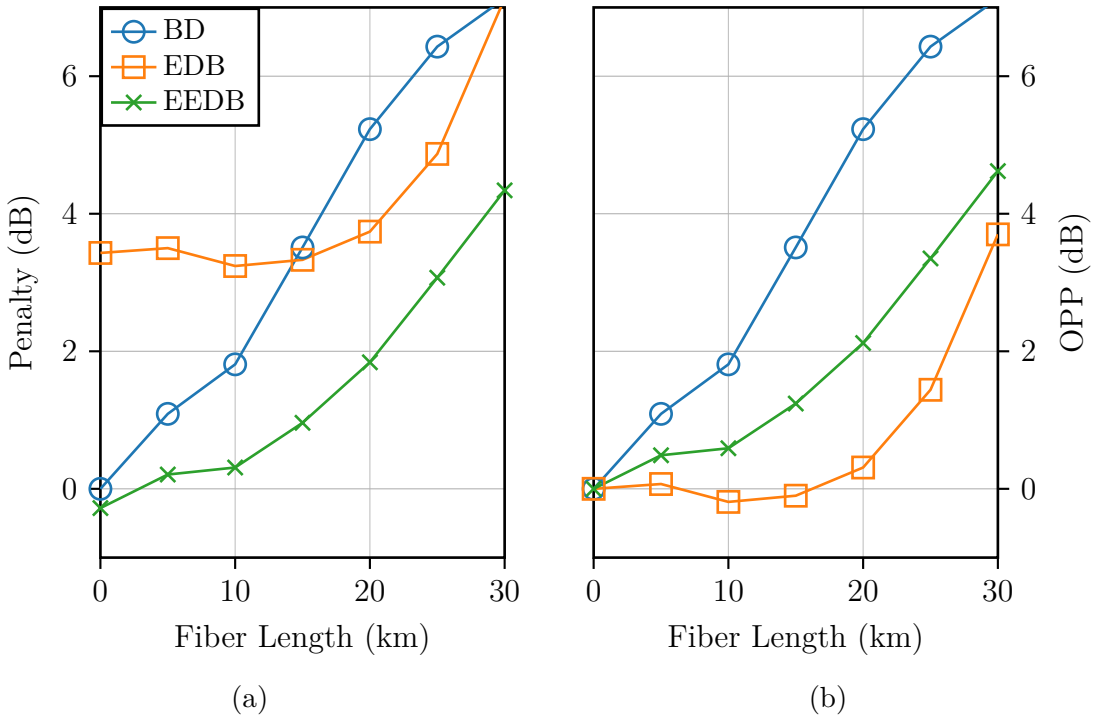

Figure 3.12: Penalty against fiber length for BD, EDB and EEDB: (a) Absolute penalty and (b) Optical path penalty

Remarkably, the influence of CD on BD is significant, as evidenced by a 2 dB penalty after 10 km of SMF, which increases to 5 dB penalty when going beyond 20 km. This experimental observation underscores the considerable impact of CD on signal integrity and underscores the pressing need for mitigation strategies in PON systems. Moreover, the effectiveness of the EDB modulation scheme in counteracting the adverse effects of CD is evident, although with an anticipated trade-off. While EDB proves adept at mitigating the detrimental impact of dispersion, this enhancement comes at the expense of reduced sensitivity. This outcome aligns with

expectations, highlighting the inherent compromise of EDB between dispersion tolerance and receiver sensitivity.

Considering EEDB, the OPP is half way between the other two detection techniques, but when examining the absolute penalty, it becomes evident that the new scheme fully leverages the ISI introduced by both the limited bandwidth of the receiver and the fiber CD. In BtB, it performs 0.1 dB better than BD, while after 20 km of SMF the absolute penalty is reduced to 2 dB, compared to 5 dB of binary detection. Moreover, if one is willing to accept an extra penalty, the scheme is able to reach 30 km with both an absolute penalty and an OPP of around 4 dB. This finding adds a further confirmation to the validity of this scheme and to its resilience against channel impairments.

EEDB in a 50 Gbps PON link

After the initial experiments at 25 Gbps, with improved component availability it was possible to perform a new set of experiments, this time at 50 Gbps. We transitioned to using 25G-class components both at Tx and Rx, similar to a 50G-PON application. As it was discussed in the previous parts of this work, one of the options for cost reduction in PON is to utilize reduced-bandwidth transmitters, particularly at ONU side. The transmitter employed for these tests was a 25G-class EML with a 3-dB bandwidth of 22 GHz. It was biased at -1.6 V and its integrated laser was set to a current of 50 mA. On the receiver side, an integrated APD+TIA with an approximate 3 dB bandwidth of 17 GHz was employed. To comprehensively evaluate various Rx bandwidth limitations, the bitrate was varied across a range from 25 to 50 Gbps and the Rx sensitivity at a BER target of 1e-2 was measured for BD, EDB and EEDB. Fig. 3.13a shows the absolute penalty compared to the best sensitivity for binary transmission (BD), which is -27.6 dBm and it is obtained at 25 Gbps. The x-axis is expressed in terms of Rx bandwidth (B) to bitrate (R_b) ratio.

In this case, the EEDB scheme is able to reduce the penalty of BD by at least 0.5 dB when the Rx bandwidth is less than half of the bitrate, and improving as the bandwidth limitations becomes more severe. If we look at the case of $B/R_b = 0.38$, that is, 44 Gbps, the EEDB scheme has a penalty of 6 dB, which is certainly not negligible, but much smaller than the one of BD (15 dB).

For further confirmation, the tests were repeated using another APD + TIA, this time with a 3-dB bandwidth of 21 GHz. Again, the results are expressed with respect to the best value of BD, which improves to -28.2 dBm, thants to the higher Rx BW. It is possible to see in Fig. 3.13b that the increased bandwidth of the receiver leads to a greater penalty in the EEDB scheme (orange line, square markers), starting from around 2 dB. This can be attributed to a better quality of the two-level part of the signal and, consequently, the degraded three-level part. However, this penalty is almost constant until $B/R_b = 0.52$, while increasing only

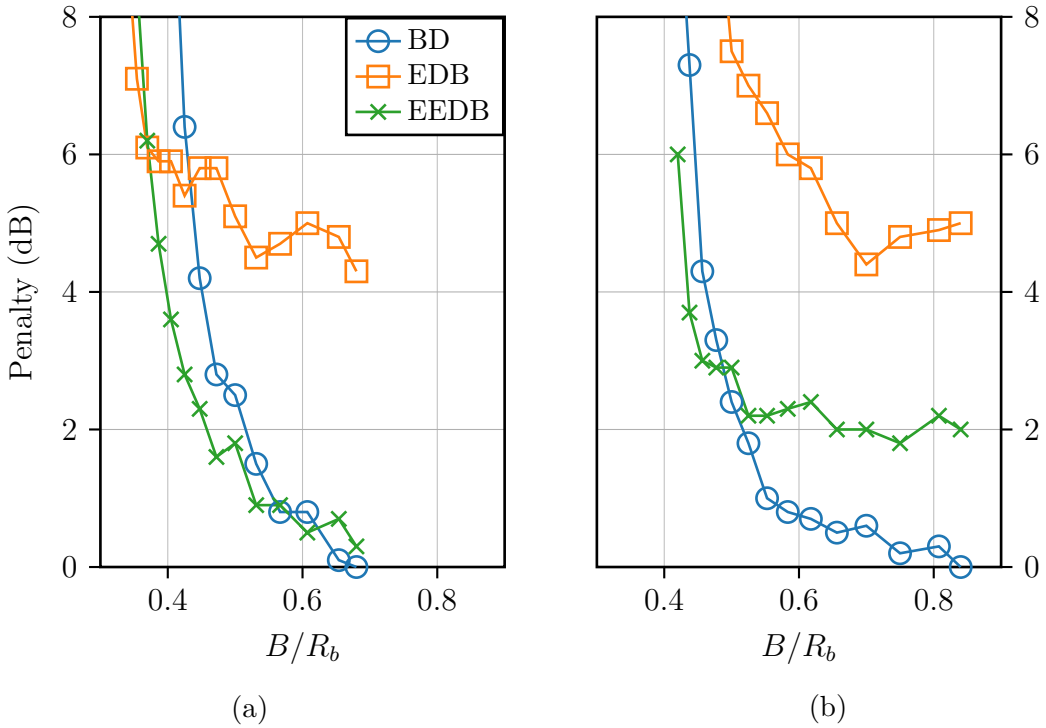

Figure 3.13: Rx sensitivity penalty using a 25G-APD when varying the bitrate. (a) B=17 GHz and (b) B=21 GHz.

2 dB for the extreme case of $B/Rb = 0.42$, that is, 50 Gbps. For comparison, the measured BD penalty for this case was 9.8 dB.

Reducing the sampling rate

In all the experiments described so far, the assumption is that an ADC works at twice the bitrate. However, for some applications such as in a ONU for PON, it is desirable to have a lower sampling rate, to reduce cost and power consumption Therefore, it is interesting to observe what happens when only one decision instant is used. For this purpose, an evaluation of receiver sensitivity was performed by sweeping the ROP and assessing the resulting BER for the EEDB scheme.

For this set of experiments, at the Tx side a PRBS-15 pattern ($2^{15} - 1$ bits). is generated by a PPG. This signal modulates an EML emitting at 1342 nm and generating a modulated optical signal with ER of 6 dB. The signal goes through 20 km SMF and a VOA, to emulate ODN losses. At Rx, the signal is detected by a 25G-APD+TIA with 17 GHz 3-dB BW. The signal is then captured using a digital oscilloscope and the BER is calculated after performing EEDB detection.

Figures 3.14a and 3.14b illustrate the BER when employing two or one samples per symbol (sps) for the decision-making process.

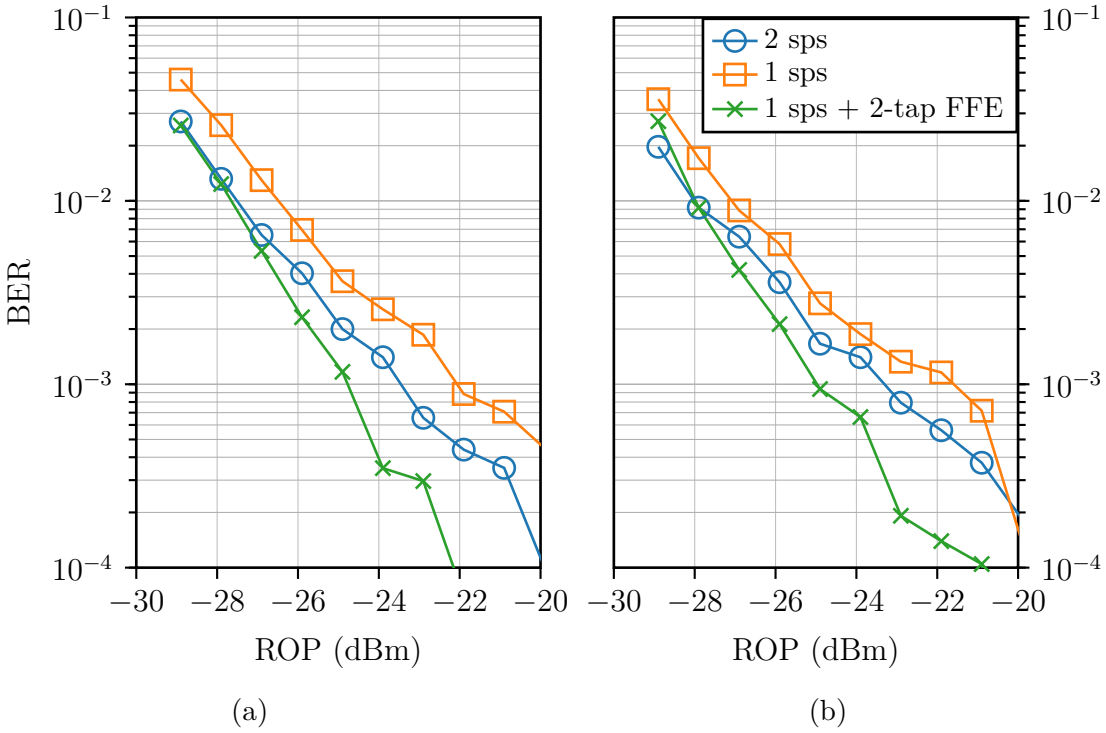

Figure 3.14: EEDB sensitivity with reduced sampling rate (a) BtB and (b) after 20 km

When looking at the 1e-2 BER threshold, a 1 dB sensitivity penalty appears when going from two to one sample per symbol (Fig. 3.14a, circle and square markers, respectively). A similar penalty is observed when a 20 km SMF spool is added. However, it is possible to compensate for this penalty by adding a 2-tap FFE in each branch of the EEDB detection scheme (cross marker in Figs. 3.14a and 3.14b). These results show that EEDB can effectively be implemented in a simple receiver employing a one-sample-per-symbol ADC can achieve comparable results to a system utilizing two sps through straightforward digital signal processing (DSP) techniques. This approach simplifies hardware requirements, offering a cost-effective solution without compromising performance.

3.2.3 Conclusions

This Chapter presented transmission techniques alternative to NRZ-OOK for bandwidth-limited systems. An introduction to duobinary signaling was provided. Next, a novel approach that combines binary and electrical duobinary detection was presented, named Enhanced Electrical Duobinary. This technique allows to correct errors on a received binary sequence in a bandwidth limited system by comparing the decoded bits also on the crossing points. After proving its validity in a variety

of simulated cases, where transceiver limitations, CD effects, and signal reflections were tested, experiments showed the validity of this scheme also in a real PON testbed.

Experimental validation carried out at 25 and 50 Gbps confirms the efficacy of the proposed scheme. Through meticulous testing with various APD-based receivers, the robustness and versatility of the EEDB was underscored, as its performance consistently withstands varied operational conditions. This comprehensive evaluation provides confidence in the applicability of the scheme.

The experiments conducted have provided valuable insights into the performance of EEDB in a 50 Gbps communication system with limited receiver bandwidth. On the basis of these findings, the extension of this technique to achieve transmission rates of 100 Gbps looks promising, supported by improvements in optical technology, which now offers components with much higher bandwidth. However, this will still require further testing.

Chapter 4

Optical access networks beyond 50 Gbps

The ongoing standardization efforts for 50G-PON are nearing completion, while research and development of access links capable of achieving bitrates beyond 50 Gbps are already underway [84]. The surge in demand for broadband and ultra-broadband internet access is compelling service providers to enhance their network capacities even further. Emerging applications, such as augmented reality (AR) and virtual reality (VR), ultra-high definition video, 5G mobile transport, and cloud services, are particularly bandwidth intensive, necessitating higher network capacities.

Looking at mobile networks, the gradual adoption of 5G and the future development of 6G networks will require that the mobile xHaul be capable of handling tens to hundreds of Gbps [72]. In this scenario, Point-to-Point networks are the most common solution, as they can provide lower latency compared to PONs, a crucial requirement in mobile links. However, PONs are particularly well suited for mobile xHaul in dense urban areas, where there is a high concentration of mobile base stations. In these areas, PONs can be used to connect multiple base stations to a single optical fiber, which can significantly reduce the cost of deploying and maintaining the mobile network. The demand and the need for commercial competitiveness is putting pressure on service providers to increase the capacity of their networks.

However, the requirement for network capacity must be accompanied at the same time by low costs and high link budget margins, particularly for PONs, in order to reuse already deployed ODNs. In this context, a two- or four-fold increase from the actual 50 Gbps is very challenging, due to the even tighter constraints already described in the previous Sections, that is, limited bandwidth of the components and increased impact of chromatic dispersion.

All PON generations so far use NRZ-OOK (also referred to as PAM-2) as the modulation format. This is the simplest modulation format achievable and can be

realized with low-cost optical devices [84]. Furthermore, when components have sufficient bandwidth and dispersion can be managed, it gives the best performance with respect to sensitivity and multipath interference tolerance [25], important for many deployed PON ODNs with poor return loss.

The next options for single-channel PONs could be 100 Gbps/λ or 200 Gbps/λ. From a research point of view, the topic has already been investigated for several years [81].

More recently, also the standardization bodies started to gather the requirements and to perform feasibility studies for 200 or even 400 Gbps links. On the PON side, a new ITU-T working program called G.suppl.VHSP was started in November 2022 to study the system requirements and characteristics of optical transmission above 50 Gbit/s [32]. In parallel, point-to-point (PtP) networks represent the main optical connectivity used in mobile networks, and represent a growing part of the market share in Datacom [72]. Although there is an ITU-T recommendation for 50G-PtP links [27], higher bitrate networks are already being considered due to the interest of operators in their application in RAN [93].

As we have seen in the previous Chapters, PON generations typically advance from one generation to the next one with a bitrate increase of four times. In a perspective of co-existence with already deployed ODN, this would result in using 200 Gbps per wavelength. Looking at the literature, it is possible to see results at this bitrate, for example, in [98]. However, when looking at the receiver sensitivity values, they are in the order of -10 dBm, making them suitable for datacenter applications, but not for access networks. In fact, if we think about PON, for example, such sensitivity would require a launch power of 19 dBm plus extra margin, unrealistic due to the nonlinearities appearing at such high powers along the fiber [2] and due to concerns about eye safety. Moreover, state-of-the-art 200G systems require complex digital signal processing techniques [3], which may not be desirable in access networks from a cost containment perspective.

For this reason, this Chapter focuses on 100 Gbps-per-wavelength access networks, which reduce challenges and requirements. After providing an overview of the state-of-the-art results from the literature in the field, new results are provided on how to achieve high link budgets with relatively simple digital signal processing and components suitable for an access network deployment.

The results of this study are presented in the following Sections, whose content is partially based on the results presented in the following works:

1. Giuseppe Caruso, Ivan N. Cano, Derek Nesset, Giuseppe Talli, and Roberto Gaudino. "Real-Time 100 Gb/s PAM-4 for Access Links With up to 34 dB Power Budget". In: *Journal of Lightwave Technology* 41.11 (2023), pp. 3491–3497. DOI: 10.1109/JLT.2023.3244028

2. Giuseppe Caruso, Ivan N. Cano, Derek Nesset, Giuseppe Talli, and Roberto Gaudino. "Real-Time 100Gb/s Downstream PAM4 PON Link with 34 dB

Power Budget". In: *2022 European Conference on Optical Communication (ECOC)*. 2022, pp. 1–4

3. Jérémy Potet, Mathilde Gay, Laurent Bramerie, Monique Thual, Ivan N. Cano, Giuseppe Caruso, Ricardo Rosales, Derek Nesset, Fabienne Saliou, Gaël Simon, and Philippe Chanclou. "Real-Time DSP-Free 100 Gbit/s/λ PAM-4 Fiber Access Link Using EML and Direct Detection". In: *IEEE Photonics Technology Letters* 34.17 (2022), pp. 895–898. DOI: 10.1109/LPT.2022.3191460

4.1 100 Gbps/λ access networks

By looking at the literature, several approaches have been considered to achieve 100G access networks. In [5], the authors present a feasibility study of a 100 Gbps PON using PAM-2. Using simulations, they foresee that a PAM-2 based 100G PON could be feasible around 2030, when full bandwidth components and more effective DSP techniques could be available.

Another approach considered is that of discrete multitone signaling (DMT), where the available bandwidth is divided into multiple frequency subchannels or tones [90]. Each tone is modulated independently, and the resulting signals are combined for transmission over the communication channel. If this technique provides flexibility (each subchannel can have a different bitrate) and good CD tolerance [69], it requires high linearity in the system components and it is likely to not overperform more common approaches, such as PAM-4 [87].

A further potential candidate for 100 Gbps links is PAM-4. This modulation format was already considered for 50G-PON, but was ultimately dropped due to its sensitivity penalty compared to OOK [84]. However, when data rates are further increased, optoelectronics limitations make NRZ-OOK more and more difficult to achieve.

To avoid being affected by bandwidth limitations, a 100 Gbps OOK link will require ≈ 70 GHz BW transceivers, while a PAM-4 signal with the same bitrate will need half the bandwidth, as we can see in Fig. 4.1. This is desirable both in a cost perspective, since devices with 30 to 50 GHz are already commercially available (and mass produced) and for CD tolerance.

Furthermore, PAM-4 is already adopted by data centers for data rates of 200 Gbps (4x50 Gbps) and 400 Gbps (4x100G or 8x50G), with fiber distances up to 10 km. In the context of access networks, it is already used in HS-PtP, also known as BiDi [27], at a nominal rate of 50 Gbps. It is likely that PAM-4 will continue to be the modulation format of choice for the next generation of BiDi networks.

Looking at the literature, extensive results have been shown with respect to PAM-4 for access links, both with direct detection and coherent receivers. In a non-extensive list: a link budget of 24 dB is achieved by [89], where a Nyquist-shaped

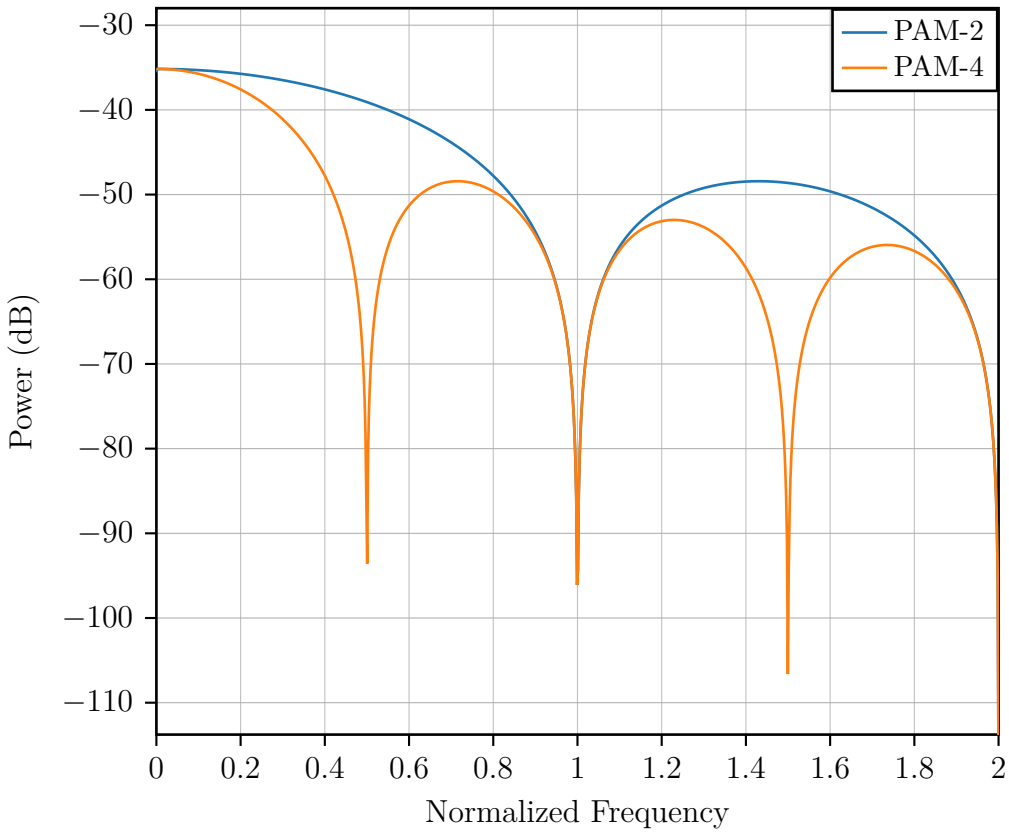

Figure 4.1: Power Spectral Density of PAM-2 and PAM-4 signals using rectangular pulse shape

signal is modulated through an 18 GHz EML. At the receiver side, a pre-amplified receiver (SOA+PIN) is used and the received signal is processed by constant modulus algorithm (CMA), Volterra, and decision-directed least mean squares (DD-LMS) equalizers. Similar results are found in [97], where 29 dB are obtained with a transmitter based on a 13 GHz DML [89]. More complex DSP techniques allowed the authors in [94] to reach the 34 dB link budget: at the transmitter side, they included a Tomlinson-Harashima precoder before Nyquist shaping, while at the receiver they added a decision-feedback equalizer (DFE). These results are even more remarkable when considering that it was achieved using a considerably limited-bandwidth system (15 GHz).

A novel approach for the future PON is that shown in [7], where the authors divide the ONT into groups according to their link budget. They present a flexible rate PON scheme that uses both NRZ and PAM-4 depending on the group needs. To achieve more granularity, they also introduce flexible FEC and probabilistic shaping, as shown in [8, 49]. The link budget achieved in this case is 31.5 dB, by using an SOA-preamplified Rx and a 23-tap FFE + 5-tap DFE. A different

approach is shown in [80], where the goal of the authors is to keep the complexity on the OLT side; they take advantage of the digital CD precompensation in C-band by using an IQ modulator. If we have a look at coherent receivers, in [54] a power budget of 30.5 dB in C-band is demonstrated with a polarization-diversity coherent receiver. On this track, the results in the O-band are not yet many (see, for example, [55]).

A summary of the results available in the literature at the time of writing this manuscript are shown in Table 4.1.

Table 4.1: Literature results on 100 Gbps PAM-4 for Access Networks

Link budget [dB]	Wavelength	TRx	Ref.
24	O-band	18 GHz EML+SOA, Volterra Eq.	[89]
29	O-band	10G-class DML, CMA + Volterra	[97]
29	O-band	MZM + PDFA	[64]
29	C-band	Digital precompensation, IQ mod	[80]
30	O-band	EML+PDFA, SOA+PIN Rx	[65]
30.5	C-band	30 GHz EML+SOA, Coh. Rx	[54]
31.5	O-band	Flex rate	[7, 8, 49]
34	O-band	Joint THP, Volterra	[94]

If the aforementioned results are interesting to understand how far low bandwidth components and/or equalization techniques can be stretched to meet high link budgets or, on the other hand, to make predictions about future developments, during this thesis another approach was attempted.

In a set of experimental tests, we tried to investigate, by implementing a real-time 100 Gbit/s PAM-4 link, what could be achieved with simple equalization, more suitable for a realistic deployment.

4.1.1 Real-time 100 Gbps testbed

In order to perform the analysis mentioned earlier, a real-time experimental testbed was implemented. Fig. 4.2 was assembled.

In the testbed, a PPG outputs two electrical OOK-NRZ PRBS-11 sequences (D_0 and D_1) at 50 Gbps. The two bitstreams are then fed to an analog PAM-4 encoder: this device includes both a continuous-time linear equalizer and a 3-tap FFE, useful for pre-emphasis in case the optical transmitter has limited BW. For these experiments, the bandwidth of the transmitter did not affect the signal quality, so the equalizer in the encoders was used to compensate only for penalties from the RF cables. Since the encoder does not include a feedback loop with the output signal, the taps must be manually adjusted. This was done by capturing the optical signal with a sampling oscilloscope and optimizing the taps to achieve

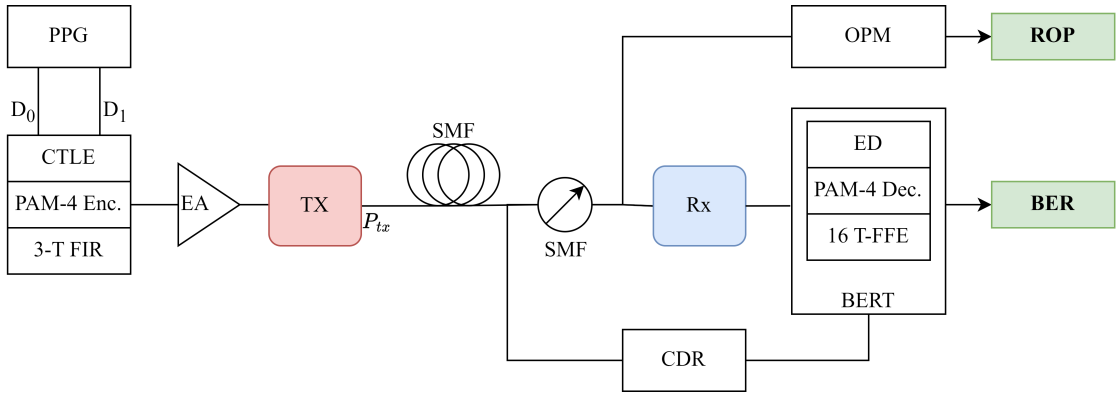

Figure 4.2: 100 Gbps PAM-4 experimental setup

maximum eye opening. Fig. 4.3a shows the eye diagram of the resulting electrical signal.

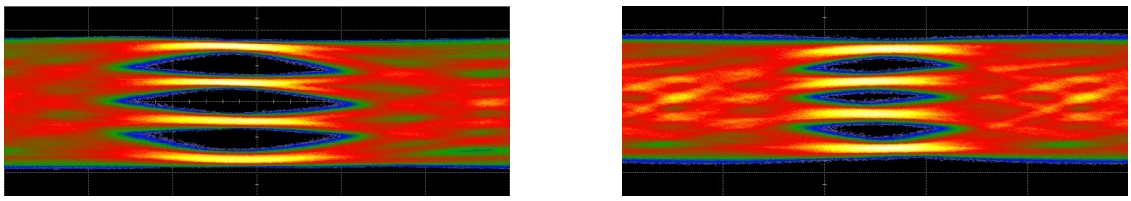

(a) Electrical signal (b) Optical signal

Figure 4.3: Measured PAM-4 eye diagrams

The four-level electrical signal is then fed to an RF amplifier, which outputs a 2 V_{pp} signal that modulates an EML (51 GHz 3-dB BW) emitting at 1310.5 nm. The distributed feedback laser (DFB) and the electroabsorption modulator (EAM) in the EML are biased at 40 mA and −3.03 V respectively and the output power (P_{tx}) is 5.3 dBm after modulation. The eye diagram of the optical signal is shown in Fig. 4.3b. The launched 50 GBaud PAM-4 optical signal has an outer extinction ratio (ER) of 6.7 dB. A summary of the various transmitter parameters is provided in Table 4.2.

As will be detailed in the following Sections, in some tests an O-band SOA was used to boost the signal power and increase the link budget. The resulting signal had an ER of 5.6 dB and an optical signal-to-noise ratio (OSNR) of 37 dB (0.1 nm), which does not limit the system performance. The booster SOA had a gain of 16 dB and noise figure (NF) of 7 dB and it was a discrete component, but this kind of amplifier is of interest since it can be monolithically integrated with the EML. Two examples of such devices are shown in [71] and [48], while recently a device of this kind with 20 dBm output power was presented [35].

After different lengths of SMF, a variable optical attenuator (VOA) simulates

Table 4.2: Optical Tx parameters

Parameter	Value	Unit
EAM 3-dB BW	51.0	GHz
λ	1310.5	nm
DFB current	40.0	mA
EAM bias	-3.0	V
Driving voltage	2.0	V_{pp}
Outer ER	6.7	dB
Output Power	5.3	dBm

Table 4.3: Optical Rx parameters

Parameter	APD	PIN	Unit
3-dB BW	21	38	GHz
R	0.8	6.5	A/W
M	10	1	

losses along the link and limits the input power in the receiver. For these experiments, the loss of the diplexers used in the transceivers to separate Tx and Rx wavelengths is not explicitly taken into account, and it is considered as part of the overall link budget.

On the receiver side, two possibilities are tested: a 25G-class APD and an optically preamplified PIN. For the latter case, a discrete SOA (gain=15 dB and NF=7 dB) and a 38 GHz p-i-n PD are used. To limit the amount of optical noise entering the photodiode, an Optical Bandpass filter (OBPF) with 20 nm width and centered at 1310 nm was used. The SOA is a discrete component on the receiver side too, but researchers have successfully shown integrated SOA+PIN, for example [9] or [10].

Both PDs have an integrated linear transimpedance amplifier (TIA) and are packaged into a receiver optical subassembly (ROSA). Table 4.3 summarizes the main parameters of the two devices, including PD responsivity (R), APD gain (M) and 3-dB bandwidth, while a block diagram of the Tx and the two Rx types is shown in Fig. 4.4.

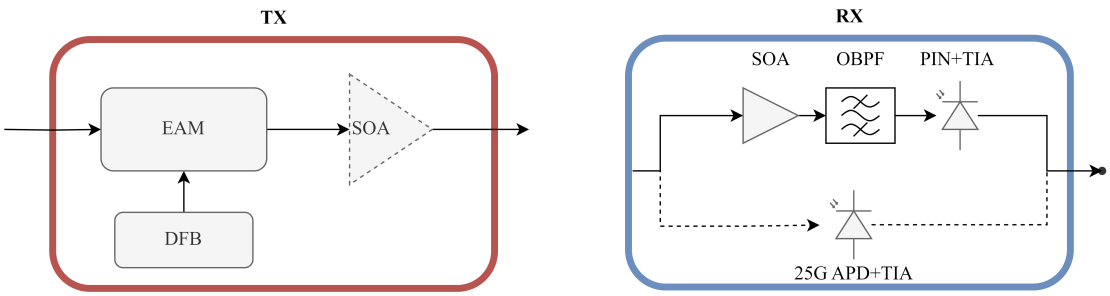

Figure 4.4: Block diagram of Tx and Rx used in the experiments

The electrical signal then passes through a 16-tap T-spaced FFE embedded in the BERT, which compensates for the BW limitation of the APD and the RF cables. An external CDR module recovers the clock signal from the optical signal

and provides it to the BERT. Finally, the PAM-4 signal is decoded, and the BER is computed in real time in the Error Detector (ED).

4.1.2 Non-amplified transmitter

The first test case was to determine the achievable performance using a non-amplified PAM-4 optical link. The expectation is that this kind of link will not reach the 29 dB budget required for PON but could potentially achieve power budgets suitable for BiDi PtP applications.

The EML-generated signal was detected with an APD+TIA after several lengths of SMF, i.e., back-to-back (BtB) to 40 km, in 10 km steps. The Tx pre-equalizer, that is, the pre and postcursor of the FFE, was first optimized to get the maximum eye-aperture of the optical signal, by observing the optical signal in a sampling oscilloscope. Subsequently, the optimal tap values for the Rx equalizer were calculated, following an offline least mean square (LMS) in BtB. It must be highlighted that the ED FFE has a main cursor with both fixed position and tap value, constraining to work with only two precursors. Furthermore, as seen in Fig. 4.5a, due to the limited equalization capabilities of the ED FFE, only two post-cursors are used in the Rx equalizer. The tap values obtained under these conditions are then kept constant for all measurements. Fig. 4.6 shows the BER results against ROP for BtB, 20 km, 30 km, and 40 km of SMF.

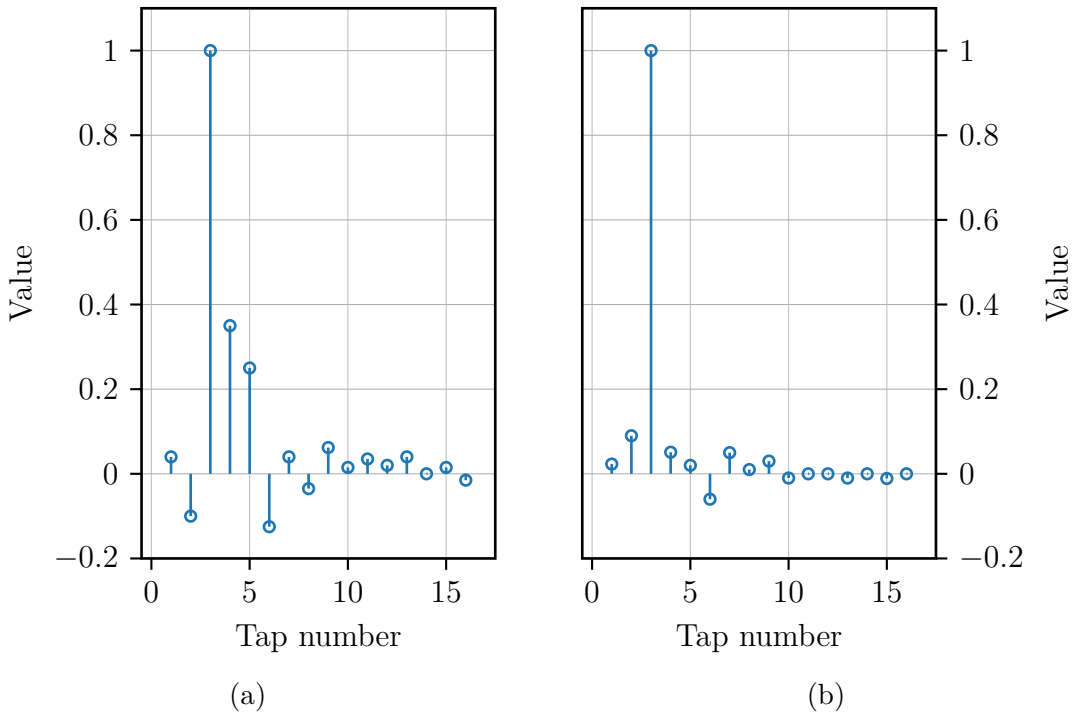

Figure 4.5: ED FFE taps for (a) APD and (b) PIN receiver

Even if current 50 Gb/s BiDi is defined with Reed-Solomon (RS) FEC codes [27] at a target input BER of $2.4*10^{-4}$, due to signal integrity becoming increasingly challenging at higher baud rates, the assumption here is that future recommendations could include low-density parity check codes (LDPC) as used in PON [26]. Therefore, BER is measured at an HD-FEC threshold of 10^{-2}, following the LDPC (17280, 14592) used in 50G-PON.

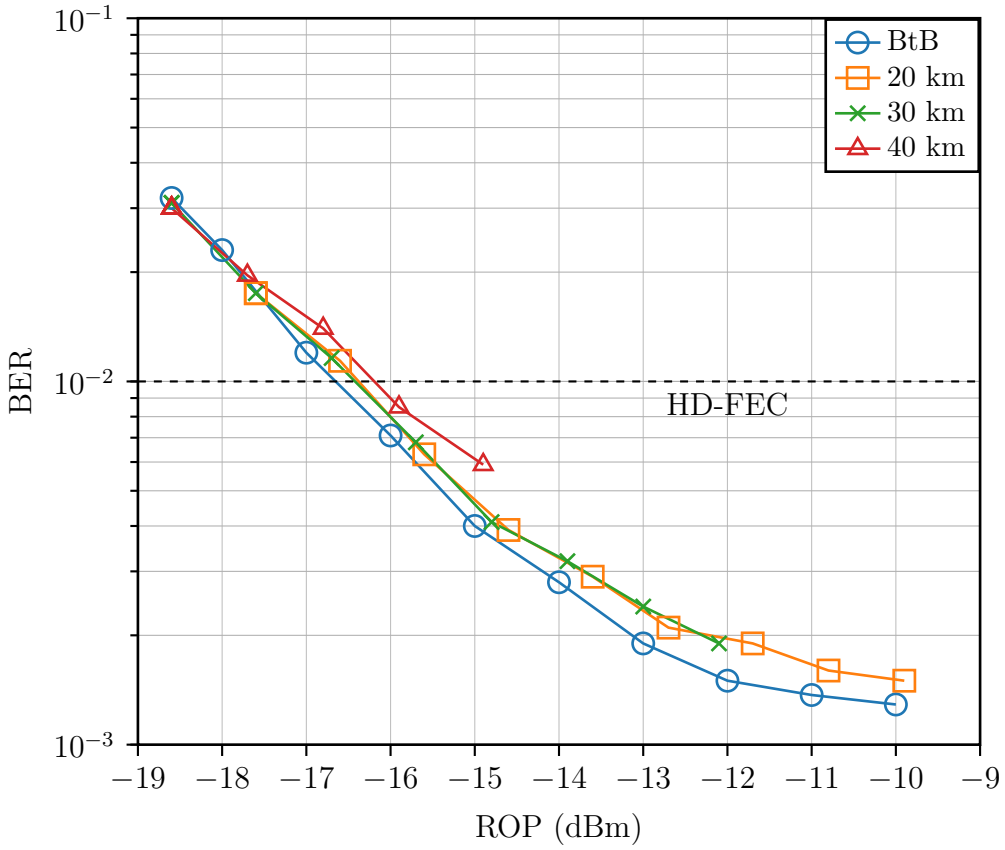

Figure 4.6: BER vs. ROP for EML-based Tx and APD-based RX

With this configuration, one can obtain sentitivities of -16.6 dBm and -16.2 dBm in BtB and after 40 km of SMF, respectively. The OPP is almost negligible, only 0.4 dB, and these results can be motivated by the emission wavelength of the EML being close to the zero-dispersion wavelength of the fiber and by the FFE being able to partially compensate for the ISI introduced by the fiber CD. In Fig. 4.6 it is also possible to observe a BER floor at $2{\cdot}10^{-3}$, which can be attributed to the limited bandwidth of Rx together with limited equalization capabilities. In fact, optimizing the APD+TIA for 50 Gbaud applications can, in principle, lower the BER floor to 10^{-8}, as shown in [37]. Taking into account a transmitted power (P_{tx}) of +5.3 dBm, the achieved optical budget is 21.5 dB, which gives 6.5 dB and 1.5 dB

margin for BiDi class S (15 dB) and class A (20 dB), respectively. It is also worth mentioning that, considering an SD-FEC threshold of $2{\cdot}10^{-2}$, after 40 km of SMF the Rx sensitivity is -17.7 dBm, achieving a power budget of 23 dB, enough for BiDi class B- (23 dB). This suggests that a 100 Gb/s/λ BiDi link can be achieved with an EML-based Tx and a properly designed APD+TIA at receiver.

Subsequently, the APD was replaced with a preamplified SOA+50G-PIN, with the expectation of an improved Rx sensitivity. A 20 nm Optical Band Pass Filter (OBPF) was added after the SOA, to limit the amount of ASE noise that enters the photodiode. For this test case, Rx has enough BW (∼36 GHz) for a 100G-PAM4 signal and the FFE coefficients are optimized primarily to compensate for any impairments deriving from the RF cables. The tap values obtained under these conditions (Fig. 4.5b) are then kept constant for all measurements. Fig. 4.7 plots BER against ROP in BtB and after 20 km, 30 km, and 40 km of SMF.

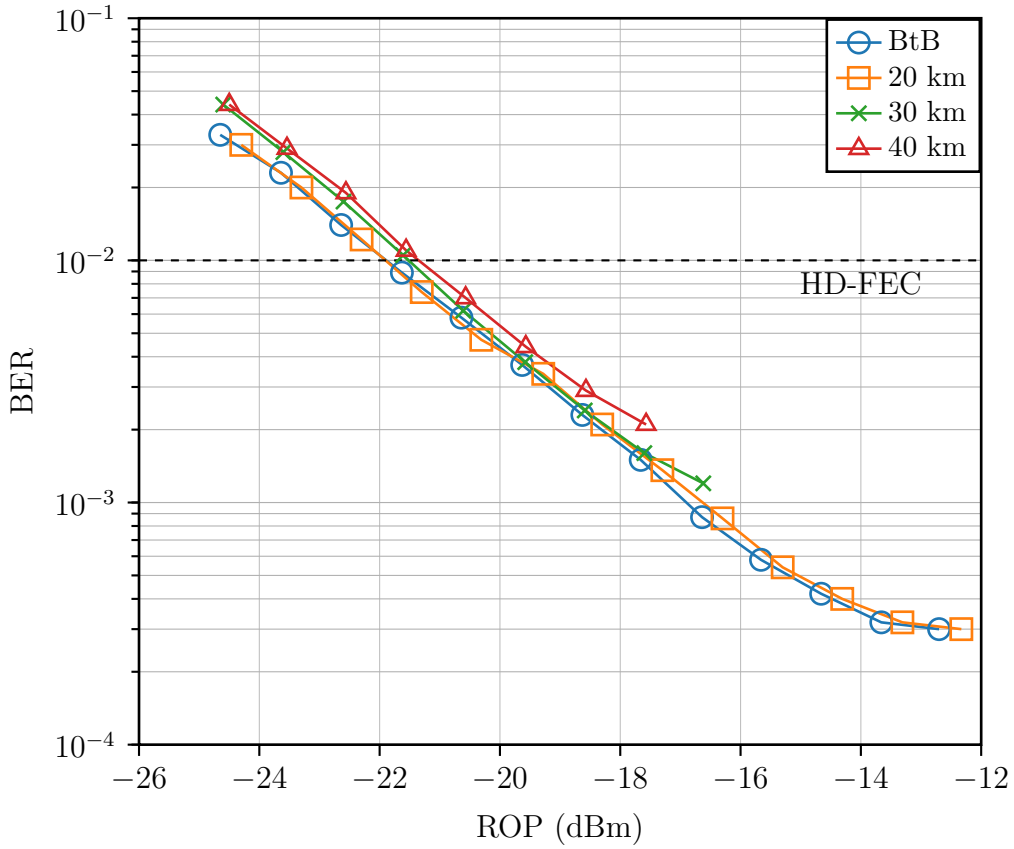

Figure 4.7: BER vs. ROP for EML-based Tx and SOA+PIN-based RX

Compared to APD, the Rx sensitivity at the HD-FEC threshold improves to -21.8 dBm in BtB and to -21.4 dBm after 40 km. The OPP is again only 0.4 dB since the accumulated CD is small, while the high BW Rx allows to lower the BER floor to

$3{\cdot}10^{-4}$. The optical budget, assuming again P_{tx}=+5.3 dBm, is increased to 26.7 dB, giving enough margin for Class B for BiDi; considering the SD-FEC threshold, the optical budget can be improved up to 28.2 dB, obtaining 3.2 dB margin. An SOA+PIN Rx with a very simple electrical equalization can be considered as a potential solution to cover the BiDi loss class at the longest transmission distance defined in [27].

4.1.3 Amplified transmitter

With the Rx sensitivity values observed in the previous Section, it becomes clear that to obtain a power budget of at least 29 dB and achieve a 100 Gbps PON link, an increase in Tx launch power is required. Therefore, for this set of experiments, an SOA was introduced on the transmitter side. This device had a gain of 15 dB and NF of 7 dB. Its bias current was set to 210 mA, to obtain a P_{tx}=+10.9 dBm. The pre-equalizer FFE coefficients were again tuned and the EAM bias was reduced to −2.95 V to obtain the maximum eye aperture of the optical signal after SOA. At receiver side, the same APD as the non-amplified setup was first tested. The Rx FFE taps were once again tuned, in order to obtain the lowest BER at an ROP of -13 dBm in BtB. Then BER was measured in BtB and after 20 km and 30 km, as shown in Fig. 4.8.

The first noticeable effect, when looking at the curve, is that the BER floor is now very close to the HD-FEC target BER of 10^{-2}. This is mainly due to the optical noise added by the SOA. After 30 km, the floor is even higher than 10^{-2}, while for a fiber distance of 40 km it is not anymore possible to detect the signal.

As already anticipated in the previous Section, a lower BER floor can be obtained by using a higher BW APD+TIA, as in [37], but its value in the presence of optically amplified systems remains to be investigated. At the HD-FEC threshold of BER=10^{-2}, the Rx sensitivity in BtB and after 20 km is -13.7 dBm and -13.4 dBm, respectively. Compared to the non-amplified case, the Rx sensitivity is degraded due to the ASE noise introduced in the Tx signal, but with an increase of 5.6 dB in P_{tx} it is possible to obtain an overall link budget of 24.3 dB (P_{tx} = 10.9 dBm). However, the HD-FEC threshold is very close to the BER floor and working under such conditions will limit the system performance and operating range.

More complex equalization techniques can help to improve Rx sensitivity, as presented in [94]. The authors show a 2 dB sensitivity improvement when introducing Volterra and DFE equalization, compared to only FFE+DFE. Furthermore, if we consider the results published in [37] and include the 3 dB penalty measured when Tx is optically amplified, a 2 dB Rx sensitivity gain can be estimated at the HD-FEC threshold when switching to a 50 GBaud APD+TIA.

When considering the SD-FEC threshold (2e-2), the Rx sensitivities improve to -16.2 dBm and -16.1 dBm in BtB and after 20 km, respectively, and a link budget of 27 dB is measured. For such a pre-FEC BER level, a Rx sensitivity of -16 dBm

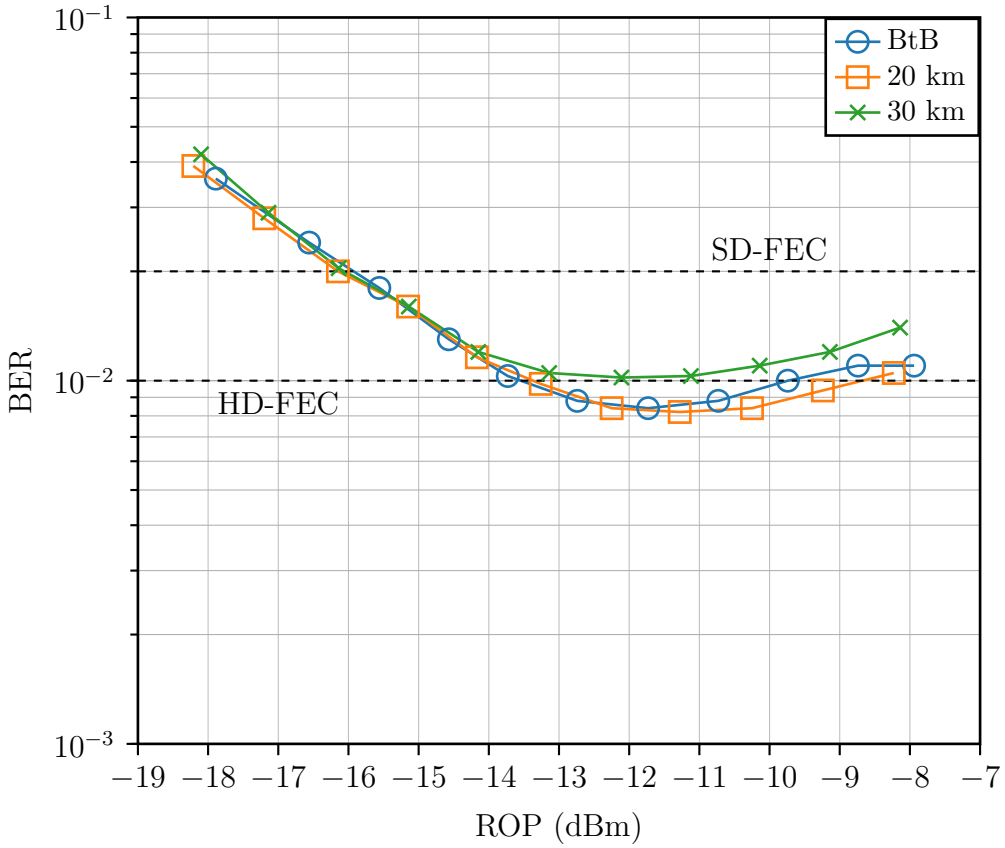

Figure 4.8: BER vs. ROP for EML+SOA-based Tx and APD-based RX

is obtained after 30 km of SMF. Although the link budget value obtained is enough to cover the highest loss BiDi class, the transmission distance of 40 km cannot be achieved.

The link budgets obtained with this system configuration are around 2 dB lower than the EML with SOA+PIN described in the previous Section. This discrepancy can be mainly justified by the limited BW APD+TIA and the limited equalization used. If the expected gain from using a 50G APD with an amplified Tx is confirmed, then the link budgets of the two configurations become comparable.

After measuring the sensitivity for the amplified transmitter, in order to assess the total achievable link budget, P_{Tx} was swept by changing the SOA bias current. The results are shown in Fig. 4.9, where the link budget is depicted against P_{Tx}.

Due to the high BER floor shown in Fig. 4.8, the Rx sensitivity was now measured at BER=$2{\cdot}10^{-2}$ after 20 km. Even if the EML emission wavelength is close to the zero dispersion wavelength and self-phase modulation causes limited pulse spreading, P_{Tx} must still be limited to 13.4 dBm to avoid nonlinearities in the fiber and from the SOA [23, 65].

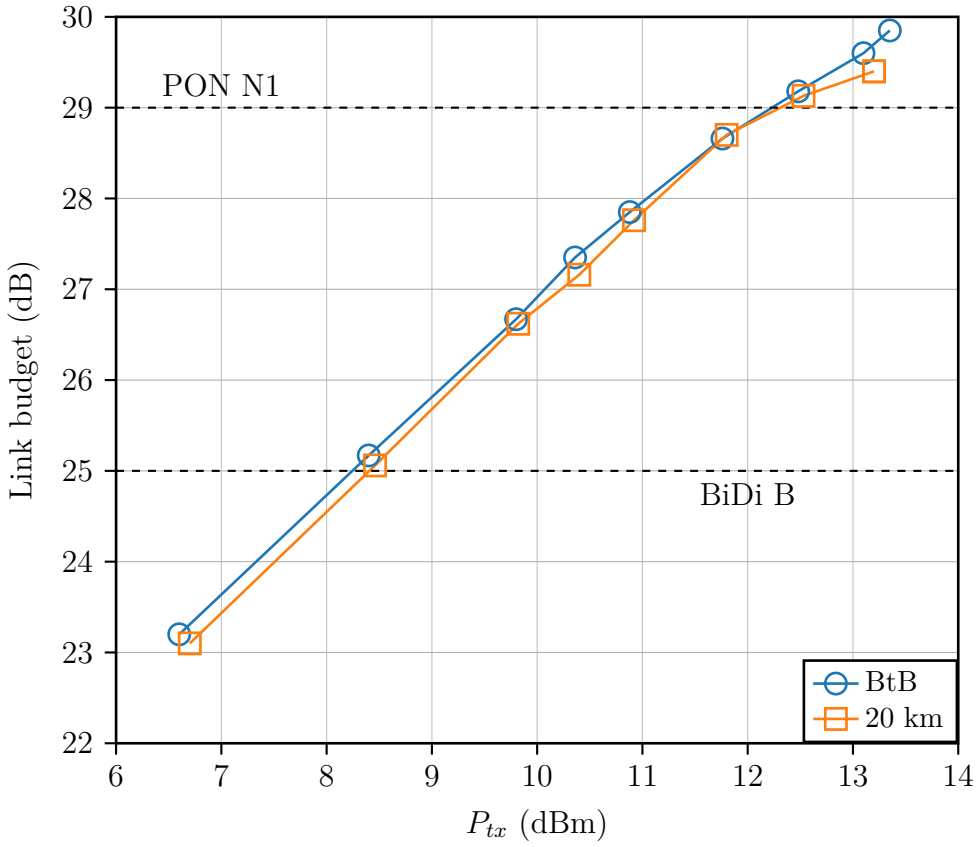

Figure 4.9: Link budget for EML+SOA Tx and 25G-APD Rx

From Fig. 4.9, it can be observed that when setting P_{Tx}=8.5 dBm (with a corresponding Rx sensitivity of -16.6 dBm), even the highest loss class of BiDi (class B) can be achieved. Furthermore, by increasing P_{Tx} to 13 dBm, the 29 dB link budget of PON is also obtained with a small margin.

These results show that an integrated EML+SOA with relatively small gain and moderate P_{Tx} is suitable for BiDi links, guaranteeing at the same time additional margin if P_{Tx} increases. In the case of PON networks, the link budget extra margin is below 1 dB, so other solutions need to be considered.

For this reason, the amplified transmitter we also tested with the preamplified Rx shown in the previous Section, up to a distance of 20 km. Initially, a P_{Tx} of +9.3 dBm was used and also in this case the FFE coefficients on the Rx side in BtB were re-optimized, this time to achieve minimum BER at ROP of -17 dBm. Fig. 4.10 shows the BER plots versus ROP.

At the HD-FEC threshold, the ROP is -20.8 dBm and -20.6 dBm in BtB and after fiber, respectively, which together with the optical power of Tx gives a link budget of 29.9 dB. It should be noted that the Rx sensitivity and power budget

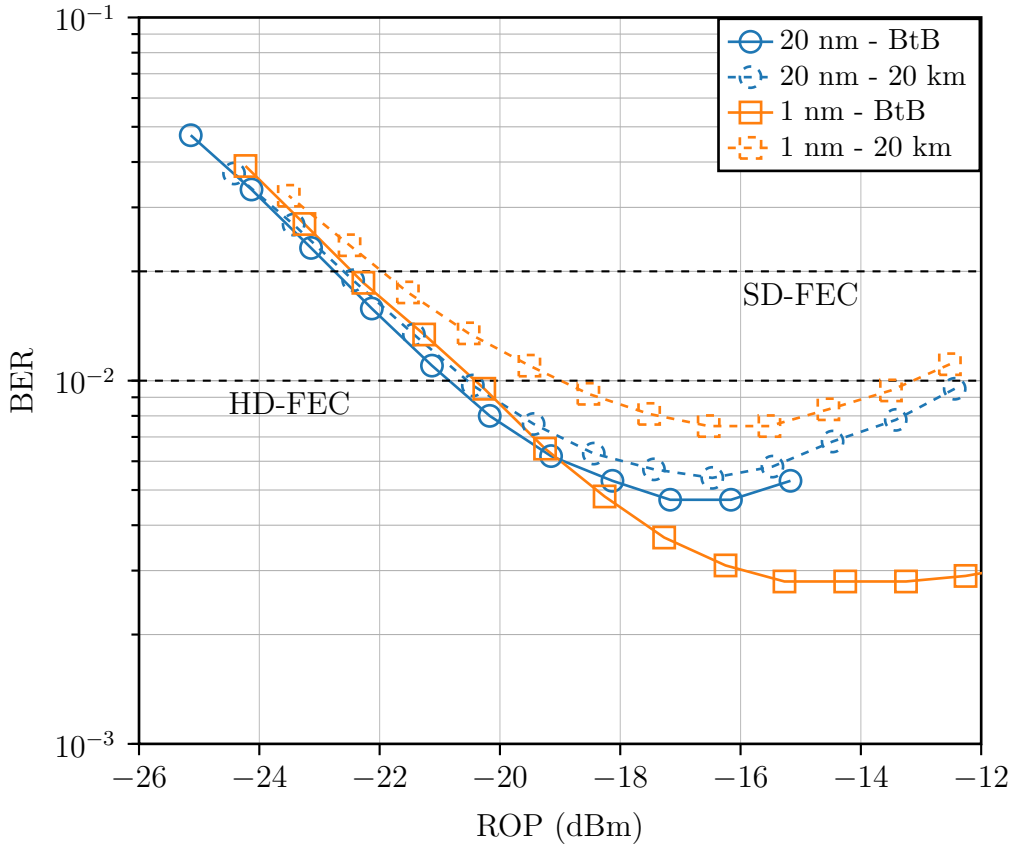

Figure 4.10: BER vs ROP measured in BtB (solid) and after 20 km (dashed) for amplified Tx and Rx

achieved are only 1.5 dB and 0.6 dB lower when comparing them with those reported in [54], where coherent amplification and offline processing were used. However, it must be highlighted once again that the experiments in the forementioned work are done in C-Band. Furthermore, looking again at the results of Fig. 4.10, the Rx sensitivity measured is almost 2 dB better than the real-time results reported in [64], where a Praseodymium-Doped Optical Amplifier (PDFA) with a NF of 5 dB was used as the Tx booster. This improvement can be attributed both to the high-BW EML and to a fine-tuning of the Tx equalizer to maximize the eye aperture after the SOA.

Instead, considering the SD-FEC threshold of $2{\cdot}10^{-2}$, the ROP improves by almost 2 dB to -22.3 dBm after fiber and a link budget of 31.8 dB can be obtained. An additional margin could be obtained by using more complex Rx DSP, such as FFE+DFE or MLSE. Furthermore, by looking again at Fig. 4.10, it is possible to see that for ROP values higher than -17 dBm, the BER increases because the optical signal starts to saturate the TIA, distorting the highest level of the PAM-4

signal. A specific TIA design could, in principle, mitigate this problem and increase the dynamic range. The second observation is that a BER floor at around $8{\cdot}10^{-3}$ which can be explained by the optical ASE noise in the Rx signal. To confirm this hypothesis, as shown in Fig. 4.10, when the optical filter was changed with one having 1 nm BW, the BER floor is reduced to $5{\cdot}10^{-3}$.

In a similar way to what was done for the APD receiver, the link budget is also evaluated for this configuration by sweeping the bias current of the Tx SOA. Fig. 4.11 shows the link budget versus P_{Tx} at the HD-FEC threshold of 10^{-2}. P_{Tx} was set to a maximum of +13.4 dBm in order to avoid nonlinearities in the fiber [77, 23]. Confirming what was observed in the previous Section, BiDi class B can be attained with P_{Tx}=+5 dBm and still have 1 dB margin. Regarding PON, the loss budget class N1 can be achieved with a launch power of at least 8.1 dBm.

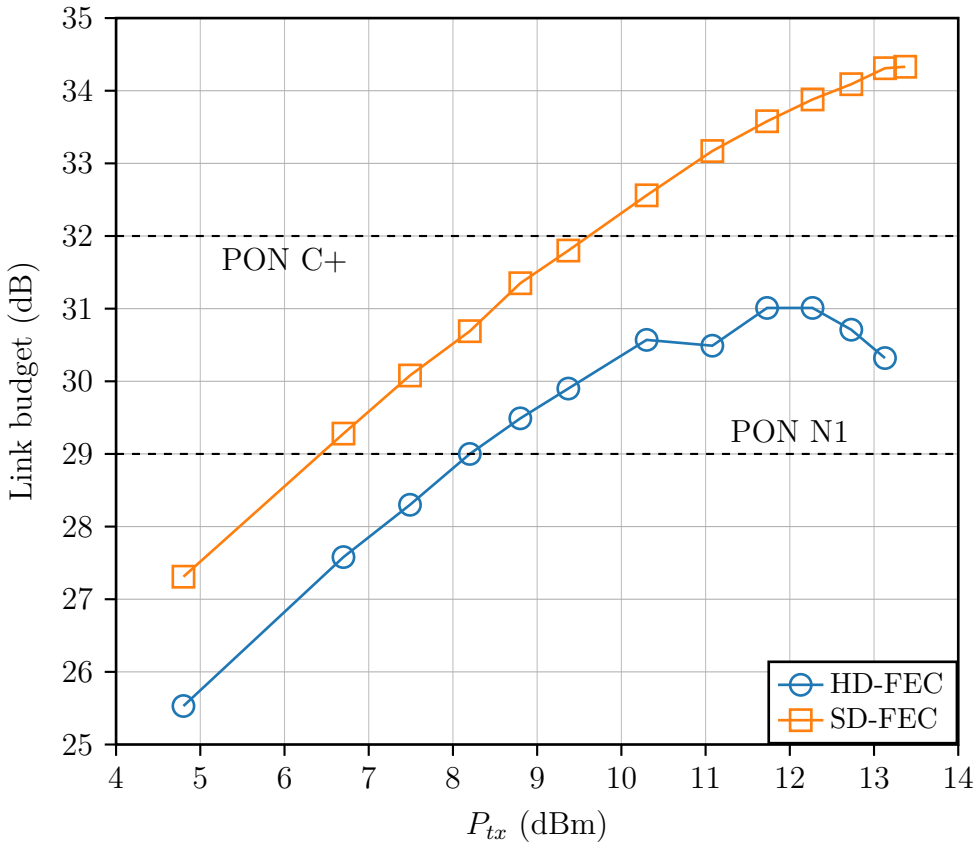

Figure 4.11: Link budget for EML+SOA Tx and SOA+PIN Rx

At a target BER of 10^{-2}, a maximum link budget of 31 dB is obtained, which gives 2 dB margin for PON class N1. When P_{Tx} increases to at least 12.3 dBm, the link budget starts to decrease. This is explained by SOA nonlinearities appearing at higher bias currents. They cause distortions in the signal and increase the BER

floor, as in Fig. 4.10, resulting in a reduced Rx sensitivity. A more complex Rx DSP could help mitigate this penalty.

When looking at the SD-FEC threshold of $2{\cdot}10^{-2}$, a maximum link budget of 34.3 dB was measured for P_{Tx}=13.4 dBm. At the time of writing this Thesis, this is the highest link budget achieved for a real-time 100G PAM-4 link. This kind of setup, therefore, could be a candidate to achieve 100 Gbps PON, achieving C+ class with margin. However, it must be highlighted that, due to Tx working emitting at 1310.5 nm (which falls in the US channel of GPON), the link budgets are computed considering a measured total CD of 4.4 ps/nm.

If an estimate of CD penalty in a PON scenario is somewhat complicated, since it must be decided which generations must coexist with a potential 100G-PON and consequently allocate a given wavelength range, the task is easier for BiDi, where coexistence is not a requirement. An estimate of the potential CD penalty can be provided by looking at the wavelength plan in the standards. BiDi systems employ two wavelengths (one per direction), which for the 100G application are considered to be centered at 1304 nm and 1309 nm [93]. For the lowest wavelength, the minimum and maximum total CD are -75.31 ps/nm and 14.65 ps/nm. Negative CD and Tx chirp will produce limited OPP and could even improve Rx sensitivity, while positive CD is low enough to limit the OPP below 1 dB. The minimum and maximum CD at 1309 nm are -56.16 ps/nm and 32.78 ps/nm respectively. In a similar way as to 1304 nm, the total negative CD will cause a negligible OPP, but the highest CD can induce ISI and produce up to 2 dB OPP. If a drift of ±1 nm is assumed, the highest CD reaches 37 ps/nm, which can increase the OPP to 2.5 dB [93], therefore additional margin should be considered.

To summarize all the results achieved in this Section, Fig. 4.12 reports the maximum power budget obtained for each transmitter and receiver configuration.

A 100G PAM-4 PtP link can be realized with an EML and a 25G-APD using simple FFE equalization, which allows to reach class B-. The highest loss Class B can be achieved by using an SOA at Tx or Rx. By looking at PON, the minimum link budget of 29 dB can be obtained by using a full BW EML followed by a booster SOA and a 25G-APD at receiver, whereas by including a pre-amplified Rx makes C+ link budget class achievable with 2.3 dB margin.

4.1.4 Summary

In summary, this Chapter has presented a comprehensive analysis and discussion of 100 Gbps optical access networks using PAM-4 as modulation format, highlighting the significant contributions and achievements made throughout the course of this thesis. The investigation was carried out with the primary aim of exploring the possibilities of using this modulation format in future access networks. Due to its reduced bandwidth requirements, 100G PAM-4 could make use of already available 50G-class components, and the results obtained have provided valuable insight into

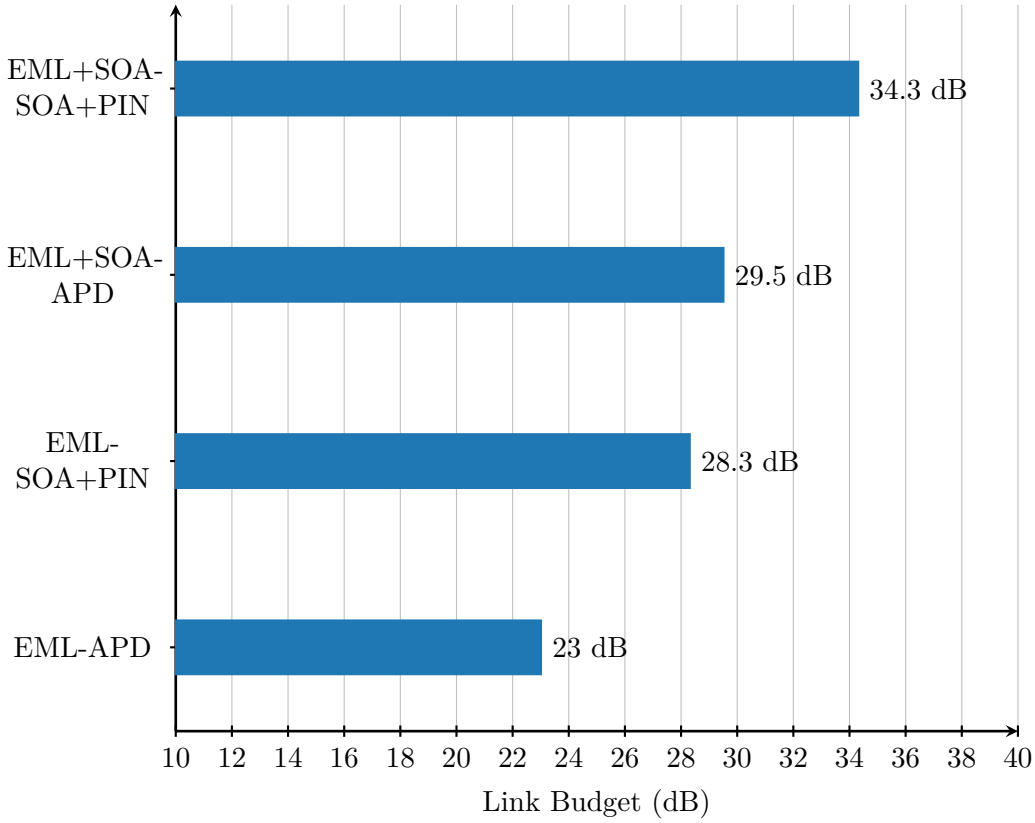

Figure 4.12: Overview of measured real-time link budgets for 100G-PAM4

the possibilities and limitations of this kind of system.

The experimental efforts carried out as part of this research have yielded robust and notable results. An experimental analysis with different kind of transmitters and receivers has shown that 100 Gbps PAM-4 links having a link budget greater than 20 dB are feasible with 50G-class components and simple receiver equalization. Specifically, PtP links with link budgets of at least 23 dB can be obtained with a full-BW EML and a 25G-class APD, while 28.3 dB can be obtained using an SOA-preamplified PIN. Regarding PON, where a link budget of at least 29 dB is required, an amplified Tx with a 25G-class APD allows to get a 29.5 dB link budget, whereas by amplifying both Tx and Rx it is possible to achieve a record 34.3 dB link budget.

These findings serve as a substantial contribution to the existing body of knowledge in the field of next generation access networks, providing a foundation for further research and advancements.

Chapter 5

Conclusions

Passive Optical Networks (PONs) represent a crucial technology in modern telecommunications infrastructure, delivering high-speed internet access to both residential and business customers. Unlike traditional copper-based networks, PONs eliminate the need for active electronic components like signal boosters and repeaters along the distribution path. By employing passive optical splitters, PONs can serve multiple users without requiring powered amplification, thereby significantly cutting down on both capital expenditure and ongoing operational expenses. Chapter 1 provides a concise history of Passive Optical Networks, highlighting the key technologies that led to the success of this kind of network and then the most influential standards in the field.

The importance of standardization in the context of PON is discussed in Chapter 2, where an overview of transmitter compliance metrics for passive optical networks is presented. The TDEC metric, introduced in 50G-PON was analyzed and new effects due to APD shot noise and receiver equalization were included in the underlying mathematics. A numerical optimization of several parameters that affected the measurement was performed, and subsequently a comparison between equivalent sampling and real-time oscilloscope was tested. It can be seen that, with proper signal processing, the two instruments provide comparable results. Later on, the metric was tested in several experimental scenarios, and it was shown that TDEC is able to predict sensitivity penalties due to the transmitter (extinction ratio, limited bandwidth) or the chromatic dispersion of the channel, both in positive and negative dispersion regime. These results show that TDEC can be a reliable and straightforward test of transmitter compliance in all the cases covered by the 50G-PON standard.

In Chapter 3, a new technique is described that exploits a mix of binary and duobinary signaling, called Enhanced Electrical Duobinary. By retrieving information both from the eye opening and the crossing point of the signal, this scheme aims to correct errors in a PAM-2 stream caused by signal degradation due to bandwidth

limitations and chromatic dispersion. An initial set of simulations showed the validity of the idea and its potential, showing better sensitivity compared to standard binary detection in the case of reduced system bandwidth and limited Rx sensitivity penalty when the bandwidth limitations were less severe. These results were later on proved in several experiments up to 50 Gbps, where bandwidth limitation and chromatic dispersion were put under test using PON-grade components.

Chapter 4 delves into the future of PON. The ever increasing demand for bandwidth and the need for signal integrity will likely require a change in modulation format, if IM/DD will still be the chosen transmission and reception technique. For this reason, in this work a 100 Gbit/s access system was experimentally analyzed, specifically a 50GBaud real-time PAM-4. After evaluating several transmitter and receiver schemes, both with and without optical amplifications on both ends, and by using relatively simple equalization (a real-time 16 taps FFE), a broad overview of the possibilities and limitations of this kind of system was presented. The results show that non-amplified setups are interesting for PtP links (also known as BiDi), where lower link budgets are required. For PON systems, the minimum link budget of 29 dB is achieved with a transmitter employing an EML followed by an SOA and an APD at receiver. Last, a record link budget of 34.3 dB is obtained when using optical amplification also at receiver side, by means by a SOA+filter+PIN.

In summary, this thesis contributes to the field of optical access networks by addressing key technological challenges, as it is the case for TDEC, and proposing novel solutions, with EEDB and 100G PAM-4 PON. The insight gained from the simulative and experimental results of this research will be an important starting point for future developments in optical access networks, where new and important challenges will rise, posed by the need for increased data rates and need for low power consumption.

Useful Formulas

BER in NRZ-OOK IM/DD communication systems

It is possible to derive the error probability for an ideal binary system as follows. Assuming that a system transmits 1 and 0 symbols, an error occurs if, due to receiver noise, a 1 is misdetected for a 0 and viceversa. The error probability can be defined as:

$$BER = p(1)P(0|1) + p(0)P(1|0) \tag{1}$$

in which $p(1)$ and $p(0)$ are the probabilities of transmitting 1 or 0, while $P(0|1)$ is the probability of decoding a 0 when a 1 was transmitted and viceversa for $P(1|0)$. We can assume that 0 and 1 are transmitted with equal probability, i.e. $p(1) = p(0) = \frac{1}{2}$, thus getting

$$BER = \frac{1}{2}\left[P(0|1) + P(1|0)\right] \tag{2}$$

The two probabilities in 2 will depend on the noise statistics, but a common approach [1] is to consider thermal and shot noise as independent Gaussian r.v. with zero mean and variance $\sigma_{T,S}$. The total noise variance is then given by $\sigma^2 = \sigma_T^2 + \sigma_S^2$.

Taking into account that average and noise variance are different for I_1 and I_0, one can write:

$$P(0|1) = \frac{1}{\sigma_1\sqrt{2\pi}} \int_{-\infty}^{I_D} \exp\left(-\frac{(I-I_1)^2}{2\sigma_1^2}\right) \mathrm{d}I = \frac{1}{2}\,\mathrm{erfc}\left(\frac{I_1 - I_D}{\sigma_1\sqrt{2}}\right) \tag{3}$$

$$P(1|0) = \frac{1}{\sigma_0\sqrt{2\pi}} \int_{I_D}^{\infty} \exp\left(-\frac{(I-I_0)^2}{2\sigma_0^2}\right) \mathrm{d}I = \frac{1}{2}\,\mathrm{erfc}\left(\frac{I_D - I_0}{\sigma_0\sqrt{2}}\right) \tag{4}$$

where I_D is the decision threshold and erfc is the well-known complementary error function. By putting together the previous equations, one obtains:

$$BER = \frac{1}{4}\left[\mathrm{erfc}\left(\frac{I_1 - I_D}{\sigma_1\sqrt{2}}\right) + \mathrm{erfc}\left(\frac{I_D - I_0}{\sigma_0\sqrt{2}}\right)\right] \tag{5}$$

From 5, it is evident that the BER can be minimized by choosing the optimum I_D. It is possible to show that the optimal value is:

$$I_D = \frac{\sigma_0 I_1 + \sigma_1 I_0}{\sigma_0 + \sigma_1} \tag{6}$$

and that, for thermal noise-limited receivers, this reduces to $(I_1 + I_0)/2$. This indicates that the BER is minimized when the decision threshold is set halfway between the two levels. Last, by defining the Q factor as $\frac{I_1 - I_0}{\sigma_1 + \sigma_0}$, it is possible to rewrite the error probability as

$$BER = \frac{1}{2}\operatorname{erfc}\left(\frac{Q}{\sqrt{2}}\right) \tag{7}$$

Q function

Not to be confused with the Q factor defined in the previous Section, the Q function is the tail distribution function of a standard normal distribution. In other words, $\mathrm{Q}(x)$ is the probability that a standard normal r.v. assumes a value greater than x.

Considering a random variable $X = N(0,1)$ having probability density function

$$f(x) = \frac{1}{\sqrt{2\pi}}\exp\left(-\frac{x^2}{2}\right) \tag{8}$$

the probability that it will assume a value greater than x will be

$$P(X > x) = \frac{1}{\sqrt{2\pi}}\int_x^\infty \exp\left(-\frac{z^2}{2}\right)\mathrm{d}z \tag{9}$$

Expressing it in terms of error function [68], it becomes

$$\mathrm{Q}(x) = \frac{1}{2}\operatorname{erfc}\left(\frac{x}{\sqrt{2}}\right) \tag{10}$$

Bibliography

[1] Govind P. Agrawal. *Fiber-optic communication systems*. 4th ed. New York: Wiley, 2008. ISBN: 0-470-92282-6.

[2] Govind P. Agrawal. *Nonlinear fiber optics*. Elsevier, 2019.

[3] Md Sabbir Bin Hossain et al. "Experimental Comparison of Cap and Cup Probabilistically Shaped PAM for O-Band IM/DD Transmission System". In: *2021 European Conference on Optical Communication (ECOC)*. 2021, pp. 1–4. DOI: 10.1109/ECOC52684.2021.9605995.

[4] Christian Bluemm et al. "FDMA Point-to-Multi-Point Fibre Access System for Latency Sensitive Applications". In: *2022 European Conference on Optical Communication (ECOC)*. 2022, pp. 1–4.

[5] Rene Bonk et al. "Perspectives on and the road towards 100 Gb/s TDM PON with intensity-modulation and direct-detection". In: *Journal of Optical Communications and Networking* 15.8 (2023), pp. 518–526.

[6] René Bonk et al. "50G-PON: The First ITU-T Higher-Speed PON System". In: *IEEE Communications Magazine* 60.3 (2022), pp. 48–54. DOI: 10.1109/MCOM.001.2100441.

[7] Robert Borkowski et al. "FLCS-PON – A 100 Gbit/s Flexible Passive Optical Network: Concepts and Field Trial". In: *Journal of Lightwave Technology* 39.16 (2021), pp. 5314–5324. DOI: 10.1109/JLT.2021.3102383.

[8] Robert Borkowski et al. "Operator Trial of 100 Gbit/s FLCS-PON Prototype with Probabilistic Shaping and Soft-Input FEC". In: *2021 European Conference on Optical Communication (ECOC)*. 2021, pp. 1–4. DOI: 10.1109/ECOC52684.2021.9606115.

[9] Christophe Caillaud et al. "Integrated SOA-PIN Detector for High-Speed Short Reach Applications". In: *Journal of Lightwave Technology* 33.8 (2015), pp. 1596–1601. DOI: 10.1109/JLT.2015.2389533.

[10] Christophe Caillaud et al. "Monolithic Integration of a Semiconductor Optical Amplifier and a High-Speed Photodiode With Low Polarization Dependence Loss". In: *IEEE Photonics Technology Letters* 24.11 (2012), pp. 897–899. DOI: 10.1109/LPT.2012.2190275.

[11] Ivan N. Cano et al. "FDMA in Point-to-Multipoint Fibre Access Systems for Non-Residential Applications". In: *2023 23rd International Conference on Transparent Optical Networks (ICTON)*. 2023, pp. 1–4. DOI: 10.1109/ICTON59386.2023.10207353.

[12] Ivan N. Cano et al. "Relation Between TDEC, Extinction Ratio and Chromatic Dispersion in 50G PON". In: *2022 13th International Symposium on Communication Systems, Networks and Digital Signal Processing (CSNDSP)*. 2022, pp. 555–557. DOI: 10.1109/CSNDSP54353.2022.9908040.

[13] Giuseppe Caruso et al. "Enhanced Electrical Duobinary Decoder with Low-BW Based Receivers for Short Reach Indoor Optical Links". In: *2021 European Conference on Optical Communication (ECOC)*. 2021, pp. 1–4. DOI: 10.1109/ECOC52684.2021.9606150.

[14] Giuseppe Caruso et al. "Real-Time 100 Gb/s PAM-4 for Access Links With up to 34 dB Power Budget". In: *Journal of Lightwave Technology* 41.11 (2023), pp. 3491–3497. DOI: 10.1109/JLT.2023.3244028.

[15] Giuseppe Caruso et al. "Real-Time 100Gb/s Downstream PAM4 PON Link with 34 dB Power Budget". In: *2022 European Conference on Optical Communication (ECOC)*. 2022, pp. 1–4.

[16] Giuseppe Caruso et al. "Study of TDEC for 50G-PON Upstream at 50 Gb/s in Negative Dispersion Regime using 25G-class Transceivers". In: *Optical Fiber Communication Conference (OFC) 2023*. Optica Publishing Group, 2023, Th1G.2. DOI: 10.1364/OFC.2023.Th1G.2.

[17] Mariacristina Casasco et al. "TDEC metric for 50G-PON using Optical Amplification". In: *2023 23rd International Conference on Transparent Optical Networks (ICTON)*. 2023, pp. 1–4. DOI: 10.1109/ICTON59386.2023.10207515.

[18] Mariacristina Casasco et al. "TDEC metric in 50G-PON: analytical and experimental investigation on several implementation aspects". In: *J. Opt. Commun. Netw.* 15.7 (July 2023), pp. 480–487. DOI: 10.1364/JOCN.489208. URL: https://opg.optica.org/jocn/abstract.cfm?URI=jocn-15-7-480.

[19] Philippe Chanclou et al. "Optical access solutions in support of 5G and beyond [Invited]". In: *Journal of Optical Communications and Networking* 15.7 (2023), pp. C48–C53. DOI: 10.1364/JOCN.480580.

[20] H.S. Chung, Y.G. Jang, and Y.C. Chung. "Directly modulated 10-gb/s signal transmission over 320 km of negative dispersion fiber for regional metro network". In: *IEEE Photonics Technology Letters* 15.9 (2003), pp. 1306–1308. DOI: 10.1109/LPT.2003.814900.

[21] F.J. Effenberger, H. Ichibangase, and H. Yamashita. "Advances in broadband passive optical networking technologies". In: *IEEE Communications Magazine* 39.12 (2001), pp. 118–124. DOI: 10.1109/35.968822.

[22] Frank Effenberger et al. "An introduction to PON technologies [Topics in Optical Communications]". In: *IEEE Communications Magazine* 45.3 (2007), S17–S25. DOI: 10.1109/MCOM.2007.344582.

[23] A. D. Ellis et al. "Performance limits in optical communications due to fiber nonlinearity". In: *Adv. Opt. Photon.* 9.3 (Sept. 2017), pp. 429–503. DOI: 10.1364/AOP.9.000429. URL: https://opg.optica.org/aop/abstract.cfm?URI=aop-9-3-429.

[24] Robert F. H. Fischer. "Precoding and Signal Shaping for Digital Transmission". In: Wiley, 2002. Chap. 2: Digital Communications via Linear Distorting Channels, pp. 14–85.

[25] C.R.S. Fludger et al. "Experimental measurements of the impact of multipath interference on PAM signals". In: *OFC 2014*. 2014, pp. 1–3. DOI: 10.1364/OFC.2014.W1F.6.

[26] *G.9804.3 : 50-Gigabit-capable passive optical networks (50G-PON): Physical media dependent (PMD) layer specification*. Standard. ITU-T, Sept. 2021.

[27] *G.9806: Higher-speed bidirectional, single fibre, point-to-point optical access system (HS-PtP)*. Standard. ITU-T, 2022.

[28] *G.983.1: Broadband optical access systems based on Passive Optical Networks (PON)*. Standard. ITU-T, Oct. 1998.

[29] *G.984.1: Gigabit-capable passive optical networks (GPON): General characteristics*. Standard. ITU-T, Mar. 2003.

[30] *G.987.2: 10-Gigabit-capable passive optical networks (XG-PON): Physical media dependent (PMD) layer specification*. Standard. ITU-T, Oct. 2010.

[31] *G.987.2: 10-Gigabit-capable symmetric passive optical network (XGS-PON)*. Standard. ITU-T, June 2016.

[32] *G.suppl.VHSP - PON transmission technologies above 50 Gb/s per wavelength*. Work programme. ITU-T, 2022.

[33] *Global Broadband Subscriptions in Q1 2023: Fibre Glides Past Two Thirds*. Report. Point Topic, July 2023. URL: https://www.point-topic.com/post/global-broadband-subscriptions-q1-2023.

[34] Thibaut Gurne et al. "First Demonstration of a 100 Gbit/s PAM-4 Linear Burst-Mode Transimpedance Amplifier for Upstream Flexible PON". In: *2022 European Conference on Optical Communication (ECOC)*. 2022, pp. 1–4.

[35] Debregeas H. et al. "Extremely High-Power Laser-Modulators with Integrated Amplifier Section (EML-SOAs)". In: *2023 European Conference on Optical Communication (ECOC)*. paper Th.B.4.1. Sept. 2023.

[36] Jeff Heynen. *50G PON moves closer to deployment*. Apr. 2023. URL: https://www.delloro.com/50g-pon-moves-closer-to-deployment/.

[37] Chingyin Hong et al. "High Speed Ge/Si Avalanche Photodiode with High Sensitivity for 50Gbit/s and 100Gbit/s Optical Access Systems". In: *2022 Optical Fiber Communications Conference and Exhibition (OFC)*. 2022, pp. 1–3.

[38] Dave Hood. *Gigabit-capable passive optical networks*. John Wiley & Sons, 2012.

[39] Vincent Houtsma et al. "100 GBd Dispersion-Tolerant Downstream PON with 35 dB Power Budget using APD and Low-Complexity Equalization". In: *2023 European Conference on Optical Communication (ECOC)*. paper We.C.1.1. Sept. 2023.

[40] Vincent Houtsma et al. "APD-based duobinary direct detection receivers for 40 Gbps TDM-PON". In: *2015 Optical Fiber Communications Conference and Exhibition (OFC)*. 2015, pp. 1–3. DOI: 10.1364/OFC.2015.Th4H.1.

[41] Rongqing Hui and Maurice O'Sullivan. *Fiber-Optic Measurement Techniques*. Academic Press, 2022.

[42] *IEEE Standard for Ethernet*. Standard. 2018. Chap. 4, Clause 75. Physical Medium Dependent (PMD) sublayer and medium for passive optical networks, type 10GBASE–PR and 10/1GBASE–PRX. DOI: 10.1109/IEEESTD.2018.8457469.

[43] *IEEE Standard for Ethernet*. Standard. 2018. Chap. 4, Clause 52: Physical Medium Dependent (PMD) sublayer and baseband medium, type 10GBASE-S (short wavelength serial), 10GBASE-L (long wavelength serial), and 10GBASE-E (extra long wavelength serial. DOI: 10.1109/IEEESTD.2018.8457469.

[44] *IEEE Standard for Ethernet*. Standard. IEEE, 2018. Chap. 6, Clause 95: Physical Medium Dependent (PMD) sublayer and medium, type 100GBASE-SR4, pp. 558–561. DOI: 10.1109/IEEESTD.2018.8457469.

[45] *IEEE Standard for Ethernet*. Standard. 2018. Chap. 8, Clause 121: Physical Medium Dependent (PMD) sublayer and medium, type 200GBASE-DR4, pp. 131–136. DOI: 10.1109/IEEESTD.2018.8457469.

[46] Shweta Jain et al. "World's First XG-PON Field Trial". In: *Journal of Lightwave Technology* 29.4 (2011), pp. 524–528. DOI: 10.1109/JLT.2010.2104313.

[47] W Kaiser et al. “Reduced complexity optical duobinary 10-Gb/s transmitter setup resulting in an increased transmission distance”. In: *IEEE Photonics Technology Letters* 13.8 (2001), pp. 884–886.

[48] Shigeru Kanazawa et al. “High output power 214-Gbit/s 4-PAM operation of Hi-FIT AXEL transmitter”. In: *2021 Opto-Electronics and Communications Conference (OECC)*. 2021, pp. 1–3.

[49] Noriaki Kaneda et al. “Experimental demonstration of flexible information rate PON beyond 100 Gb/s with probabilistic and geometric shaping”. In: *Journal of Optical Communications and Networking* 14.1 (2022), A23–A30. DOI: 10.1364/JOCN.438127.

[50] Jonathan King, David Leyba, and Greg D. LeCheminant. “TDECQ (Transmitter Dispersion Eye Closure Quaternary) replaces historic eye-mask and TDP test for 400 Gb/s PAM4 optical transmitters”. In: *2017 Optical Fiber Communications Conference and Exhibition (OFC)*. 2017, pp. 1–3.

[51] G. Kramer, B. Mukherjee, and G. Pesavento. “IPACT a dynamic protocol for an Ethernet PON (EPON)”. In: *IEEE Communications Magazine* 40.2 (2002), pp. 74–80. DOI: 10.1109/35.983911.

[52] Adam Lender. “The duobinary technique for high-speed data transmission”. In: *IEEE Transactions on Communication and Electronics* 82.2 (1963), pp. 214–218. DOI: 10.1109/TCE.1963.6373379.

[53] Borui Li et al. “DSP enabled next generation 50G TDM-PON”. In: *Journal of Optical Communications and Networking* 12.9 (2020), pp. D1–D8. DOI: 10.1364/JOCN.391904.

[54] Xiang Li, Md. Saifuddin Faruk, and Seb J. Savory. “Bidirectional Symmetrical 100 Gb/s/λ Coherent PON Using a Simplified ONU Transceiver”. In: *IEEE Photonics Technology Letters* 34.16 (2022), pp. 838–841. DOI: 10.1109/LPT.2022.3168294.

[55] Aaron Maharry et al. “First Demonstration of an O-Band Coherent Link for Intra-Data Center Applications”. In: *Journal of Lightwave Technology* (2023), pp. 1–8. DOI: 10.1109/JLT.2023.3290487.

[56] Michael P. McGarry, Martin Reisslein, and Martin Maier. “Ethernet passive optical network architectures and dynamic bandwidth allocation algorithms”. In: *IEEE Communications Surveys & Tutorials* 10.3 (2008), pp. 46–60.

[57] Derek Nesset. “Next Generation PON Technologies: 50G PON and Beyond (Invited)”. In: *2023 International Conference on Optical Network Design and Modeling (ONDM)*. 2023, pp. 1–6.

[58] *NGMN 6G drivers and vision*. Whitepaper 1.0. https://www.ngmn.org/work-programme/ngmn-6g-drivers-and-vision.html: NGMN, Apr. 2021.

[59] OECD. "Broadband networks of the future". In: (2022). URL: https://www.oecd-ilibrary.org/science-and-technology/broadband-networks-of-the-future_755e2d0c-en.

[60] OIF-CEI. *Implementation Agreement OIF-CEI-04.0 Common Electrical: Common Electrical I/O (CEI) - Electrical and Jitter Interoperability agreements for 6G+ bps, 11G+ bps and 25G+ bps I/O*. https://www.oiforum.com/wp-content/uploads/2019/01/OIF-CEI-04.0.pdf. 2017.

[61] P. Ossieur et al. "A 1.25-gb/s burst-mode receiver for GPON applications". In: *IEEE Journal of Solid-State Circuits* 40.5 (2005), pp. 1180–1189. DOI: 10.1109/JSSC.2005.845984.

[62] *Passive Optical Network (PON) Market Size, Share & COVID-19 Impact Analysis, Regional Forecast, 2023-2030*. Report. Forbes Business Insight, Mar. 2023.

[63] John Petrilla, Piers Dawe, and Greg D. LeCheminant. "New Metric Offers More Accurate Estimate of Optical Transmitter's Impact on Multimode Fiber-optic Links". In: *DesignCon 2015*. 2015.

[64] Jeremy Potet et al. "Real Time 100 Gbit/s/λ PAM-4 Experiments for Future Access Networks over 20 km with 29 dB Optical Budget". In: *2021 European Conference on Optical Communication (ECOC)*. 2021, pp. 1–3. DOI: 10.1109/ECOC52684.2021.9606149.

[65] Jeremy Potet et al. "Real-Time DSP-Free 100 Gbit/s/λ PAM-4 Fiber Access Link using EML and Direct Detection". In: *IEEE Photonics Technology Letters* 34.17 (2022), pp. 895–898. DOI: 10.1109/LPT.2022.3191460.

[66] Jérémy Potet et al. "Real-Time DSP-Free 100 Gbit/s/λ PAM-4 Fiber Access Link Using EML and Direct Detection". In: *IEEE Photonics Technology Letters* 34.17 (2022), pp. 895–898. DOI: 10.1109/LPT.2022.3191460.

[67] Richard Poulo et al. "Statistical Principles and Trends in Mask Testing". In: *DesignCon 2015*. 2015.

[68] John G. Proakis and Masoud Salehi. "Digital Communications". In: 5th ed. McGraw-Hill Higher Education, 2008. Chap. 10: Adaptive Equalization, pp. 689–705. ISBN: 9780071263788.

[69] Chuan Qin et al. "40 Gbps PON with 23 dB power budget using 10 Gbps optics and DMT". In: *Optical Fiber Communication Conference*. Optica Publishing Group. 2017, M3H–5.

[70] *Recommendation G.9804.3 (2021) Amendment 1 (02/23)*. Standard. ITU-T, Feb. 2023.

[71] Ricardo Rosales et al. “Achieving high budget classes in the downstream link of 50G-PON”. In: *Journal of Optical Communications and Networking* 13.8 (2021), pp. D13–D21. DOI: 10.1364/JOCN.426009.

[72] Fabienne Saliou et al. “Optical access network interfaces for 5G and beyond [Invited]”. In: *Journal of Optical Communications and Networking* 13.8 (2021), pp. D32–D42. DOI: 10.1364/JOCN.425039.

[73] D.V. Sarwate and M.B. Pursley. “Crosscorrelation properties of pseudorandom and related sequences”. In: *Proceedings of the IEEE* 68.5 (1980), pp. 593–619. DOI: 10.1109/PROC.1980.11697.

[74] David Schaber et al. “PON Downstream Scheme Supporting Simultaneously Different ONU Categories”. In: *IEEE Photonics Technology Letters* 35.21 (2023), pp. 1171–1174. DOI: 10.1109/LPT.2023.3308372.

[75] G. Simon et al. “Experimental Analysis of TDEC for Higher Speed PON Including Linear Equalization”. In: *2022 European Conference on Optical Communication (ECOC)*. 2022, pp. 1–4.

[76] JR Stern et al. “Passive optical local networks for telephony applications and beyond”. In: *Electronics Letters* 24.23 (1987), pp. 1255–1256.

[77] N. Taengnoi et al. “AMI for Nonlinearity Mitigation in O-Band Transmission”. In: *2019 Optical Fiber Communications Conference and Exhibition (OFC)*. 2019, pp. 1–3.

[78] Minghui Tao et al. “Improved Dispersion Tolerance for 50G-PON Downstream Transmission via Receiver-Side Equalization”. In: *2019 Optical Fiber Communications Conference and Exhibition (OFC)*. 2019, pp. 1–3.

[79] *The Connecting Europe Broadband Fund*. URL: https://digital-strategy.ec.europa.eu/en/library/connecting-europe-broadband-fund.

[80] Pablo Torres-Ferrera et al. “Experimental Demonstration of 100 Gbps/λ C-Band Direct-Detection Downstream PON Using Non-Linear and CD Compensation with 29 dB+ OPL Over 0 Km - 100 Km”. In: *Journal of Lightwave Technology* 40.2 (2022), pp. 547–556. DOI: 10.1109/JLT.2021.3129446.

[81] Pablo Torres-Ferrera et al. “Experimental Demonstration of 100 Gbps/λ C-Band Direct-Detection Downstream PON Using Non-Linear and CD Compensation with 29 dB+ OPL Over 0 Km-100 Km”. In: *Journal of Lightwave Technology* 40.2 (2022), pp. 547–556. DOI: 10.1109/JLT.2021.3129446.

[82] Pablo Torres-Ferrera et al. “Impact of the overall electrical filter shaping in next-generation 25 and 50 Gb/s PONs”. In: *Journal of Optical Communications and Networking* 10.5 (2018), pp. 493–505. DOI: 10.1364/JOCN.10.000493.

[83] Pablo Torres-Ferrera et al. "Optimization of Band-Limited DSP-Aided 25 and 50 Gb/s PON Using 10G-Class DML and APD". In: *Journal of Lightwave Technology* 38.3 (2020), pp. 608–618. DOI: 10.1109/JLT.2019.2946959.

[84] Pablo Torres-Ferrera et al. "Overview of high-speed TDM-PON beyond 50 Gbps per wavelength using digital signal processing [Invited Tutorial]". In: *Journal of Optical Communications and Networking* 14.12 (2022), pp. 982–996. DOI: 10.1364/JOCN.468920.

[85] Joris Van Kerrebrouck et al. "NRZ, Duobinary, or PAM4?: Choosing Among High-Speed Electrical Interconnects". In: *IEEE Microwave Magazine* 20.7 (2019), pp. 24–35. DOI: 10.1109/MMM.2019.2909517.

[86] Dora van Veen et al. "Interoperability and Experimental Evaluation of TDEC(Q) Testing for 50 and 100G PONs". In: *2023 Optical Fiber Communications Conference and Exhibition (OFC)*. 2023, pp. 1–3. DOI: 10.23919/OFC49934.2023.10117203.

[87] Doutje van Veen and Vincent Houtsma. "Strategies for economical next-generation 50G and 100G passive optical networks". In: *Journal of Optical Communications and Networking* 12.1 (2020), A95–A103.

[88] Doutje van Veen et al. "26-Gbps PON transmission over 40-km using duobinary detection with a low cost 7-GHz APD-based receiver". In: *2012 38th European Conference and Exhibition on Optical Communications*. 2012, pp. 1–3. DOI: 10.1364/ECEOC.2012.Tu.3.B.1.

[89] Kaihui Wang et al. "100-Gbit/s/ PAM-4 Signal Transmission over 80-km SSMF Based on an 18-GHz EML at O-Band". In: *2020 Optical Fiber Communications Conference and Exhibition (OFC)*. 2020, pp. 1–3.

[90] Wei Wang et al. "100 Gbit/s/λ DMT-PON System Based on Intensity Modulation and Heterodyne Coherent Detection". In: *IEEE Photonics Technology Letters* 33.18 (2021), pp. 1014–1017. DOI: 10.1109/LPT.2021.3079982.

[91] Yang Jing Wen, Yan Cui, and Yusheng Bai. "Mitigation of optical multipath interference impact for directly detected PAMn system". In: *Opt. Express* 28.25 (Dec. 2020), pp. 38317–38333. DOI: 10.1364/OE.413054. URL: https://opg.optica.org/oe/abstract.cfm?URI=oe-28-25-38317.

[92] Jun Shan Wey. "The Outlook for PON Standardization: A Tutorial". In: *Journal of Lightwave Technology* 38.1 (2020), pp. 31–42. DOI: 10.1109/JLT.2019.2950889.

[93] Jun Shan Wey et al. *ITU-T G.9806Am3 Update*. Meeting. Nov. 2022.

[94] Lei Xue et al. "100G PAM-4 PON with 34 dB Power Budget Using Joint Nonlinear Tomlinson-Harashima Precoding and Volterra Equalization". In: *2021 European Conference on Optical Communication (ECOC)*. 2021, pp. 1–4. DOI: 10.1109/ECOC52684.2021.9606041.

[95] Dezhi Zhang et al. “Carrier Lab Trial of a Real Time 50G-PON Prototype”. In: *2021 European Conference on Optical Communication (ECOC)*. 2021, pp. 1–4. DOI: 10.1109/ECOC52684.2021.9605843.

[96] Dezhi Zhang et al. “Progress of ITU-T higher speed passive optical network (50G-PON) standardization”. In: *Journal of Optical Communications and Networking* 12.10 (2020), pp. D99–D108. DOI: 10.1364/JOCN.391830.

[97] Jiao Zhang et al. “Demonstration of 100-Gb/s/λ PAM-4 TDM-PON Supporting 29-dB Power Budget with 50-km Reach using 10G-class O-Band DML Transmitters”. In: *2019 Optical Fiber Communications Conference and Exhibition (OFC)*. 2019, pp. 1–3.

[98] Jiao Zhang et al. “Demonstration of Terabit/s LAN-WDM for the Evolution of B5G/6G Fronthaul Networks”. In: *IEEE Photonics Journal* 15.4 (2023), pp. 1–9. DOI: 10.1109/JPHOT.2023.3300705.

[99] Ying Zhao et al. “BER and TDECQ Correlation for Different Impairments in 400Gbps PAM4 System”. In: *2020 Optical Fiber Communications Conference and Exhibition (OFC)*. 2020, pp. 1–3.

This Ph.D. thesis has been typeset by means of the TEX-system facilities. The typesetting engine was pdfLATEX. The document class was `toptesi`, by Claudio Beccari, with option `tipotesi=scudo`. This class is available in every up-to-date and complete TEX-system installation.